Satellite Formation Maintenance Using Differential Atmospheric Drag

by

Francis Bellefeuille

Department of Mechanical Engineering

McGill University, Montreal

November 2011

A thesis submitted to McGill University in partial fulfilment of the requirements of the degree of Master of Engineering

Acknowledgements

First and foremost, I would like to thank my advisor Professor Arun K. Misra for his help and guidance throughout my graduate studies. This thesis would not have been possible without his vast knowledge of control and dynamics and his willingness to share it. I would also like to thank him for encouraging me to attend and participate at multiple conventions during the past years. The experience and knowledge gained from doing so is invaluable.

I must thank Tyler Reid for his help as well. His work on formation flying dynamics under the supervision of professor Misra was the foundation upon which this thesis was built. He also helped me in the early stages of coding.

To my family, friends and especially my parent, thank you for your patience, constant support and encouragements. You have been pivotal in my decision of pursuing and completing my graduate studies.

Abstract

Satellite formation flying is a very promising field for future space missions as it holds many advantages over the common monolithic satellite. However, in order for the formations to be effective, a formation maintenance scheme is required to overcome perturbations arising from different sources. In this thesis the effect of atmospheric drag on a formation is examined. To do so the Schweighart and Sedwick equations, which describe the motion of a spacecraft, called deputy spacecraft, relative to another spacecraft, referred to as the chief spacecraft, placed in a circular orbit, are modified to account for atmospheric drag. The modified equations keep the effects arising from the oblateness of the Earth, known as the J_2 effects, which were included in the model proposed by Schweighart and Sedwick. A similar set of equation is then developed for satellite formations placed in orbits of small eccentricity. A formation maintenance scheme which uses differential atmospheric as a means of control is then introduced. Numerical simulation results showing the evolution of formations through time with and without active control are also provided.

Résumé

Le vol de satellite en formation est un domaine très prometteur pour de futures missions spatial étant donnés les nombreux avantages que cette technologie détient le satellite monolitique commun. Toutefois, pour que ces formations soient efficaces, un système de maintenance de formation est nécessaire pour surmonter les perturbations provenant de multiples sources. Dans cette these, l'effet du freinage atmosphérique sur une formation est examiné. Pour ce faire, les equations de Schweighart et Sedwick, qui décrivent le mouvement d'un engin spatial, appelé meneur, relative à un autre engine, nommé suiveur, place sur une orbite circulaire, sont modifiées pour tenir compte du freinage atmosphérique. Les equations modifiées conservent les effets découlant du fait que la Terre n'est pas parfaitement sphérique, connus comme les effets J_2, qui sont inclus dans le modèle proposé par Schweighart et Sedwick. Un ensemble d'équations similaire est ensuite développé pour des formations de satellites placées sur des orbites de petites eccentricités. Un système de maintenance de formation qui utilise le freinage atmosphérique comme moyen de contrôle est introduit. Des resultats de simulations numériques montrant l'évolution dans le temps de formations avec et sans contrôle sont également fournis.

Table of Contents

List of Symbols

$\mathbf{A}$	State matrix used in the state-space form of the equation of motion for the circular case
$\mathbf{A}_e$	State matrix used in the state-space form of the equation of motion for the elliptical case
A	Projected area of spacraft
δA	Change in projected area of spacecraft
$\mathbf{a}_{Drag}$	Drag perturbative acceleration vector acting on the reference orbit expressed in the Hill frame
$\Delta\mathbf{a}_{Drag}$	Aceleration vector of deputy spacecraft relative to the chief spacecraft due to drag expressed in the Hill frame
$\mathbf{a}_{J_2}$	J_2 perturbative acceleration vector acting on the reference orbit expressed in the Hill frame
$\Delta\mathbf{a}_{J_2}$	Aceleration vector of deputy spacecraft relative to the chief spacecraft due to J_2 perturbations expressed in the Hill frame
a	Semi-major axis of reference orbit
$\mathbf{B}$	Input vector used in the state-space form of the equation of motion for the elliptical case
$\mathbf{C}$	Damping matrix of the dynamic system for the circular reference orbit case
$\mathbf{C}_e$	Damping matrix of the dynamic system for the elliptical reference orbit case
C_D	Drag coefficient of spacecraft
c	Parameter used in Schweighart and Sedwick formulation, see Appendix B
d	Characteristic length associated with the desired formation's geometry

$\mathbf{E}^*$	Error in the signal given to the feedback law
E	Eccentric anomaly of reference orbit
e	Eccentricity of reference orbit
$\mathbf{F}$	Constant matrix used in Floquet-Lyapunov theory
$\mathbf{f}_{Drag}$	Absolute acceleration vector of spacecraft due to drag
$\Delta\mathbf{f}_{Drag}$	Acceleration vector of the deputy spacecraft relative to the chief spacecraft due to drag
$\mathbf{f}$	Forcing function vector of the dynamic system for the circular reference orbit case
$\mathbf{f}_e$	Forcing function vector of the dynamic system for the elliptical reference orbit case
f	True anomaly of reference orbit
$\mathbf{G}$	Control gain matrix
h	Magnitude of the specific angular moment vector of the reference orbit
i	Inclination of reference orbit
J_2	Second spherical harmonic of Earth's gravitational potential
$\nabla\mathbf{J}_2$	J_2 potential field gradient matrix
$\mathbf{K}$	Damping matrix of the dynamic system for the circular reference orbit case
$\mathbf{K}_e$	Damping matrix of the dynamic system for the elliptical reference orbit case
k	Parameter used in Schweighart and Sedwick formulation, see Appendix B
$\mathbf{L}$	Time dependant Matrix used in Floquet-Lyapunov theory

l	Parameter used in Schweighart and Sedwick formulation, see Appendix B
$\mathbf{M}$	Generalized inertia matrix of the dynamic system for the circular reference orbit case
$\mathbf{M}_e$	Generalized inertia matrix of the dynamic system for the elliptical reference orbit case
M	Mean anomaly of reference orbit
m	Mass of spacecraft
n	Mean orbital rate of reference orbit
n_0	Initial mean orbital rate of reference orbit
p	Semi-latus rectum
q	Parameter used in Schweighart and Sedwick formulation, see Appendix B
R_e	Mean equatorial radius of the Earth
r_{ref}	Radial distance of the origin of the Hill frame from the center of the Earth
s	Parameter used in Schweighart and Sedwick formulation, see Appendix B
$\tilde{s}$	Parameter defined in Chapter 4, Eq. (4.53)
t	Time
u	Control input used in the state-space form of the equation of motion
$\mathbf{v}_{rel}$	Velocity vector of spacecraft relative to the rotating atmosphere
$\mathbf{W}$	Vector related to the forcing function used in the state-space form of the equation of motion for the circular case
$\mathbf{W}_e$	Vector related to the forcing function used in the state-space form of the equation of motion for the elliptical case

$\mathbf{X}$	State vector used in the state-space form of the equation of motion
$\mathbf{x}$	Relative position vector of spacecraft
x	Radial component of the relative position vector expressed in the Hill frame
y	In-track component of the relative position vector expressed in the Hill frame
z	Cross-track component of the relative position vector expressed in the Hill frame

α	Parameter used in stability condition, Eq. (2.100)
β	Dimensionless ballistic coefficient of spacecraft
θ	True latitude of reference orbit
κ_y	Parameter defined in Chapter 2, Eq. (2.84)
κ_z	Parameter defined in Chapter 2, Eq. (2.85)
μ	Earth's gravitational constant
ξ	Parameter used in stability condition, Eq. (2.100)
ρ	Local atmospheric density
$\hat{\sigma}$	Dimensionless parameter defined in Chapter 2, Eq. (2.54)
$\tilde{\sigma}_1$	Dimensionless parameter defined in Chapter 4, Eq. (4.92)
$\tilde{\sigma}_2$	Dimensionless parameter defined in Chapter 4, Eq. (4.93)
$\hat{\varsigma}$	Parameter defined in Chapter 2, Eq. (2.55)
τ	Dimensionless time parameter
$\mathbf{\Phi}$	State transition matrix
φ	Parameter used in Schweighart and Sedwick formulation to indicate initial phase angle for the cross-track motion, see Appendix B
Ω	Right ascension of ascending node of reference orbit

ω	Argument of perigee of reference orbit
$\boldsymbol{\omega}_e$	Angular velocity vector of the Earth
ω_e	Angular velocity of the Earth

A dot over a variable indicates differentiation with respect to time.

An apostrophe next to a variable indicates differentiation with respect to dimensionless time parameter τ.

A hat over a variable indicates non-dimensionalization of the variable.

An overbar indicates orbit-averaging of the variable.

List of Figures

List of Tables

Chapter 1 - Introduction

1.1 Formation Flying

There is a recent tendency in the space industry to replace large satellites with multiple smaller satellites working in unison to achieve specific mission objectives. These satellites formations offer various advantages over their traditional alternative. The smaller satellites constituting the formation will likely be cheaper and quicker to build. Since the formation can be altered, they offer greater versatility. Having multiple satellites and redundancy also allows for a malfunctioning satellite to be replaced, avoiding having to abort the mission. Even if the malfunctioning satellite was impossible to replace, the formation could be altered to perform, at least partially, the mission with the remaining satellites. While, the resolution of a single satellite's onboard radar dish is limited by size and cost constraints at launch, satellite formations can be configured to create a much larger dish and, therefore, can offer greater resolution. These multiple advantages make satellite formation flying an ideal technology for astronomical observations, communications, meteorology and environmental applications.

The use of a formation brings some complications though. For the formation to be effective, the satellites must maintain a certain configuration and relative positions become of the utmost importance. Examples of such configurations are formations operating on projected circular orbits (PCO) or along track orbits (ATO). In the case of a projected circular formation, the motion of the deputy spacecraft relative to the chief spacecraft forms an ellipse whose projection in the x-y plane of the Hill frame described in Section 2.1 forms a circle. As for the along track formation, both spacecraft's share the same ground track, meaning they pass over the Earth in the exact same locations one after the other. Since these relative positions and motions are subject to drift caused by perturbation forces such as the ones due to the oblateness of the Earth (often referred to as the J_2 perturbations) and solar radiation pressure, active formation control becomes imperative. Another perturbation force that will affect relative motion between two spacecraft is atmospheric drag. This last perturbation force increases in magnitude as the altitude of the formation decreases. It is therefore usually seen as an obstacle to formation flight at low altitudes.

1.2 Differential Atmospheric Drag Control

Although atmospheric drag is typically seen as a nuisance when planning a mission involving formation flying at low altitudes, it can be used as a means of formation keeping. Through the implementation of drag panels that can be rotated, one can control the projected area of each spacecraft and, as a consequence, the differential drag between them. In fact, the solar panels mounted on the satellites can be used as drag panels if they, or the spacecraft, can be rotated. Using differential drag would decrease the use of impulsive thrusters and the products of the combustion associated with such thrusters can contaminate sensitive sensors and optical equipment. It would also reduce the cost associated with fuel and increase the life of the spacecraft, as they would not be as dependent on onboard fuel. Since, the accelerations arising from differential are much smaller in magnitude to the ones coming from conventional thrusters, it might be preferable if the spacecraft carries something fragile or is fragile in fabrication.

1.3 Objectives of the Thesis

The objectives of this thesis are to evaluate the effect of atmospheric drag on a formation of satellites orbiting the Earth at low altitudes and to assess the feasibility of using differential drag as a means of maintaining such formation. Simplified linearized models taking into account J_2 perturbations and atmospheric drag will be developed for both circular and elliptical reference orbits. The effect of eccentricity on a formation will then be investigated. Finally, control schemes for both the circular and elliptic cases will be developed and tested through numerical simulations.

1.4 Literature Review

The literature reviewed in this section will be divided into two subsections. The first subsection will deal with the work that has been done in the field of dynamics of spacecraft formations and relative position. The following subsection will go over some of the work done in the field of formation control and formation maintenance. The last subsection will be related to the control of linear, periodically time-varying systems. This subsection is essential because we seek to control a spacecraft formation flying in circular orbits as well as elliptic orbits and, once we increase the eccentricity, the system remains linear, but becomes periodically time-varying.

1.4.1 Dynamics of Spacecraft Formation Flying and Relative Positions

There are two main ways of describing the motion of deputy spacecraft relative to a chief spacecraft. The first way is to express the state of the deputy in the Hill frame ($x, y, z, \dot{x}, \dot{y}, \dot{z}$) which is explained in details Section 2.1. This frame is an orthogonal coordinate frame centered on the chief placed on the reference orbit. This method will be the one used in this thesis and the Hill frame will be described in more details in section 2.1. There have been several works done in the field of dynamics of formation flying using this method to characterize the relative motion.

The most well known equations in the field of spacecraft relative motion are the Clohessy-Wiltshire equations (Clohessy and Wiltshire, 1960). They are a set of constant coefficient linear ordinary differential equations describing the motion of a deputy spacecraft relative to a chief spacecraft. The chief spacecraft is assumed to be traveling in an unperturbed circular orbit. Since perturbations are not considered, errors tend to grow large over time. Despite this limitation, these equations can be used quite effectively in the context of rendezvous missions, since the time frame for such missions is small enough for the equations to still be accurate. In the context of formation flying, however, the time frame is significantly larger and the errors can grow too large for this set of equations to be of much use.

Tschauner and Hempel (1965) provided a solution for the problem of relative motion between two spacecraft placed in an elliptic orbit. Similarly to the Clohessy-Wiltshire, these equations do not account for any perturbations. They, therefore, have limited applications for formation flying, but can be useful for rendezvous missions.

Kechichian (1998) developed a set of second-order nonlinear differential equations describing the motion of a deputy spacecraft relative to a chief spacecraft placed in an elliptic orbit. These equations factor in the effects of both atmospheric drag and J_2 perturbations. This system of equations cannot be solved in closed form.

Carter and Humi worked on modifying the Clohessy-Wiltshire to include the effect of atmospheric drag on the relative motion of spacecraft. In their first work (Carter and Humi, 2002a), they presented equations and solutions representing the terminal phase of a rendezvous in the presence of atmospheric drag. The drag was assumed to be linear in the velocity of the spacecraft. In their second work (Carter and Humi, 2002b), the atmospheric drag model was changed to be proportional to the square of the velocity of each spacecraft in order to be more realistic. The model is given in the forms of a set of ordinary differential equations and of a state transition matrix. When the drag constants of each spacecraft are identical, the solution simplifies to that obtained by Tschauner and Hempel. The equations also simplify to Clohessy-Wiltshire equations if the eccentricity is then set to zero. Since they worked with rendezvous missions in mind, they did not include the effect of J_2 perturbations. The solution, therefore, loses in accuracy over long periods of time.

Schweighart and Sedwick (2002) modified the Clohessy-Wiltshire equations to increase their precision. To do so, they addressed the assumption made by Clohessy and Wiltshire that the Earth was perfectly spherical which leads to large errors with time. The result is a set of constant coefficient, linearized, differential equations similar in form to the equations they modified, but that now captures the effect of J_2 perturbations. These equations can be solved analytically and the solution is provided by Shweighart and Sedwick. This solution has periodic errors of no more than 0.4% when compared numerically to a high precision orbit propagator including the effects of the J_2 potential. Like the Clohessy-Wiltshire equations, they are only valid for circular orbits.

Yamanaka and Ankersen (2002) developed a state transition matrix to obtain the position and velocity of the deputy spacecraft relative to the chief spacecraft at any given time. The state transition matrix is valid for any elliptical orbit and does not have a singularity at $e = 0$. Like the Clohessy-Wiltshire equations, the state transition matrix given here does not account for perturbations. In fact, for circular reference orbits, the state transition matrix and the Clohessy-Wiltshire equations give the same results.

The second way of describing relative motion is more recent and uses orbit element differences. That is to take the vector of the difference in orbital elements between the two satellites to express the state of the deputy relative to the chief (δa, δe, δi, $\delta \Omega$, $\delta \omega$, δM). There is a substantial amount of work that has been done in the field of dynamics of formation flying using this method to characterize the relative motion as well.

While it might not be as easy to visualize the instantaneous relative position using the state vector given by this method, it has other advantages. One of those is given by Schaub and Junkins (2003), when going over relative orbit description: “Simply starting out with the Hill frame initial conditions [...], the relative geometry is determined only after solving the differential equations. However, by describing the relative orbit in terms of orbit element differences, it is possible to make certain statements regarding the relative orbit geometry”. More details regarding relative orbit description and formation flying can also be found in that book.

Schaub (2004) used mean orbital element differences to express the relative motion between two spacecraft placed on an elliptical orbit. The spacecraft are assumed to be under the effect of J_2 perturbations. The mapping between the orbital element differences and the Hill-frame coordinates is also provided.

Sengupta and Vadali (2007), studied the effects of eccentricity on the relative motion of spacecraft flying in Keplerian orbits. They also derive a new linear condition for bounded relative motion. This condition is valid for any eccentricity or perigee altitude. Using the effects of eccentricity, they also determine the desired geometry of the relative motion.

Hamel and de Lafontaine (2007) built upon the work of Schaub to obtain an analytical state transition matrix that models the relative motion between two spacecraft placed in a J_2-perturbed elliptical orbit. The advantage of the state matrix lies in the fact that the reference orbit doesn`t need to be propagated. In order to obtain the state transition matrix, Hamel and de Lafontaine provide the mapping between the mean orbital elements and the osculating orbital elements.

1.4.2 Formation Control

The most common way of controlling a satellite formation is through the use of thrusters to provide the instantaneous acceleration needed. Although this method will not be used in this thesis, the control laws developed for systems controlled by thrusters are still of interest and will thus be presented in the first part of this section.

Ulybyshev (1998) developed a discrete-time linear quadratic regulator (LQR) to perform formation keeping for satellite constellations placed in circular orbits. The control law minimizes relative displacements in the along-track direction. It also minimizes the orbital period displacements relative to the reference orbit period.

Vadali et al. (2002) modified the Clohessy-Wiltshire equations to include the time-averaged effects of the J_2 perturbations. They then provided a method to obtain initial conditions that result in quasi-periodic relative motion. Finally, they presented a linear-quadratic regulator that minimizes fuel consumption and maintains equal average fuel consumption for each spacecraft.

Schaub and Alfriend (2002) developed a hybrid continuous feedback control law using both orbit element differences and Hill frame coordinates. The controller is given the desired relative orbit geometry in terms of orbit element differences and the actual orbit in terms of Hill-frame coordinates. In order for this controller to work properly the mapping between both state vectors must be done accurately. The method used for mapping is therefore presented and numerical results demonstrate its accuracy.

Tillerson et al. (2002) used linear program optimization in order to perform trajectory planning. A bounding box is defined around the spacecraft's desired position. Once the spacecraft reaches the edge of this box, a return trajectory is planned. This control algorithm can be used both for formation maintenance and reconfiguration. The controller accounts for actuator saturation while remaining valid despite disturbances and model uncertainties.

Blake (2008) used quasi-rigid body formulation in order to describe a satellite formation as one entity. Once this is done, it is showed that formation control can be separated in a torque to control the orientation and forces to maintain its rigidity. From there, two controllers acting on the formation as a whole are presented. The first is based on Lyapunov theory while the second prescribes a series of linear feedback matrices. Simulations are provided to show the controllers ability to perform formation maintenance and constrained reorientations.

In the second part of this section, the work done in the literature using differential atmospheric drag to control satellite formations will be provided.

Leonard et al. (1986, 1989) first examined the feasibility of using differential drag to control the relative positions between spacecraft. To do so, the Clohessy-Wiltshire equations were modified to include the effect of atmospheric drag, which was modeled as a constant force acting in the direction opposite to the velocity. This force could be positive, negative or equal to zero depending on the control applied, since both chief and deputy spacecraft were assumed to have drag panels that could be rotated to have an angle of attack of either 0 or 90 degrees. After a coordinate transformation, the problem was reduced to the simultaneous solutions of the double integrator and harmonic oscillator. A control law was then developed and was successful in performing formation manoeuvring and maintenance.

Franconeri (2003) examined how differential atmospheric drag could be used to perform station keeping for satellite constellations. He shows how differential atmospheric drag can be obtained by changing the projected area of each spacecraft through the rotation of solar panels or through attitude adjustments. The example chosen in the paper is an in-plane constellation where the distances between each spacecraft are very large. However, detailed calculations are not provided.

Mishne (2004) worked on formation maintenance in low-Earth orbits. He developed a method to compensate for the effects of atmospheric drag and J_2 perturbation on the formation using impulsive velocity corrections. An optimality condition is also developed in order to make these impulses as small as possible.

Fourcade (2004) presented the results of the mission analysis the interferometric wheel patented by the French space agency, CNES (Centre National d'Études Spatiales), operating at low-Earth orbit. This formation is comprised of three small satellites flying in a circular wheel relative to a larger satellite. The mission analysis goes over how the initial orbital elements were chosen in order to satisfy all the constraints provided by the mission. It also provides orbit positioning strategies such as reconfiguration of the wheel in order to modify its size. Finally the mission analysis provides the station keeping strategies used. One of those strategies uses differential atmospheric drag to control the mean nodal elongation between the satellites of the wheel.

Sabatini and Palmerini (2006) presented a linear quadratic regulator for low-Earth orbit formations. Their control law is based on the equations developed by Carter and Humi (2002) which include the effects of aerodynamic drag. They assumed that thrust could be applied continuously for control purposes. Numerical simulations taking into account the effects of atmospheric drag and J_2 perturbations show that the LQR based on the Carter-Humi equations is significantly more efficient than an LQR based on the Clohessy-Wiltshire.

Jigang and Yulin (2006) worked on using differential drag to control co-planar formations. To do so they used phase plane methods and assumed the rate of change of the difference between the semi-major axes of the two satellites to be constant. Simulation results show that the control scheme developed is able to reduce the drift in the formation and keep it bounded.

Kumar, Bang and Tahk (2007) studied the feasibility of using differential atmospheric drag to maintain a formation of nano-satellites. Using a commercial simulator (the Precision Orbit Propagator within the program Satellite Tool Kit [STK]), they were able to determine the range for which differential atmospheric drag could be used to perform formation maintenance. A simple proportional-integral-derivative (PID) controller is then developed to control the spacecraft's cross sectional area and thus control the drag forces. The PID uses the orbit's energy as input. It is shown that the controller can maintain the formation within reasonable boundaries.

Kumar, Ng, Yoshihara and De Ruiter (2007) examined the feasibility of using atmospheric drag as a means of relative position control in the context of a proposed formation flight mission of the Canadian Space Agency. A PID controller for formation keeping was designed. The controller compares the difference in energies between the orbits of both spacecraft to assign a change in projected area to either spacecraft. The controller is successful for small difference in energies, but is designed for circular orbits.

Bevilacqua and Romano (2008) presented a method tha uses atmospheric drag in order to perform rendezvous manoeuvres in low-Earth orbits. The Schweighart and Sedwick equations (2002) are used to model the relative motion and the control methods developed are an improvment on those first developed by Leonard et al. (1986, 1989). The dynamics are decoupled in a periodic oscillation and a secular motion. First, the secular motion is controlled using differential atmospheric drag and then a oscillation reduction scheme is used. Unlike the method developed by Leonard and al., this new control scheme is not left with a residual distance at the end of the manoeuvre. Also, since the manoeuvres are based on analytical expressions, there is no longer a need for a numerical optimization routine. Numerical simulations are provided which validate the effectiveness of the control method.

1.4.3 Linear Periodically Time-Varying Systems

Calico and Wiesel (1984) worked on developing the complete algorithm capable of solving Floquet Systems. They then examine the case of scalar control and explain how this approach has limited effectiveness as it is unable to move pairs of conjugate roots. For a more rigorous method they analyse the case of vector control and come up with a new algorithm for pole placement.

An expression for the feedback gain giving pole placement was introduced by Kabamba (1986). He also demonstrated that if a periodic system is controllable over one period, then the monodromy matrix was assignable in its entirety. He therefore concluded that periodic controllers would likely be better than time invariant ones for feedback control of time-invariant systems.

Sinha and Joseph (1994) were the first to propose a method for computing the Lyapunov-Floquet transformation matrix for linear, periodically varying systems. To do so the state transition matrix is expressed as a function of time in terms of Chebyshev polynomials, which allows for the Lyapunov-Floquet transformation matrix to be expressed as a function of time in a closed form as well. This transformation matrix can then be used to transform the system to a form that is suitable for time-invariant control methods.

After noting that the method developed by Sinha and Joseph could not always ensure the stability of the system, Lee and Balas (1999) introduce a new control technique based on the output feedback algorithm with time-varying control gains. A full state-feedback controller is designed first followed by a controller with state estimator.

1.5 Outline of the Thesis

In Chapter 2, the objective is to obtain as set of linearized equations of motion for a formation placed in a circular orbit around the Earth under the effect of atmospheric drag and J_2 perturbations. To do so the linearized ordinary differential equations developed by Schweighart and Sedwick will serve as starting point. They will then be modified to include the effect of aerodynamic drag. A stability analysis will then be performed on the system to find a gain matrix that can be used to perform formation maintenance using atmospheric drag.

Simulation results building on the model developed in Chapter 2 will be presented in the next chapter. From these simulations, the effects of drag will be defined. Finally the controller developed in the Chapter 2 will be tested in order to see if it can be used to perform formation maintenance.

A major goal of this thesis being to develop a differential drag controller able of performing formation maintenance in elliptical orbits, a set of equations similar to the ones developed in Chapter 2 are needed. In Chapter 4, the small eccentricity assumption is made to find such a formulation. Two formation maintenance schemes using drag as means of control will then presented.

In chapter 5, the models developed in Chapters 4 and 5 will be compared for circular orbits. Then simulation results will be presented to see what the effects of eccentricity on a formation are. Finally the control schemes will be tested on formations placed in elliptical orbits.

Chapter 2 – Relative Motion Equations for Circular Orbits

In this chapter, we will analyse the relative motion between two spacecraft flying in formation. These spacecraft will be assumed to be placed in a circular orbit around the Earth and under the effect of J_2 and drag perturbations. The first step will be to establish the coordinate frames that will be used during the analysis. Then, the Schweighart and Sedwick equations (2002) of motion describing the relative motion of spacecraft placed in a circular orbit under the effect of the J_2 potential will be introduced. Since the equations do not account for atmospheric drag, the equations will have to be modified. They will also be non-dimensionalized to facilitate their understanding and for future computational efficiency. A stability analysis will be performed based on the equations of motion obtained. Finally, numerical simulation results will be shown to demonstrate the effect of both J_2 and atmospheric drag perturbations on formations orbiting the Earth at low altitudes, where atmospheric drag is more active, and to assess the effectiveness of differential drag as a means of control for formation maintenance.

2.1 Coordinate Frames

To describe the motion and position of the spacecraft over time, we need to establish the reference frames that will be used. In this thesis, two reference frames will be used: the Earth-Centered Inertial (ECI) and Hill frames. The two frames are shown in Fig. 2.1.

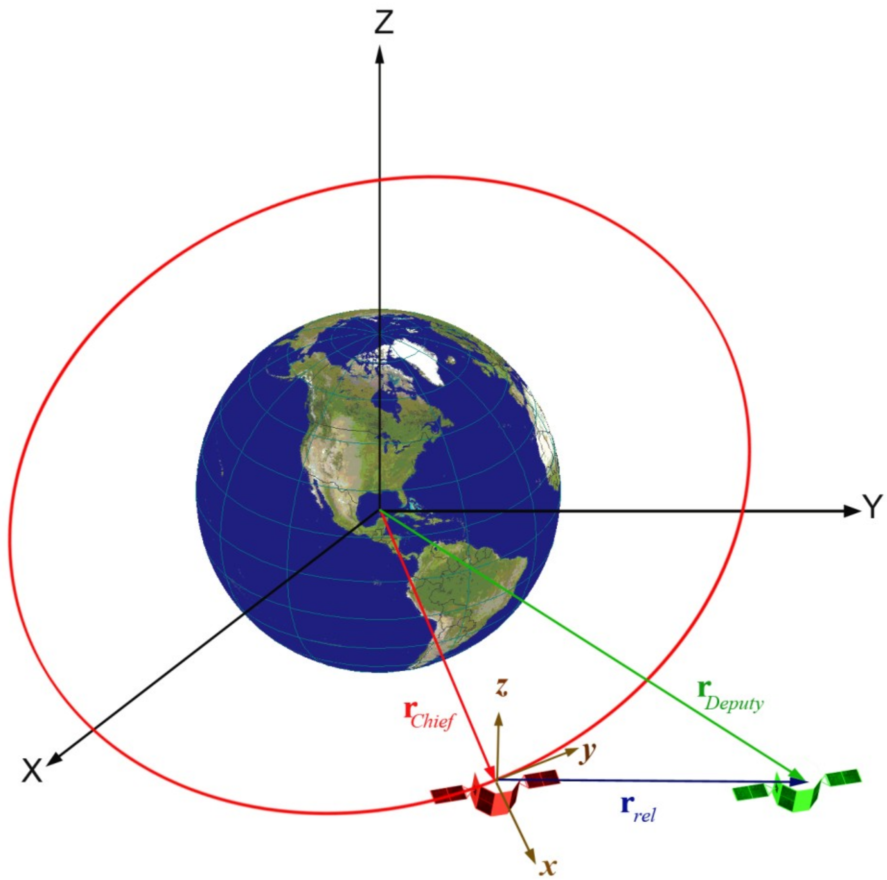

Figure 2.1: ECI and Hill Coordinate Frames

The origin of the ECI is attached the center of the Earth and is composed of the X, Y and Z axes. The Z-axis is along the Earth's axis of rotation, the X-axis points towards the vernal equinox and the Y-axis completes the right-hand rules, such that the X-Y plane intersects the Earth along its equator. This reference frame is mainly used to define the spacecraft' position over time relative to the Earth, allowing us to evaluate the local atmospheric density. For relative motion, the Hill frame is better suited. This frame is a moving one and has its origin on an imaginary spacecraft called the Chief. The x-axis points in the same direction as $\vec{r}_{Chief}$, which is the vector from the center of the Earth to the chief's position. The z-axis is perpendicular to the chief's orbit plane and the y-axis completes the right hand orthogonal system. In the case where the chief is in a circular orbit, y-

axis is along the chief's velocity vector. The x, y and z directions are commonly referred to as the radial, in-track and cross-track directions respectively.

To describe a spacecraft's state, one needs 6 independent quantities. These quantities can differ in their form though. For example, in the ECI a spacecraft's state $\boldsymbol{X}$ can be described as:

$$\boldsymbol{X} = \left[X\ Y\ Z\ \dot{X}\ \dot{Y}\ \dot{Z}\right]^T \tag{2.1}$$

A more common way of expressing the state of a spacecraft in orbit is through the classical orbital elements:

$$\boldsymbol{X} = [a\ e\ i\ \Omega\ \omega\ M]^T \tag{2.2}$$

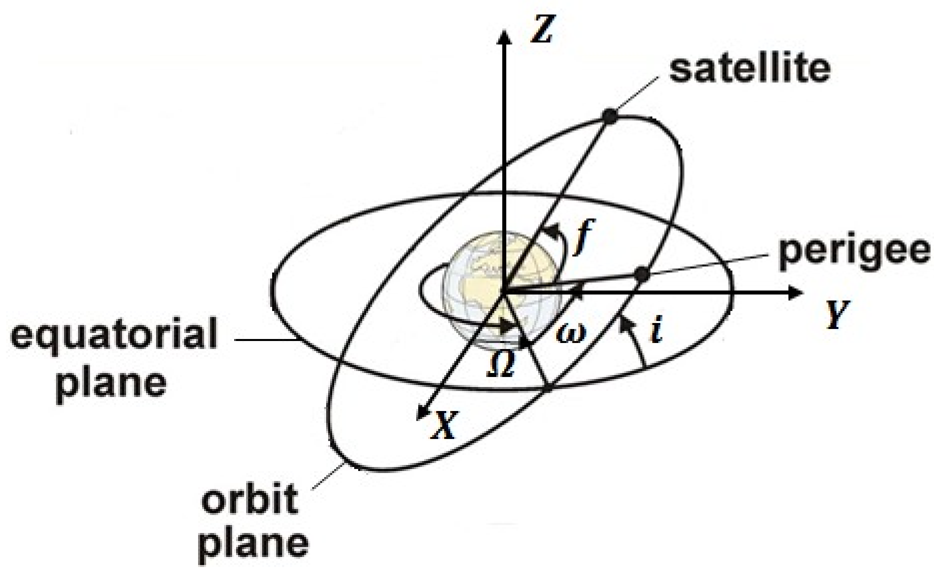

Figure 2.2: Classical Orbital Elements

In this case, a is the orbit's semi-major axis and e its eccentricity. If the orbit is circular, then a is simply the orbit's radius and e is equal to zero. The inclination i refers to then angle between the orbit plane and the Earth's equatorial plane while Ω, ω and M are the right ascension of the ascending node, the argument of perigee and the mean anomaly respectively. The mean anomaly is a function of both the eccentricity and the true anomaly f. The right ascension of ascending node is the angle between the X-axis of the ECI frame and the intersection of the orbital and equatorial plane (ascending node). The argument of the perigee is the angle between the ascending node and the perigee. Finally, the true anomaly is the angle between the perigee and the current position of the satellite. Another angle worth mentioning is the true latitude θ, which is defined as the sum of the argument of perigee and true anomaly:

$$\theta = f + \omega \tag{2.3}$$

2.2 Relative Motion Equations

The equations developed by Schweighart and Sedwick (2002) were selected as a starting point due to their simple form. They are a set of linearized, constant coefficient ordinary differential equations. They are similar in form to the Clohessy-Wiltshire equations and, like them, are only valid in the case of a circular reference orbit. The Schweighart and Sedwick equations allow to model the motion of a spacecraft relative to a J_2 perturbed reference orbit though. To obtain the relative motion between two satellites, one therefore needs to obtain the relative motion of both satellites with respect to the same reference orbit and then take the difference between the two. The equations that will be used in this chapter are:

$$\begin{gathered}\ddot{x} - 2(nc)\dot{y} - (5c^2 - 2)n^2 x = -3n^2 J_2\left(R_e^2/r_{ref}\right) \\ \times\left\{\frac{1}{2} - \left[3\sin^2 i_{ref}\sin^2(kt)/2\right] - \left[\left(1 + 3\cos 2i_{ref}\right)/8\right]\right\} + f_{Drag,x}\end{gathered} \tag{2.4}$$

$$\begin{gathered}\ddot{y} + 2(nc)\dot{x} = -3n^2 J_2\left(R_e^2/r_{ref}\right)\sin^2 i_{ref}\sin(kt)\cos(kt) \\ + f_{Drag,y}\end{gathered} \tag{2.5}$$

$$\ddot{z} + q^2 z = 2lq\cos(qt + \varphi) + f_{Drag,z} \tag{2.6}$$

where the x, y and z terms refer to the Hill frame coordinates, R_e is the Earth's mean equatorial radius, r_{ref} is the initial radius of the circular reference orbit, i_{ref} is the reference orbit's initial inclination, and J_2 is a dimensionless quantity representing the second spherical harmonic of the Earth's gravitational potential. J_2 has a constant value of 1.08263×10^{-3}. Time is denoted by t, while the orbital rate n is defined as:

$$n = \sqrt{\mu / r_{ref}^3} \tag{2.7}$$

where μ is Earth's gravitational constant and has a constant value of $3.986005 \times 10^{14}\ \mathrm{m^3/s^2}$. The other constants are specific to the Schweighart and Sedwick equations and are given in Appendix B along with other details about the equations.

The $f_{Drag,x}$, $f_{Drag,y}$ and $f_{Drag,z}$ terms represent the acceleration due to drag in x, y and z respectively. This acceleration is given by (Vallado, 2007):

$$\mathbf{f}_{Drag} = -\frac{1}{2}\frac{C_D A}{m}\rho \|\mathbf{v}_{rel}\| \mathbf{v}_{rel} \tag{2.8}$$

where C_D is the spacecraft's drag coefficient, A its cross sectional area, m its mass, ρ the local atmospheric density and $\boldsymbol{v}_{rel}$ the spacecraft velocity relative to the rotating atmosphere. The atmosphere is assumed to rotate at the same angular velocity as the Earth. The velocity of the spacecraft with respect to the rotating atmosphere is then given as (Vallado, 2007):

$$\mathbf{v}_{rel} = \mathbf{v} - \boldsymbol{\omega}_e \times \mathbf{r}_s \tag{2.9}$$

where $\mathbf{v}$ is the spacecraft's absolute velocity, $\boldsymbol{r}_s$ its position vector relative to the Earth's center and $\boldsymbol{\omega}_e$ is the angular velocity vector of the Earth. We wish to express the atmospheric drag effects in the Hill frame. To do so, we first need to express $\mathbf{v}_{rel}$ in terms of Hill coordinates. A detailed explanation of the coordinate transformations leading to the expression of $\mathbf{v}_{rel}$ in the Hill frame is provided in

Appendix A. The expression for the spacecraft's velocity relative to the rotating atmosphere is given by:

$$\mathbf{v}_{rel} = \begin{bmatrix} \dot{x} + \dot{r}_{ref} - y(nc - \omega_e \cos i) - z\omega_e \cos\theta \sin i \\ \dot{y} + \left(r_{ref} + x\right)\left(\dot{\theta} - \omega_e \cos i\right) + z\omega_e \sin\theta \sin i \\ \dot{z} + \left(r_{ref} + x\right)\omega_e \cos\theta \sin i - y\omega_e \sin\theta \sin i \end{bmatrix} \tag{2.10}$$

If we assume the reference orbit to be circular and if we use the formulation provided by Schweighart and Sedwick (2002), this expression can be simplified to:

$$\mathbf{v}_{rel} = \begin{bmatrix} \dot{x} - y(nc - \omega_e \cos i) - z\omega_e \cos\theta \sin i \\ \dot{y} + \left(r_{ref} + x\right)(nc - \omega_e \cos i) + z\omega_e \sin\theta \sin i \\ \dot{z} + \left(r_{ref} + x\right)\omega_e \cos\theta \sin i - y\omega_e \sin\theta \sin i \end{bmatrix} \tag{2.11}$$

since $\dot{r}_{ref}$ vanishes when dealing with a circular orbit and $\dot{\theta}$ can be expressed as nc, the constant orbital rate of the circular reference orbit used by Schweighart and Sedwick.

2.3 Non-Dimensionalization of the Equations of Motion

In this section, the equations of motion introduced in the previous section will be non-dimensionalized. Doing this will reduce the computing time needed later for simulations and increase the robustness of the program needed for the numerical simulations. The non-dimensionalized equations will also be simpler to handle since it will be easier to get a sense of relative importance between each term especially that of the perturbation forces.

2.3.1 Definition of Dimensionless Terms

Before we can perform the non-dimensionalization of the equations, we need to introduce the definition of the dimensionless quantities which will be used. The first step is to define a dimensionless time parameter:

$$\tau = n_0 t \tag{2.12}$$

where n_0 is the initial mean orbital rate of the reference circular orbit. The reason the initial orbital rate has to be used instead of the instantaneous orbital rate is to make sure the scaling between τ and t remains constant. Using n would not accomplish that since, due to the drag forces, n changes with time. This initial mean orbital rate is defined as:

$$n_0 = \sqrt{\mu / r_{ref,0}^3} \tag{2.13}$$

In order to transform x, y and z into dimensionless distances, they will be normalized with respect to a reference length parameter, L_{ref}:

$$\hat{x} = x / L_{ref} \tag{2.14}$$

$$\hat{y} = y / L_{ref} \tag{2.15}$$

$$\hat{z} = z / L_{ref} \tag{2.16}$$

From these definitions, we can obtain the velocities:

$$\dot{x} = \frac{dx}{dt} = \frac{d(\hat{x} L_{ref})}{d(\tau / n_0)} = n_0 L_{ref} \frac{d\hat{x}}{d\tau} = n_0 L_{ref} \hat{x}' \tag{2.17}$$

$$\dot{y} = n_0 L_{ref} \hat{y}' \tag{2.18}$$

$$\dot{z} = n_0 L_{ref} \hat{z} \tag{2.19}$$

and the accelerations:

$$\ddot{x} = \frac{d^2x}{dt^2} = \frac{d^2(\hat{x}L_{ref})}{d(\tau/n_0)^2} = {n_0}^2 L_{ref} \frac{d^2\hat{x}}{d\tau^2} = {n_0}^2 L_{ref} \hat{x}'' \tag{2.20}$$

$$\ddot{y} = {n_0}^2 L_{ref} \hat{y}'' \tag{2.21}$$

$$\ddot{z} = {n_0}^2 L_{ref} \hat{z}'' \tag{2.22}$$

It is convenient to set $L_{ref} = d$, where d is a value associated with the geometry of the desired formation motion geometry such as the desired radius of a projected circular formation or the desired distance between the spacecraft in an in-track (also known as along track), leader-follower formation. By doing so, we will ensure that $\hat{x}$, $\hat{y}$ and $\hat{z}$ remain of the order of 1.

2.3.2 Non-Dimensionalized Equations of Motion

With the dimensionless terms defined in the previous section, we can now present the non-dimensionalized equations of motion. To do so, the equations of motion, Eqs. (2.4), (2.5) and (2.6), are modified to become functions of the dimensionless parameters $\hat{x}$, $\hat{y}$ and $\hat{z}$:

$$\begin{aligned} &{n_0}^2 d\hat{x}'' - 2(nc)n_0 d\hat{y}' - (5c^2 - 2)n^2 d\hat{x} = -3n^2 J_2\left(R_e^2/r_{ref}\right) \\ &\times \left\{\tfrac{1}{2} - \tfrac{3}{2}\sin^2 i_{ref} \sin^2(k\tau/n_0) - \tfrac{1}{8}\left(1 + 3\cos 2i_{ref}\right)\right\} + f_{Drag,x} \end{aligned} \tag{2.23}$$

$$\begin{aligned} &{n_0}^2 d\hat{y}'' + 2(nc)n_0 d\hat{x}' = \\ &\quad -3n^2 J_2\left(R_e^2/r_{ref}\right)\sin^2 i_{ref} \sin(k\tau/n_0)\cos(k\tau/n_0) + f_{Drag,y} \end{aligned} \tag{2.24}$$

$${n_0}^2 d\hat{z}'' + q^2 d\hat{z} = 2lq\cos(q\tau/n_0 + \varphi) + f_{Drag,z} \tag{2.25}$$

Dividing these equations by ${n_0}^2 d$, we obtain:

$$\hat{x}'' - 2\hat{n}c\hat{y}' - (5c^2 - 2)\hat{n}^2\hat{x} = -3\hat{n}^2 J_2\left(R_e^2/r_{ref}d\right) \tag{2.26}$$

$$\times\left\{\frac{1}{2}-\frac{3}{2}\sin^2 i_{ref}\sin^2\left(\hat{k}\tau\right)-\frac{1}{8}\left(1+3\cos 2i_{ref}\right)\right\}+\hat{f}_{Drag,x}$$

$$\hat{y}''+2\hat{n}c\hat{x}'=-3\hat{n}^2J_2\left(R_e^2/r_{ref}d\right)\sin^2 i_{ref}\sin(\hat{k}\tau)\cos(\hat{k}\tau)+\hat{f}_{Drag,y} \tag{2.27}$$

$$\hat{z}''+\hat{q}^2\hat{z}=2\frac{l}{n_0 d}\hat{q}\cos(\hat{q}\tau+\varphi)+\hat{f}_{Drag,z} \tag{2.28}$$

where

$$\hat{n}=n/n_0 \tag{2.29}$$

$$\hat{k}=k/n_0 \tag{2.30}$$

$$\hat{q}=q/n_0 \tag{2.31}$$

$$\hat{\mathbf{f}}_{Drag}=\mathbf{f}_{Drag}/(n_0^2 d) \tag{2.32}$$

Here, it can be noted that $\hat{\mathbf{f}}_{Drag}$ is the dimensionless drag acceleration.

2.4 Dimensionless Drag Terms

2.4.1 Basic Expression for the Dimensionless Drag

In this section, the dimensionless drag expression will be derived. The starting point of our analysis is to substitute Eq. (2.8) into Eq. (2.32) to obtain an expression for the dimensionless drag:

$$\hat{\mathbf{f}}_{Drag}=\frac{\mathbf{f}_{Drag}}{n_0^2 d}=-\frac{1}{2}\frac{1}{n_0^2 d}\rho\frac{C_D A}{m}\|\mathbf{v}_{rel}\|\mathbf{v}_{rel}=-\frac{1}{2}\rho\frac{C_D A}{m}d\|\hat{\mathbf{v}}_{rel}\|\hat{\mathbf{v}}_{rel} \tag{2.33}$$

where $\hat{\boldsymbol{v}}_{rel}$ is the spacecraft's dimensionless velocity relative to the rotating atmosphere and is obtained by dividing Eq. (2.11) by $n_0 d$:

$$\hat{\mathbf{v}}_{rel} = \frac{\mathbf{v}_{rel}}{n_0 d} = \frac{1}{n_0 d}\begin{bmatrix} \dot{x} - y(nc - \omega_e \cos i) - z\omega_e \cos\theta \sin i \\ \dot{y} + \left(r_{ref} + x\right)(nc - \omega_e \cos i) + z\omega_e \sin\theta \sin i \\ \dot{z} + \left(r_{ref} + x\right)\omega_e \cos\theta \sin i - y\omega_e \sin\theta \sin i \end{bmatrix} \quad (2.34)$$

This dimensionless velocity for a circular orbit for can be rewritten as a function of $\hat{x}$, $\hat{y}$ and $\hat{z}$:

$$\hat{\mathbf{v}}_{rel} = \begin{bmatrix} \hat{x}' - \hat{y}(\hat{n}c - \widehat{\omega}_e \cos i) - \hat{z}\widehat{\omega}_e \cos\theta \sin i \\ \hat{y}' + \left(\frac{r_{ref}}{d} + \hat{x}\right)(\hat{n}c - \omega_e \cos i) + \hat{z}\widehat{\omega}_e \sin\theta \sin i \\ \hat{z}' + \left(\frac{r_{ref}}{d} + \hat{x}\right)\widehat{\omega}_e \cos\theta \sin i - \hat{y}\widehat{\omega}_e \sin\theta \sin i \end{bmatrix} \quad (2.35)$$

where

$$\widehat{\omega}_e = \omega_e / n_0 \quad (2.36)$$

2.4.2 Linearization of the Dimensionless Drag Expression

Now that the dimensionless drag term has been defined, we can begin simplifying and linearizing the expression. Let us first define a new quantity, the dimensionless ballistic drag coefficient:

$$\beta = \left(\rho \frac{C_D A}{m} r_{ref}\right)^{-1} \quad (2.37)$$

such that Eq. (2.33) can now be rewritten as:

$$\hat{\mathbf{f}}_{Drag} = -\frac{1}{2}\frac{1}{\beta}\frac{d}{r_{ref}}\|\hat{\mathbf{v}}_{rel}\|\hat{\mathbf{v}}_{rel} \quad (2.38)$$

Note that the ballistic coefficient is usually defined as:

$$B = \left(\frac{C_D A}{m}\right)^{-1} \tag{2.39}$$

To simplify the linearization process, the dimensionless relative velocity vector $\hat{\boldsymbol{v}}_{rel}$ will be split into two vectors: one of which will hold the zeroeth terms while the other will contain the first order terms in $\hat{x}$, $\hat{y}$, $\hat{z}$, $\hat{x}'$, $\hat{y}'$ and $\hat{z}'$. Thus, the spacecraft's dimensionless velocity relative to the rotating atmosphere is expressed as:

$$\hat{\mathbf{v}}_{rel} = \mathbf{v}_0 + \mathbf{v}_1 \tag{2.40}$$

where

$$\mathbf{v}_0 = \begin{bmatrix} 0 \\ \frac{r_{ref}}{d}(\hat{n}c - \widehat{\omega}_e \cos i) \\ \frac{r_{ref}}{d}\widehat{\omega}_e \cos\theta \sin i \end{bmatrix} \tag{2.41}$$

$$\mathbf{v}_1 = \begin{bmatrix} \hat{x}' - \hat{y}(\hat{n}c - \widehat{\omega}_e \cos i) - \hat{z}\widehat{\omega}_e \cos\theta \sin i \\ \hat{y}' + \hat{x}(\hat{n}c - \widehat{\omega}_e \cos i) + \hat{z}\widehat{\omega}_e \sin\theta \sin i \\ \hat{z}' + \hat{x}\widehat{\omega}_e \cos\theta \sin i - \hat{y}\widehat{\omega}_e \sin\theta \sin i \end{bmatrix} \tag{2.42}$$

It is important to note that the magnitude of $\mathbf{v}_1$ is of the order of 1 while the magnitude of $\mathbf{v}_0$ is of the order of 10^4 and, thus, significantly larger. To linearize the dimensionless drag expression, the $\|\hat{\mathbf{v}}_{rel}\|\hat{\mathbf{v}}_{rel}$ must be linearized. With the definition given previously, this term can be written as:

$$\|\hat{\mathbf{v}}_{rel}\|\hat{\mathbf{v}}_{rel} = \|\mathbf{v}_0 + \mathbf{v}_1\|(\mathbf{v}_0 + \mathbf{v}_1) \tag{2.43}$$

Note that, using the vector norm definition, the $\|\mathbf{v}_0 + \mathbf{v}_1\|$ term can be seen as:

$$\begin{gathered} \|\mathbf{v}_0 + \mathbf{v}_1\| = [(\mathbf{v}_0 + \mathbf{v}_1).(\mathbf{v}_0 + \mathbf{v}_1)]^{1/2} \\ \|\mathbf{v}_0 + \mathbf{v}_1\| = [\|\mathbf{v}_0\|^2 + 2\mathbf{v}_0.\mathbf{v}_1 + \|\mathbf{v}_1\|^2]^{1/2} \end{gathered} \tag{2.44}$$

Thus:

$$\|\mathbf{v}_0 + \mathbf{v}_1\|(\mathbf{v}_0 + \mathbf{v}_1) = [\|\mathbf{v}_0\|^2 + 2\mathbf{v}_0.\mathbf{v}_1 + \|\mathbf{v}_1\|^2]^{1/2}(\mathbf{v}_0 + \mathbf{v}_1) \tag{2.45}$$

The square root term can be linearized if a binomial series expansion is used. To do so, a slight modification must be brought to Eq. (2.43):

$$\|\mathbf{v}_0 + \mathbf{v}_1\|(\mathbf{v}_0 + \mathbf{v}_1) = \|\mathbf{v}_0\|\left[1 + \frac{2\mathbf{v}_0.\mathbf{v}_1}{\|\mathbf{v}_0\|^2} + \frac{\|\mathbf{v}_1\|^2}{\|\mathbf{v}_0\|^2}\right]^{1/2}(\mathbf{v}_0 + \mathbf{v}_1) \tag{2.46}$$

Now, taking the binomial series expansion of the square root and neglecting terms of second or higher orders, we obtain:

$$\begin{gathered}\|\mathbf{v}_0 + \mathbf{v}_1\|(\mathbf{v}_0 + \mathbf{v}_1) \approx \|\mathbf{v}_0\|\left(1 + \frac{\mathbf{v}_0.\mathbf{v}_1}{\|\mathbf{v}_0\|^2}\right)(\mathbf{v}_0 + \mathbf{v}_1) \\ \|\mathbf{v}_0 + \mathbf{v}_1\|(\mathbf{v}_0 + \mathbf{v}_1) \approx \|\mathbf{v}_0\|\mathbf{v}_0 + \|\mathbf{v}_0\|\mathbf{v}_1 + \left(\frac{\mathbf{v}_0.\mathbf{v}_1}{\|\mathbf{v}_0\|}\right)\mathbf{v}_0\end{gathered} \tag{2.47}$$

The reason higher order terms can be neglected comes from the difference in magnitude between $\mathbf{v}_0$ and $\mathbf{v}_1$. While $\mathbf{v}_0$ represents the absolute velocity of the imaginary chief placed on the reference orbit, $\mathbf{v}_1$ represents the relative velocity of the deputy spacecraft relative to that imaginary chief. Since the orbit of the deputy follows that of the imaginary chief, the relative velocity between the two is significantly smaller in magnitude than the absolute velocity $\boldsymbol{v}_0$.

Let us now evaluate each term of Eq. (2.47) individually:

$$\begin{gathered}\|\mathbf{v}_0\| = \frac{r_{ref}}{d}\sqrt{(\hat{n}c - \widehat{\omega}_e \cos i)^2 + (\widehat{\omega}_e \cos\theta \sin i)^2} \\ \|\mathbf{v}_0\| \approx \frac{r_{ref}}{d}(\hat{n}c - \widehat{\omega}_e \cos i) = v_{0,y}\end{gathered} \tag{2.48}$$

The reason, the second term is neglected is because while the first term will be of order one, the second one will be at least of 2 orders less. Therefore, higher order terms in $\widehat{\omega}_e$ can always be neglected when compared with terms of the order of one. Then we can obtain the three terms as:

$$\|\mathbf{v}_0\|\mathbf{v}_0 \approx v_{0,y}\begin{bmatrix} 0 \\ v_{0,y} \\ v_{0,z} \end{bmatrix} \tag{2.49}$$

$$\|\mathbf{v}_0\|\mathbf{v}_1 \approx v_{0,y}\begin{bmatrix} v_{1,x} \\ v_{1,y} \\ v_{1,z} \end{bmatrix} \tag{2.50}$$

$$\left(\frac{\mathbf{v}_0 . \mathbf{v}_1}{\|\mathbf{v}_0\|}\right)\mathbf{v}_0 \approx \frac{1}{v_{0,y}}\begin{bmatrix} 0 \\ v_{0,y}\left(v_{0,y}v_{1,y} + v_{0,z}v_{1,z}\right) \\ v_{0,z}\left(v_{0,y}v_{1,y} + v_{0,z}v_{1,z}\right) \end{bmatrix} \tag{2.51}$$

Summing all three terms we get the linearized expression for $\|\hat{\mathbf{v}}_{rel}\|\hat{\mathbf{v}}_{rel}$:

$$\|\hat{\mathbf{v}}_{rel}\|\hat{\mathbf{v}}_{rel} \approx \begin{bmatrix} v_{0,y}v_{1,x} \\ v_{0,y}^2 + 2v_{0,y}v_{1,y} + v_{0,z}v_{1,z} \\ v_{0,y}v_{0,z} + v_{0,y}v_{1,z} + v_{0,z}v_{1,y} + \dfrac{v_{0,z}^2}{v_{0,y}}v_{1,z} \end{bmatrix} \tag{2.52}$$

Neglecting the higher order terms and factoring out $v_{0,y}$, we obtain:

$$\|\hat{\mathbf{v}}_{rel}\|\hat{\mathbf{v}}_{rel} \approx v_{0,y}\begin{bmatrix} v_{1,x} \\ v_{0,y} + 2v_{1,y} \\ v_{0,z} + v_{1,z} \end{bmatrix} \tag{2.53}$$

The linearized drag expression can then be written as:

$$\hat{\mathbf{f}}_{Drag} \approx -\frac{1}{2}\frac{1}{\beta}\frac{d}{r_{ref}}v_{0,y}\begin{bmatrix} v_{1,x} \\ v_{0,y} + 2v_{1,y} \\ v_{0,z} + v_{1,z} \end{bmatrix} \tag{2.54}$$

The following dimensionless parameters will be introduced to further simplify the notation:

$$\hat{\sigma} = \hat{n}c - \widehat{\omega}_e \cos i \tag{2.55}$$

$$\hat{\varsigma} = \widehat{\omega}_e \sin i \tag{2.56}$$

The final linearized drag expression is therefore:

$$\hat{\mathbf{f}}_{Drag} \approx -\frac{1}{2}\frac{1}{\beta}\hat{\sigma}\begin{bmatrix} \hat{x}' - \hat{y}\hat{\sigma} - \hat{z}\dot{\hat{\varsigma}}\cos\theta \\ \frac{r_{ref}}{d}\hat{\sigma} + 2(\hat{y}' + \hat{x}\hat{\sigma} + \hat{z}\hat{\varsigma}\sin\theta) \\ \frac{r_{ref}}{d}\hat{\varsigma}\cos\theta + \hat{z}' + \hat{x}\hat{\varsigma}\cos\theta - \hat{y}\hat{\varsigma}\sin\theta \end{bmatrix} \tag{2.57}$$

2.5 Final Equations of Motion

In this section, the final equations of motion describing the relative motion between the deputy and chief spacecraft will be presented. To get those equations, the linearized drag expression obtained in the previous section will be introduced in the Sedwick and Schwieghart equations.

As it stands, the linearized drag expression, Eq. (2.57), and Eqs (2.26), (2.27) and (2.28) are for a spacecraft with respect to an unperturbed reference orbit. To obtain the relative motion between both spacecraft the equations must evaluated for both spacecraft and then subtracted from one another. Doing so, we obtain:

$$\begin{aligned} \Delta\hat{x}'' - 2\hat{n}c\Delta\hat{y}' - (5c^2 - 2)\hat{n}^2\Delta\hat{x} &= -3\hat{n}^2 J_2\left(R_e^2/r_{ref}d\right) \\ &\times\left\{\tfrac{1}{2} - \tfrac{3}{2}\sin^2 i_{ref}\sin^2\left(\hat{k}\tau\right) - \tfrac{1}{8}\left(1 + 3\cos 2i_{ref}\right)\right\} + \\ &\Delta\hat{f}_{Drag,x} \end{aligned} \tag{2.58}$$

$$\begin{aligned} \Delta\hat{y}'' + 2\hat{n}c\Delta\hat{x}' &= -3\hat{n}^2 J_2\left(R_e^2/r_{ref}d\right)\sin^2 i_{ref}\sin\left(\hat{k}\tau\right)\cos\left(\hat{k}\tau\right) \\ &+\Delta\hat{f}_{Drag,y} \end{aligned} \tag{2.59}$$

$$\Delta\hat{z}'' + \hat{q}^2\Delta\hat{z} = 2\frac{l}{n_0 d}\hat{q}\cos(\hat{q}\tau + \varphi) + \Delta\hat{f}_{Drag,z} \tag{2.60}$$

where $\Delta\hat{x} = \hat{x}_D - \hat{x}_C$, $\Delta\hat{y} = \hat{y}_D - \hat{y}_C$ and $\Delta\hat{z} = \hat{z}_D - \hat{z}_C$ give the position of the deputy relative to the chief. The relative drag term is then:

$$\Delta\hat{\mathbf{f}}_{Drag} \approx -\frac{1}{2}\frac{d}{r_{ref}}v_{0,y}\left\{\left(\frac{1}{\beta}\begin{bmatrix} v_{1,x} \\ v_{0,y}+2v_{1,y} \\ v_{0,z}+v_{1,z}\end{bmatrix}\right)_D - \left(\frac{1}{\beta}\begin{bmatrix} v_{1,x} \\ v_{0,y}+2v_{1,y} \\ v_{0,z}+v_{1,z}\end{bmatrix}\right)_C\right\} \quad (2.61)$$

where the subscripts C and D denote the chief and deputy respectively.

To simplify our analysis, we will assume both spacecraft have the same projected area and local atmospheric density. This second assumption is made because although they differ, they only do so very slightly when both spacecraft are relatively close such as is the case here. We can now state both spacecraft's dimensionless ballistic coefficients to be identical. The relative drag can then be simplified to:

$$\Delta\hat{\mathbf{f}}_{Drag} \approx -\frac{1}{2}\frac{1}{\beta}\frac{d}{r_{ref}}v_{0,y}\begin{bmatrix}\Delta v_{1,x} \\ 2\Delta v_{1,y} \\ \Delta v_{1,z}\end{bmatrix} \quad (2.62)$$

where

$$\Delta v_{1,x} = \Delta\hat{x}' - \Delta\hat{y}(\hat{n}c - \hat{\omega}_e\cos\imath) - \Delta\hat{z}\hat{\omega}_e\cos\theta\sin\imath \quad (2.63)$$

$$\Delta v_{1,y} = \Delta\hat{y}' + \Delta\hat{x}(\hat{n}c - \omega_e\cos i) + \Delta\hat{z}\hat{\omega}_e\sin\theta\sin i \quad (2.64)$$

$$\Delta v_{1,z} = \Delta\hat{z}' + \Delta\hat{x}\hat{\omega}_e\cos\theta\sin i - \Delta\hat{y}\hat{\omega}_e\sin\theta\sin i \quad (2.65)$$

Note, that this second assumption will not be made when performing the simulations. It only serves to simplify the stability analysis that will follow. Writing Eqs. (2.58), 2.59 and (2.60) with the relative drag defined in Eq. (2.62) in matrix form, we obtain:

$$\mathbf{M}\Delta\hat{\mathbf{x}}'' + \mathbf{C}\Delta\hat{\mathbf{x}}' + \mathbf{K}\Delta\hat{\mathbf{x}} = \mathbf{f} \quad (2.66)$$

where the relative position vector $\Delta\hat{\mathbf{x}}$, the generalized inertia matrix $\mathbf{M}$, the damping matrix $\mathbf{C}$, the stiffness matrix $\mathbf{K}$ and the forcing function vector $\mathbf{f}$ are:

$$\Delta\hat{\mathbf{x}} = \begin{bmatrix}\Delta\hat{x} \\ \Delta\hat{y} \\ \Delta\hat{z}\end{bmatrix} \quad (2.67)$$

$$\mathbf{M} = \mathbf{I} = \begin{bmatrix} 1 & 0 & 0 \\ 0 & 1 & 0 \\ 0 & 0 & 1 \end{bmatrix} \tag{2.68}$$

$$\mathbf{C} = \begin{bmatrix} \frac{1}{2}\frac{1}{\beta}\hat{\sigma} & -2\hat{n}c & 0 \\ 2\hat{n}c & \frac{1}{\beta}\hat{\sigma} & 0 \\ 0 & 0 & \frac{1}{2}\frac{1}{\beta}\hat{\sigma} \end{bmatrix} \tag{2.69}$$

$$\mathbf{K} = \begin{bmatrix} -(5c^2 - 2)\hat{n}^2 & -\frac{1}{2}\frac{1}{\beta}\hat{\sigma}^2 & -\frac{1}{2}\frac{1}{\beta}\hat{\sigma}\hat{\varsigma}\cos\theta \\ \frac{1}{\beta}\hat{\sigma}^2 & 0 & \frac{1}{\beta}\hat{\sigma}\hat{\varsigma}\sin\theta \\ \frac{1}{2}\frac{1}{\beta}\hat{\sigma}\hat{\varsigma}\cos\theta & -\frac{1}{2}\frac{1}{\beta}\hat{\sigma}\hat{\varsigma}\sin\theta & \hat{q}^2 \end{bmatrix} \tag{2.70}$$

$$\mathbf{f} = \begin{bmatrix} 0 \\ 0 \\ 2\frac{l}{n_0 d}\hat{q}\cos(\hat{q}\tau + \varphi) \end{bmatrix} \tag{2.71}$$

The system can also be written in state-space form as:

$$\Delta\mathbf{X}' = \mathbf{A}\Delta\mathbf{X} + \mathbf{W} \tag{2.72}$$

where

$$\Delta\mathbf{X} = \begin{bmatrix} \Delta\hat{\mathbf{x}} \\ \Delta\hat{\mathbf{x}}' \end{bmatrix} \tag{2.73}$$

$$\mathbf{A} = \begin{bmatrix} \mathbf{0}_{3\times3} & \mathbf{M} \\ -\mathbf{K} & -\mathbf{C} \end{bmatrix} \tag{2.74}$$

$$\mathbf{W} = \begin{bmatrix} \mathbf{0}_{3\times1} \\ \mathbf{f} \end{bmatrix} \tag{2.75}$$

2.6 Stability Analysis

To assess the feasibility of using atmospheric as a means of formation maintenance, a stability analysis needs to be undertaken. To do so, the liner model developed in the previous sections will be used. In this analysis, it will be assumed that both spacecraft can increase their projected area to increase the drag they experience.

2.6.1 Differential Drag Analysis

In this analysis, both spacecraft are assumed to have the same physical parameters. That is to say that both spacecraft have identical mass m, drag coefficient C_D and baseline area A_0. It will also be assumed that both spacecraft are close enough such that their local atmospheric density ρ can, in turn, be assumed to be the same.

While both the chief and deputy have the same baseline area A_0, their total projected area can be increased by an amount δA by rotating some differential drag panels attached to each spacecraft. Their drag area can therefore be defined as:

$$A_C \equiv A_0 + \delta A_C \tag{2.76}$$

$$A_D \equiv A_0 + \delta A_D \tag{2.77}$$

Based on this, Eq. (2.61) can be modified to:

$$\Delta\hat{\mathbf{f}}_{Drag} \approx -\frac{1}{2}\frac{d}{r_{ref}} v_{0,y}\left(\rho\frac{C_D}{m} r_{ref}\right) \times$$
$$\left\{ A_0 \begin{bmatrix} \Delta v_{1,x} \\ 2\Delta v_{1,y} \\ \Delta v_{1,z} \end{bmatrix} + \delta A_D \begin{bmatrix} v_{1,x} \\ v_{0,y} + 2v_{1,y} \\ v_{0,z} + v_{1,z} \end{bmatrix}_D - \delta A_C \begin{bmatrix} v_{1,x} \\ v_{0,y} + 2v_{1,y} \\ v_{0,z} + v_{1,z} \end{bmatrix}_C \right\} \tag{2.78}$$

For control purposes, we want δA to be related to the dimensionless state vector. The change in area will therefore be defined as the product of a gain matrix with the state vector:

$$\delta A = \mathbf{G}\begin{bmatrix} \hat{\mathbf{x}} \\ \hat{\mathbf{x}}' \end{bmatrix} \tag{2.79}$$

where $\mathbf{G}$ is a row vector defined as:

$$\mathbf{G} = [g_1 \quad g_2 \quad g_3 \quad g_4 \quad g_5 \quad g_6] \tag{2.80}$$

Now that δA has been defined, it can be introduced into equation 2.78 and the resulting expression can be linearized. The resulting expression is:

$$\Delta\hat{\mathbf{f}}_{Drag} \approx -\frac{1}{2}\frac{d}{r_{ref}} v_{0,y}\left(\rho\frac{C_D}{m} r_{ref}\right)$$
$$\times \left\{ A_0 \begin{bmatrix} \Delta v_{1,x} \\ 2\Delta v_{1,y} \\ \Delta v_{1,z} \end{bmatrix} + \left(\mathbf{G}_D \begin{bmatrix} \hat{\mathbf{x}}_D \\ \hat{\mathbf{x}}_D{}' \end{bmatrix} - \mathbf{G}_C \begin{bmatrix} \hat{\mathbf{x}}_C \\ \hat{\mathbf{x}}_C{}' \end{bmatrix} \right) \begin{bmatrix} 0 \\ v_{0,y} \\ v_{0,z} \end{bmatrix} \right\} \tag{2.81}$$

The differential drag expression can be further simplified if the gain matrix is assumed to be the same for both spacecraft. In fact, the expression can then be written in terms of the relative position vector:

$$\Delta\hat{\mathbf{f}}_{Drag} \approx - -\frac{1}{2}\frac{d}{r_{ref}} v_{0,y} \frac{1}{\beta_0} \left\{ \begin{bmatrix} \Delta v_{1,x} \\ 2\Delta v_{1,y} \\ \Delta v_{1,z} \end{bmatrix} + \frac{1}{A_0} \left(\mathbf{G} \begin{bmatrix} \Delta\hat{\mathbf{x}} \\ \Delta\hat{\mathbf{x}}' \end{bmatrix} \right) \begin{bmatrix} 0 \\ v_{0,y} \\ v_{0,z} \end{bmatrix} \right\} \tag{2.82}$$

where β_0 is the dimensionless ballistic coefficient taken with an the baseline area A_0.

2.6.2 Eigenvalue Analysis

In this section an eigenvalue analysis for the case of marginal stability will be performed on the controlled system defined in the previous section. Using this analysis, the elements of the gain matrix needed to stabilize the system will be determined.

Once the control gains are included in the equations of motion, new terms, related to those gains, will be included in the matrices **C** and **K**. The new matrices are:

$$\mathbf{C} = \begin{bmatrix} \frac{1}{2}\frac{1}{\beta_0}\hat{\sigma} & -2\hat{n}c & 0 \\ 2\hat{n}c + g_4\kappa_y & \frac{1}{\beta_0}\hat{\sigma} + g_5\kappa_y & g_6\kappa_y \\ g_4\kappa_z & g_5\kappa_z & \frac{1}{2}\frac{1}{\beta_0}\hat{\sigma} + g_6\kappa_z \end{bmatrix} \tag{2.83}$$

$$\mathbf{K} = \begin{bmatrix} -(5c^2-2)\hat{n}^2 & -\frac{1}{2}\frac{1}{\beta}\hat{\sigma}^2 & -\frac{1}{2}\frac{1}{\beta_0}\hat{\sigma}\hat{\varsigma}\cos\theta \\ \frac{1}{\beta_0}\hat{\sigma}^2 + g_1\kappa_y & g_2\kappa_y & \frac{1}{\beta_0}\hat{\sigma}\hat{\varsigma}\sin\theta + g_3\kappa_y \\ \frac{1}{2}\frac{1}{\beta_0}\hat{\sigma}\hat{\varsigma}\cos\theta + g_1\kappa_z & -\frac{1}{2}\frac{1}{\beta_0}\hat{\sigma}\hat{\varsigma}\sin\theta + g_2\kappa_z & \hat{q}^2 + g_3\kappa_z \end{bmatrix} \tag{2.84}$$

where

$$\kappa_y = \frac{1}{2}\frac{1}{\beta_0}\frac{1}{A_0}\frac{r_{ref}}{d}\hat{\sigma}^2 \tag{2.85}$$

$$\kappa_z = \frac{1}{2}\frac{1}{\beta_0}\frac{1}{A_0}\frac{r_{ref}}{d}\hat{\sigma}\hat{\varsigma}\cos\theta \tag{2.86}$$

For this analysis, we will only consider the in-plane (x-y) portion of the system. That is because the terms coupling the out-of-plane (z) equation with the in-plane equations are significantly smaller than the other terms of the matrices and can thus be neglected. This means that we will not be able to have control over the relative motion in the z-direction. The components g_3 and g_6 can therefore be set to zero as they are related to the out-of-plane motion. For the in-plane case, the matrices $\mathbf{C}$ and $\mathbf{K}$ are reduced to the 2×2 matrices:

$$\mathbf{C} = \begin{bmatrix} \frac{1}{2}\frac{1}{\beta_0}\hat{\sigma} & -2\hat{n}c \\ 2\hat{n}c + g_4\kappa_y & \frac{1}{\beta_0}\hat{\sigma} + g_5\kappa_y \end{bmatrix} \tag{2.87}$$

$$\mathbf{K} = \begin{bmatrix} -(5c^2-2)\hat{n}^2 & -\frac{1}{2}\frac{1}{\beta_0}\hat{\sigma}^2 \\ \frac{1}{\beta_0}\hat{\sigma}^2 + g_1\kappa_y & g_2\kappa_y \end{bmatrix} \tag{2.88}$$

and $\mathbf{M}$ becomes the 2×2 Identity matrix.

To determine the stability of the in-plane system, we can analyse its eigenvalues. Those eigenvalues can be obtained as the roots of the characteristic equation:

$$\left\| \begin{bmatrix} 1 & 0 \\ 0 & 1 \end{bmatrix} \lambda^2 + \begin{bmatrix} A & B \\ C & D \end{bmatrix} \lambda + \begin{bmatrix} E & F \\ G & H \end{bmatrix} \right\| = 0 \tag{2.89}$$

$$\begin{vmatrix} \lambda^2 + A\lambda + E & B\lambda + F \\ C\lambda + G & \lambda^2 + D\lambda + H \end{vmatrix} = 0 \tag{2.90}$$

$$\begin{aligned} &\lambda^4 + (A+D)\lambda^3 + (H + AD + E - BC)\lambda^2 \\ &\quad + (AH + ED - BG - CF)\lambda + (HE - FG) = 0 \end{aligned} \tag{2.91}$$

where A, B, C, D, E, F, G and H are used to replace the components of the $\mathbf{C}$ and $\mathbf{K}$ matrices for simplicity.

To obtain asymptotic stability, the roots of the characteristic equation must all have negative real parts. Finding such roots analytically is very complicated in this case. However, marginal stability can be obtained if the first and third order terms of the characteristic polynomial are set to zero. This will transform the equation into a quadratic equation in λ^2.

Setting the third order term to zero yields:

$$A + D = 0 \tag{2.92}$$

$$\frac{1}{2}\frac{1}{\beta_0}\hat{\sigma} + \frac{1}{\beta_0}\hat{\sigma} + g_5\kappa_y = 0 \tag{2.93}$$

$$g_5 = \frac{-3}{2\beta_0\kappa_y}\hat{\sigma} = -3A_0\frac{d}{\hat{\sigma}r_{ref}} \tag{2.94}$$

Now, setting the first order term to zero yields:

$$AH + ED - BG - CF = 0 \tag{2.95}$$

$$\begin{gathered}\frac{1}{2}\frac{1}{\beta_0}\hat{\sigma}g_2\kappa_y - (5c^2-2)\hat{n}^2\left(\frac{1}{\beta_0}\hat{\sigma} + g_5\kappa_y\right) \\ +2\hat{n}c\left(\frac{1}{\beta_0}\hat{\sigma}^2 + g_1\kappa_y\right) + \frac{1}{2}\frac{1}{\beta_0}\hat{\sigma}^2\left(2\hat{n}c + g_4\kappa_y\right) = 0\end{gathered} \tag{2.96}$$

which simplifies to:

$$\hat{\sigma}g_2\kappa_y + 4\hat{n}cg_1\kappa_y\beta_0 + \hat{\sigma}^2g_4\kappa_y = -\hat{\sigma}(5c^2-2)\hat{n}^2 - 6\hat{n}c\hat{\sigma}^2 \tag{2.97}$$

Since the first and third order terms have been set to zero, the characteristic equation now is:

$$\lambda^4 + (H + AD + E - BC)\lambda^2 + (HE - FG) = 0 \tag{2.98}$$

and the following roots:

$$\lambda_{1,2} = \pm\frac{j}{2}\sqrt{(H + AD + E - BC) + \sqrt{(H + AD + E - BC)^2 - 4(HE - FG)}} \tag{2.99}$$

$$\lambda_{3,4} = \pm\frac{j}{2}\sqrt{(H + AD + E - BC) - \sqrt{(H + AD + E - BC)^2 - 4(HE - FG)}} \tag{2.100}$$

where $j = \sqrt{-1}$. To obtain marginal stability, the roots must be purely imaginary. For that to be the case, the following conditions must be met:

i) $H + AD + E - BC > 0$

ii) $0 < 4(HE - FG) < (H + AD + E - BC)^2$

It is difficult to deal with such inequalities. Thus, we will rewrite those condition as equalities. Condition i can written as:

$$H + AD + E - BC = \xi \tag{2.101}$$

with $\xi > 0$. Condition ii can be rewritten as well:

$$HE - FG = \frac{1}{4\alpha}(H + AD + E - BC)^2 \tag{2.102}$$

with $\alpha > 1$. Note, that Eq. (2.10)2 will satisfy both sides of condition (ii) since its right hand side will always be positive and larger than zero. The remaining three components of the gain matrix, g_1, g_2 and g_4, can be obtained from Eqs. (2.97), (2.101) and (2.102). The expression for each of those gains is not provided here due to their high complexity.

Chapter 3 – Numerical Simulation for Circular Reference Orbits

In this section, numerical simulations will be provided based on the equations developed in chapter 2. The non-dimensionalized equations of motion were used for robustness and computational efficiency. The numerical simulations shown in this chapter were done using MATLAB and the differential equations were solved using its ode45 numerical integration function. The ode45 function is based on the Dormand-Price method, which is a mixed 4th and 5th order Runge-Kutta adaptive step method. To obtain the local atmospheric densities at each spacecraft, the method outlined in Appendix C was used.

3.1 Spacecraft Physical Parameters

In order to perform the simulations, the spacecraft physical parameters must be specified. These parameters will be crucial in modeling the impact of atmospheric drag on the formation. Two sets of physical parameters will be used in this section, both based on planned formation flying and rendezvous missions.

3.1.1 TECSAS Physical Parameters

The TECSAS mission was a technology demonstration mission planned to be launched in 2009. Its objective was to demonstrate the technologies needed in order to perform on-orbit servicing. The mission was led by the German Space Organization (DLR) with cooperation from the Canadian Space Agency (CSA) and the Federal Space Agency of Russia (ФКА).

Figure 3.1: TECSAS Spacecraft after Rendezvous (image credit: DLR)

Unfortunately, the mission was cancelled before it could fly. Nonetheless, the physical parameters are still relevant to our interest since the spacecraft were intended to perform a rendezvous.

TECSAS Spacecraft Physical Parameters		
Parameter	**Value**	**Units**
Mass	175	[kg]
Area	2.22	[m^2]
C_D	2.3	[-]

Table 3.1: TECSAS Spacecraft Parameters

3.1.2 JC2Sat Physical Parameters

The JC2Sat mission is a collaborative formation flying technology demonstration mission between the Canadian Space Agency (CSA) and the Japanese Aerospace Exploration Agency (JAXA). Differential drag will be the main means of formation maintenance and control during this mission. The launch date for this mission is yet to be determined.

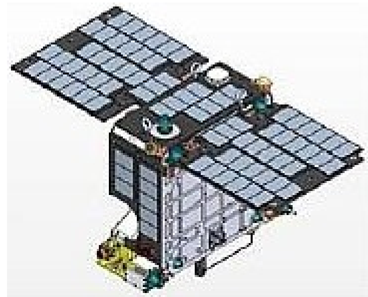

Figure 3.2: One of Two Identical JC2Sat Spacecraft (image credit: JAXA and CSA)

Since the mission plans to use atmospheric drag for formation maintenance, the JC2Sat spacecraft parameters are ideal for use in our simulations.

JC2Sat Spacecraft Physical Parameters		
Parameter	**Value**	**Units**
Mass	20	[kg]
Area	0.09	[m^2]
C_D	2.2	[-]

Table 3.2: JC2Sat Spacecraft Parameters (Shankar Kumar and Ng, 2009)

3.2 Uncontrolled Projected Circular Formation

The first set of simulations will be for a projected circular formation. For this particular type of formation, the spacecraft are placed in orbit such that motion of the deputy relative to the chief forms an ellipse centered on the chief. The ellipse's projection on the y-z plane is a circle. The motion in the y-z plane is therefore subject to the constraint:

$$y^2 + z^2 = d^2 \tag{3.1}$$

where d is the radius of the projected circle. For the simulations performed in this thesis this radius is set to 100 meters.

The initial conditions for the chief and deputy spacecraft required to achieve such a formation, taking into account the J_2 perturbations, are given as (Landry, 2005):

$$
\begin{aligned}
x_{0,D} &= \frac{d}{2}\cos\alpha \\
y_{0,D} &= d\sin\alpha \\
z_{0,D} &= d\cos\alpha \\
\dot{x}_{0,D} &= -\frac{n}{2c}(1-s)y_{0,D} \\
\dot{y}_{0,D} &= -2ncx_{0,D} + \frac{3}{4}\frac{n^2}{k}J_2\frac{R_e^2}{r_{ref}}\sin i_{ref} \\
\dot{z}_{0,D} &= \frac{n}{c}(1-s)y_{0,D}
\end{aligned}
\tag{3.2}
$$

and

$$
\begin{aligned}
x_{0,C} &= 0 \\
y_{0,C} &= 0 \\
z_{0,C} &= 0 \\
\dot{x}_{0,C} &= 0 \\
\dot{y}_{0,C} &= \frac{3}{4}\frac{n^2}{k}J_2\frac{R_e^2}{r_{ref}}\sin i_{ref} \\
\dot{z}_{0,C} &= 0
\end{aligned}
\tag{3.3}
$$

If we set the phase angle α to zero and non-dimensionalize the conditions, we obtain the following dimensionless initial conditions:

$$
\begin{aligned}
\hat{x}_{0,D} &= \frac{1}{2} \\
\hat{y}_{0,D} &= 0 \\
\hat{z}_{0,D} &= 1 \\
\hat{x}'_{0,D} &= 0 \\
\hat{y}'_{0,D} &= -c + \frac{3}{4}\frac{n}{k}J_2\frac{R_e^2}{dr_{ref}}\sin i_{ref} \\
\hat{z}'_{0,D} &= 0
\end{aligned}
\tag{3.4}
$$

and

$$\hat{x}_{0,C} = 0$$
$$\hat{y}_{0,C} = 0$$
$$\hat{z}_{0,C} = 0$$
$$\hat{x}'_{0,C} = 0 \tag{3.5}$$
$$\hat{y}'_{0,C} = \frac{3}{4}\frac{n}{k} J_2 \frac{R_e^2}{dr_{ref}} \sin i_{ref}$$
$$\hat{z}'_{0,C} = 0$$

The term common to both spacecraft's initial in-track velocity is specific to the Schweighart and Sedwick model and is needed to avoid drift between with respect to the reference orbit. More details are provided in Appendix B.

3.2.1 Results for TECSAS

The first set of results will be presented for two TECSAS satellites placed in a projected circular formation. The satellites are not given any control input and thus keep constant projected area. For all simulations performed the reference orbit parameters remain the same apart from the altitude. These parameters are provided in Table 3.3 and represent the planned reference orbit parameters for the TECSAS mission.

Circular Reference Orbit Parameters		
Parameter	**Value**	**Units**
e	0	[-]
i	78	[deg]
Ω	320	[deg]

Table 3.3: Initial Reference Orbit Parameters

The first simulation result (Fig. 3.3) shows the formation without any perturbations which is the desired motion. This motion will remain unchanged for any altitude or spacecraft parameters and is simply the result of the Clohessy-

Wiltshire equations. This first simulation will serve as a basis for comparison for the other simulation results presented. Note that for all simulations shown, distances are given in meters.

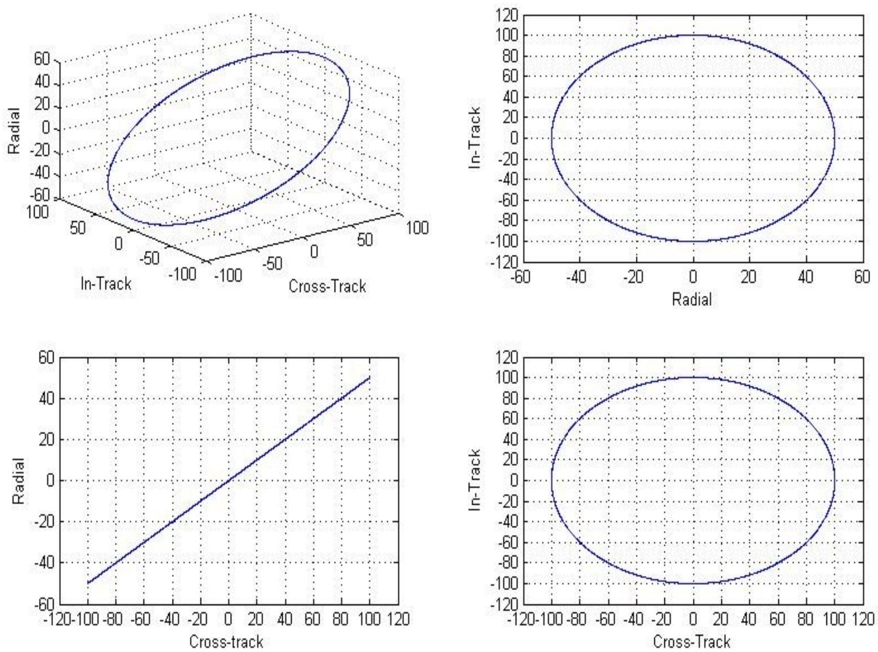

Figure 3.3: Projected Circular Motion – Unperturbed

To view the effect of the J_2 perturbations on the formation, a simulation with only this perturbative force was done. The effect of the J_2 perturbations will not change with altitude. The results obtained (Fig. 3.4) are consistent with those obtained by Landry (2005). It is interesting to note that the in-plane motion does not seem to be altered.

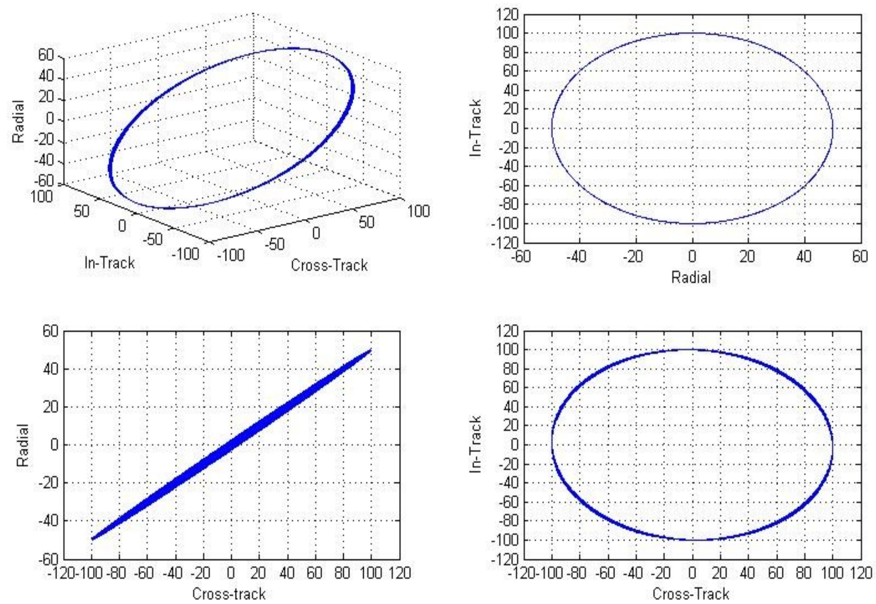

Figure 3.4: Projected Circular Motion – J_2 Perturbations only – 24 hours

The next step is to include the effect of atmospheric drag on the formation. Fig. 3.5 indicates that, at an altitude of 450 km, the effect of atmospheric drag on the relative motion is negligible as the motion is nearly indistinguishable from that of formation solely J_2 perturbed. If the altitude is lowered by 100 km however (Fig. 3.6), the effect of drag becomes apparent. At 250 km of altitude the effect grows significantly larger yet (Fig. 3.7). The main effects of atmospheric drag seem to be in the x and y directions. A small in-track drift appears along with a damping of the in-plane motion as the in-plane ellipse shrinks with time. The damping can be traced to the diagonal elements of the damping matrix $\mathbf{C}$, which represent dissipative damping on the system and theses elements are non-zero in the presence of drag. Fig. 3.8 shows a simulation with parameters identical to those of Fig. 3.7, but without J_2 perturbations. The result is very interesting as it seems that while the damping remains, the in-track drift has reduced significantly. Hence, it can be concluded that the in-track drift is a consequence of the coupling of the two pertubative forces.

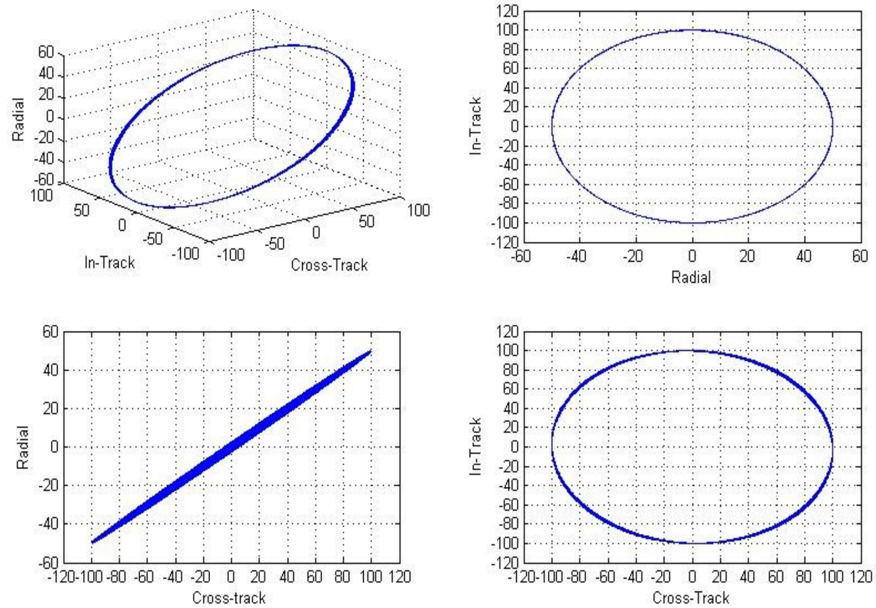

Figure 3.5: Projected Circular Motion – J_2 and Drag Perturbations – Altitude of 450 km – TECSAS Physical Parameters – Uncontrolled – 24 hours

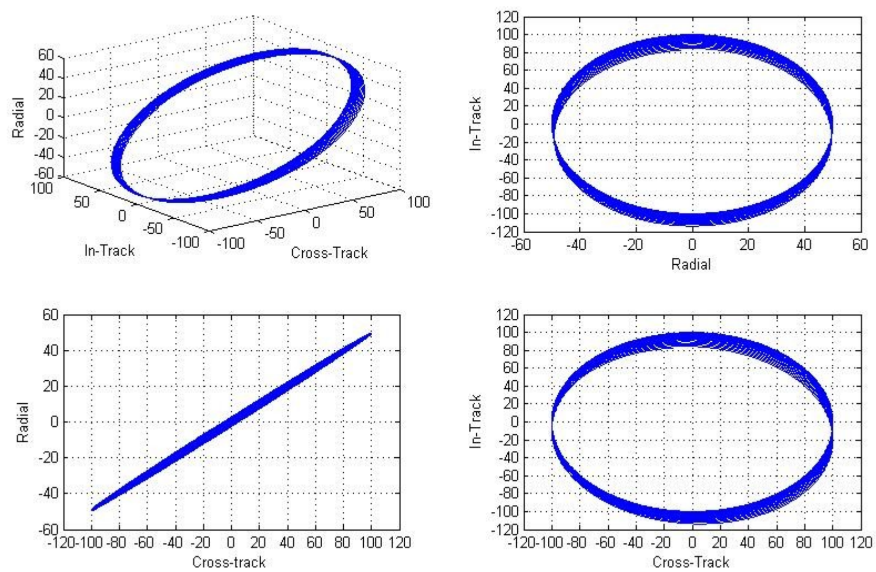

Figure 3.6: Projected Circular Motion – J_2 and Drag Perturbations – Altitude of 350 km – TECSAS Physical Parameters – Uncontrolled – 24 hours

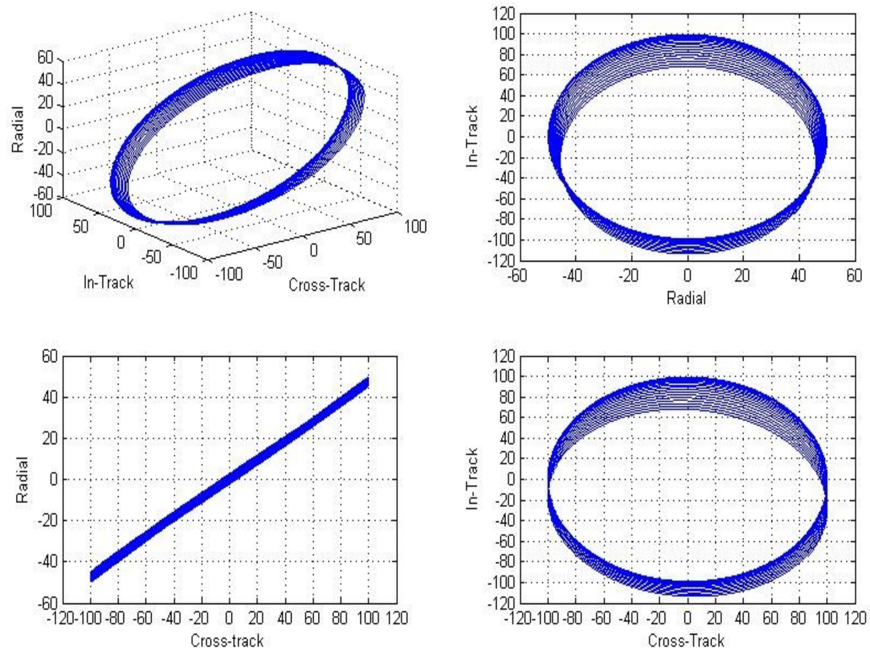

Figure 3.7: Projected Circular Motion – J_2 and Drag Perturbations – Altitude of 250 km – TECSAS Physical Parameters – Uncontrolled – 24 hours

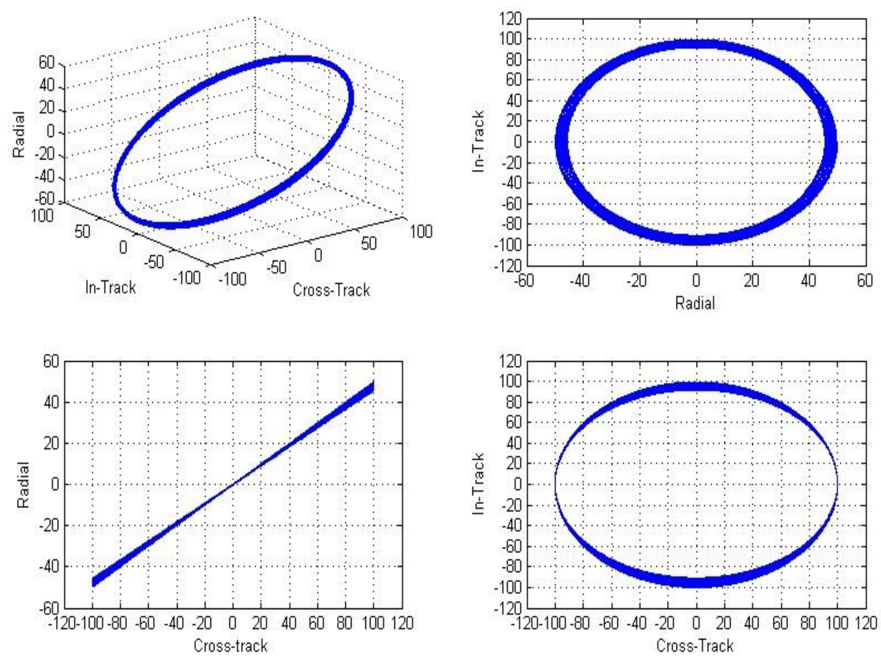

Figure 3.8: Projected Circular Motion – Drag Perturbations only – Altitude of 250 km – TECSAS Physical Parameters – 24 hours

3.2.2 Results for JC2Sat

In this section results for JC2Sat spacecraft parameters will be presented. The simulations performed use the same initial orbit parameters as the ones used for the TECSAS simulations. The unperturbed motion and motion under the effect only of J_2 perturbations will therefore be the same for both sets of spacecraft.

The results are very similar to the ones obtained with the TECSAS physical parameters. At an altitude of 450 km the effects of atmospheric drag are negligible (Fig. 3.9), but they become apparent at the lower altitudes of 350 and 250 km(Figs. 3.10 and 3.11) . Furthermore, the effects of atmospheric drag are the same: a reduction in size of the in-plane ellipse and a slight in-track drift. These effects are slightly smaller in magnitude than those observed with the TECSAS parameters as expected since the ballistic coefficient is smaller for JC2Sat.

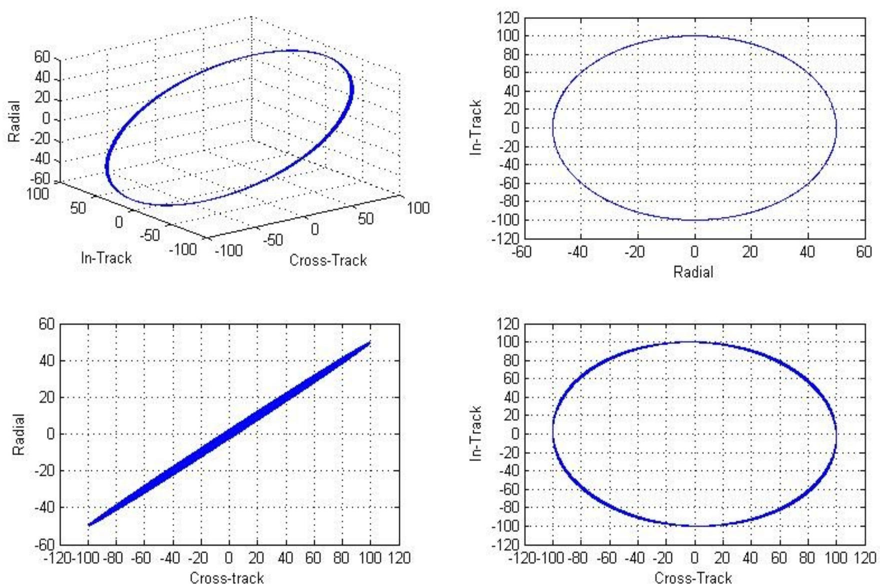

Figure 3.9: Projected Circular Motion – J_2 and Drag Perturbations – Altitude of 450 km – JC2Sat Physical Parameters – Uncontrolled – 24 hours

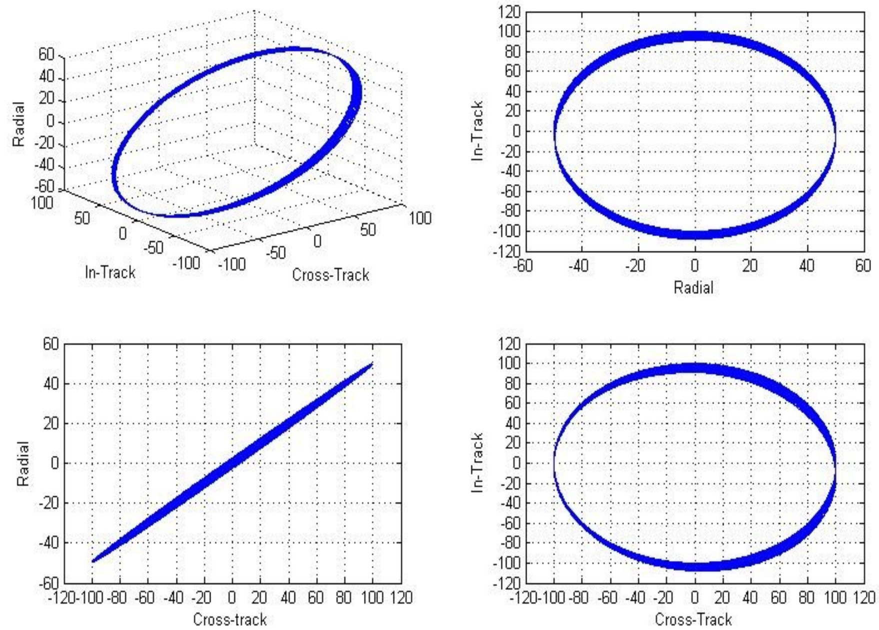

Figure 3.10: Projected Circular Motion – J_2 and Drag Perturbations – Altitude of 350 km – JC2Sat Physical Parameters – Uncontrolled – 24 hours

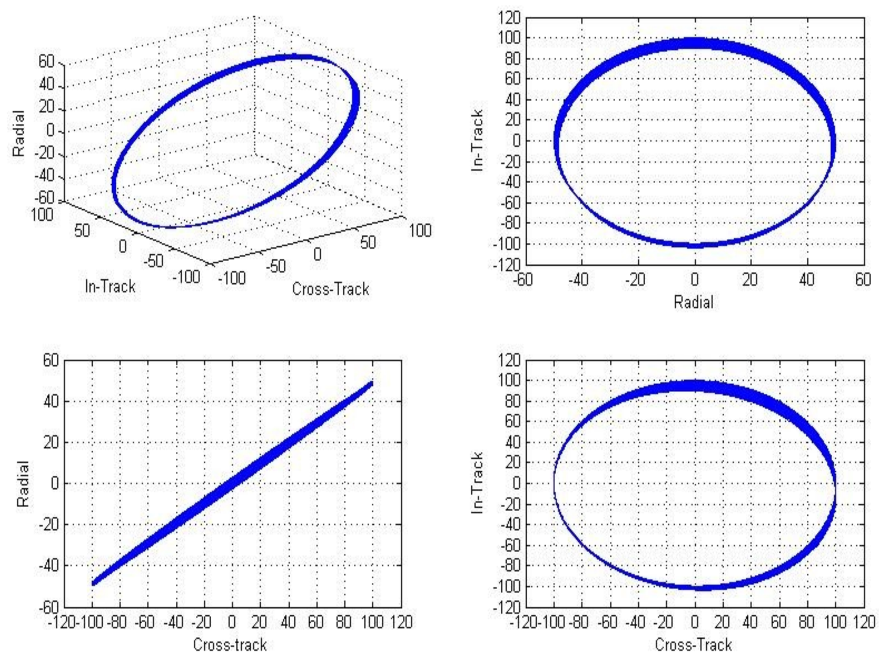

Figure 3.11: Projected Circular Motion – J_2 and Drag Perturbations – Altitude of 250 km – JC2Sat Physical Parameters – Uncontrolled – 24 hours

3.3 Uncontrolled In-Track Formation

In this section, simulation results for an in-track formation will be presented. For this particular formation, both spacecraft share the same ground track, but are separated by a desired distance. Here, ground track refers to the path of the satellite projected on the surface of the rotating Earth. In order to share this ground track both spacecraft have to on slightly differential orbital planes forming an angle $\Delta\Omega$ with each other (Fig. 3.12). This slight difference in right ascension of ascending node accounts for the rotation of the Earth.

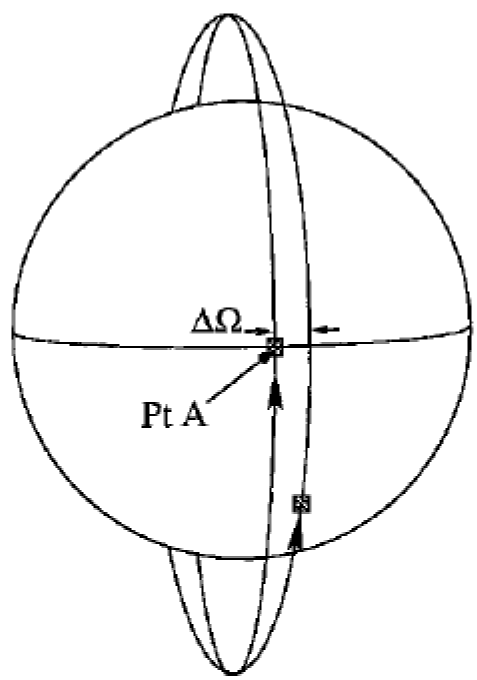

Figure 3.12: Schematic of an In-Track Formation (Sabol et al., 2001)

The desired motion for this type of formation is given by Sabol et al. (2001) as:

$$\begin{aligned} \Delta x_d &= 0 \\ \Delta y_d &= d \\ \Delta z_d &= -\frac{\omega_e}{nc} d \sin i \cos(nct) \end{aligned} \tag{3.6}$$

$$\Delta\dot{x}_d = 0$$
$$\Delta\dot{y}_d = 0$$
$$\Delta\dot{z}_d = \omega_e d \sin i \sin(nct)$$

where d is the desired in-track separation desired. The initial conditions for the deputy and chief satellites can then be given as:

$$\begin{aligned} x_{0,D} &= 0 \\ y_{0,D} &= d \\ z_{0,D} &= -\frac{\omega_e}{nc} d \sin i_{ref} \\ \dot{x}_{0,D} &= 0 \\ \dot{y}_{0,D} &= \frac{3}{4}\frac{n^2}{k} J_2 \frac{R_e^2}{r_{ref}} \sin i_{ref} \\ \dot{z}_{0,D} &= 0 \end{aligned} \tag{3.7}$$

and

$$\begin{aligned} x_{0,C} &= 0 \\ y_{0,C} &= 0 \\ z_{0,C} &= 0 \\ \dot{x}_{0,C} &= 0 \\ \dot{y}_{0,C} &= \frac{3}{4}\frac{n^2}{k} J_2 \frac{R_e^2}{r_{ref}} \sin i_{ref} \\ \dot{z}_{0,C} &= 0 \end{aligned} \tag{3.8}$$

Note that the in-track velocity comes again from the Schweighart and Sedwick formulation.

3.3.1 Results for TECSAS

In this section, simulation results for two TECSAS spacecraft placed in an in-track formation will be presented. The first simulation was performed for the case without any perturbations in order to obtain the desired relative motion (Fig. 3.13). It will later serve as a benchmark for comparative analysis. As expected, the radial distance between both satellites remain equal to zero while the in-track distance remains constant at 100 m. The oscillations in the cross-track direction come from the right ascension of ascending node offset between both orbits. The next 3 simulation results are for a formation under the effect of atmospheric drag and J_2 perturbations at 3 different altitudes (Figs. 3.14, 3.15 and 3.16). Figs. 3.14 and 3.15 show drifts in both the in-track and radial directions, but the magnitude of those drifts are so small that this can be neglected and applying control for such small drifts is not needed. However, when the formation is at an altitude of 250km (Fig. 3.16), these drifts become significant. The cross track motion remains unaffected at all altitudes.

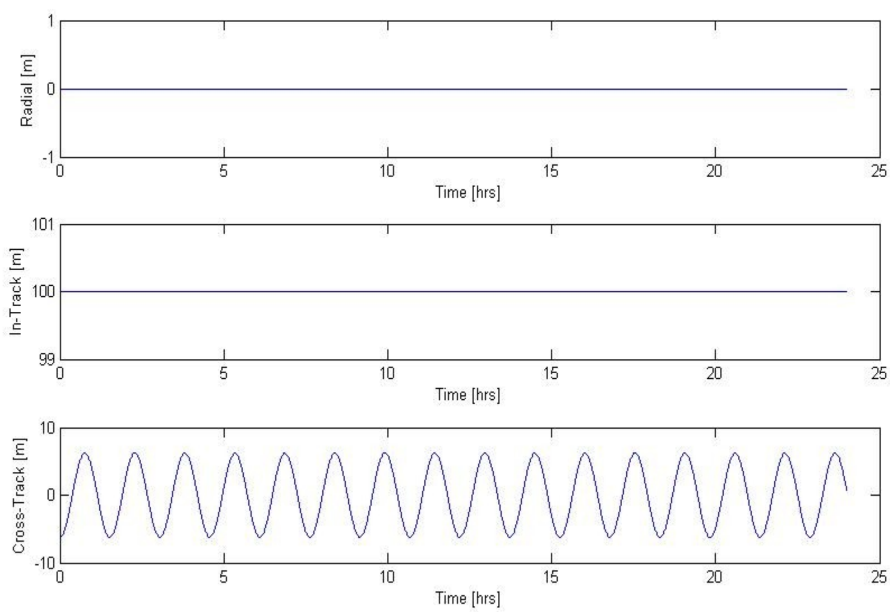

Figure 3.13: In-track Motion - Unperturbed

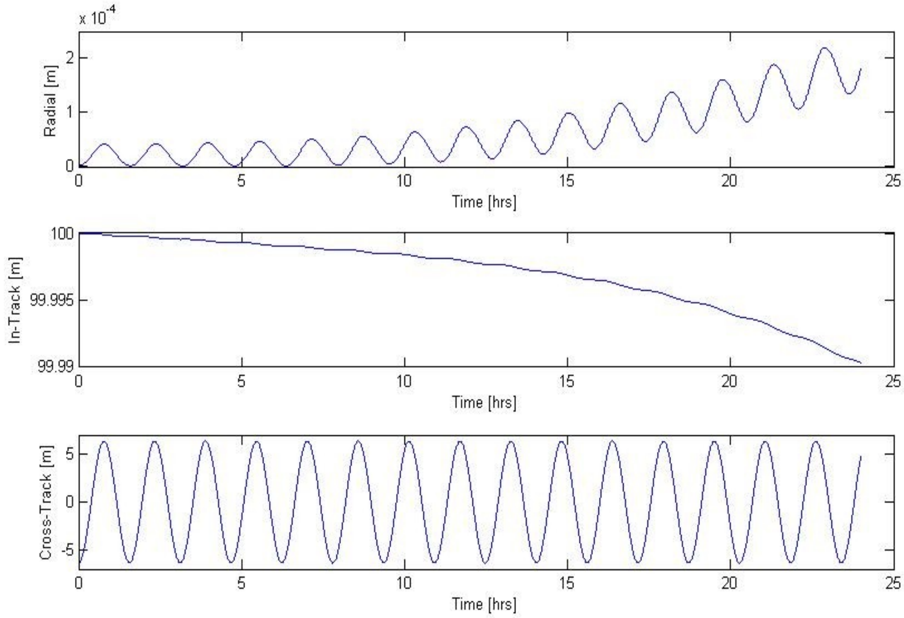

Figure 3.14: In-track Motion – J_2 and Drag Perturbations – Altitude of 450 km – TECSAS Physical Parameters – Uncontrolled – 24 hours

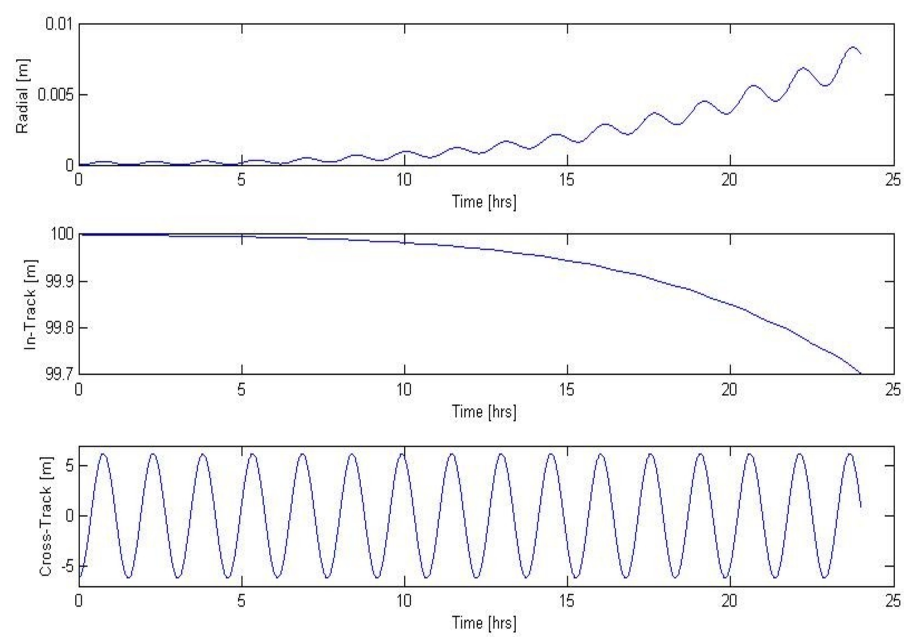

Figure 3.15: In-track Motion – J_2 and Drag Perturbations – Altitude of 350 km – TECSAS Physical Parameters – Uncontrolled – 24 hours

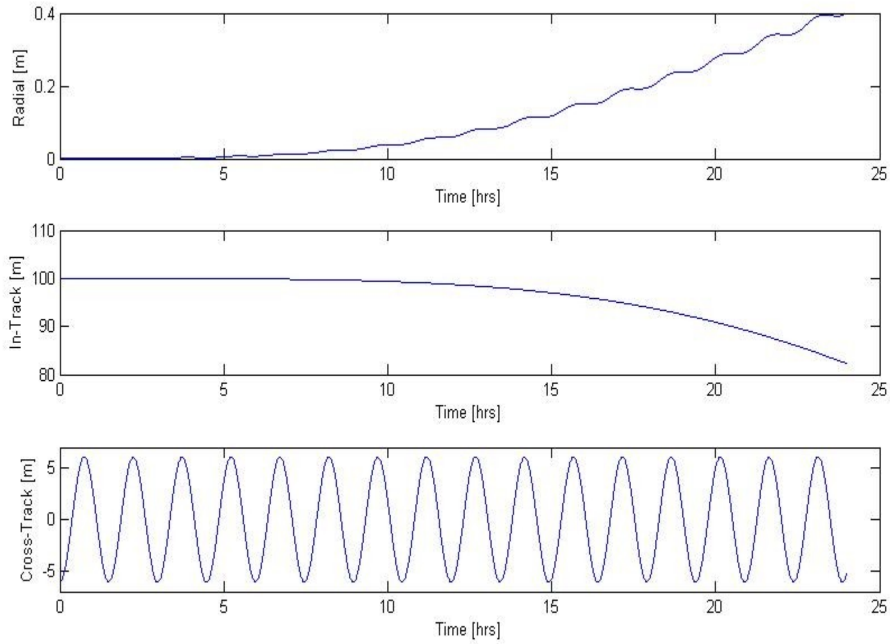

Figure 3.16: In-track Motion – J_2 and Drag Perturbations – Altitude of 250 km – TECSAS Physical Parameters – Uncontrolled – 24 hours

3.4 Effectiveness of the Gain Matrix

In this section the gain matrix developed in Chapter 2 will be tested to gage its effectiveness as a formation maintenance scheme. In order to do so, the spacecraft will be placed in a projected circular formation orbiting the Earth at the same altitudes as the uncontrolled formation of section 3.2.1.

3.4.1 Results for TECSAS

The gain matrix will first be tested using the TECSAS physical properties. Figs. 3.17 and 3.19 show the effect of using the gain matrix developed in Chapter

2 to control each spacecraft's projected area in order to maintain the formation at 350 and 450 km respectively. While there is a significant improvement in the relative motion, the gain matrix does not seem to eliminate the drift entirely. This might be due to the lack of a clearly defined method to obtain the values for α and ξ and resorting to trial and error is obviously not ideal as there are countless possible pairings. Figs. 3.18 and 3.20 show the additional area needed to control each satellite. A positive value indicates area added to the chief while a negative value indicates area added to the deputy. The additional area needed doesn't seem too large when compared to the baseline area of the spacecraft indicating that it would be feasible.

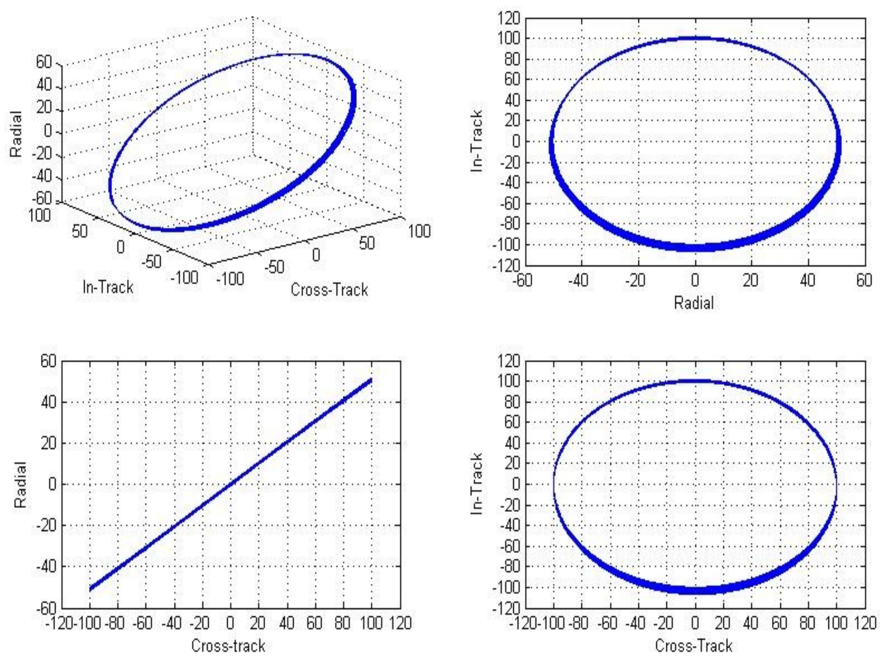

Figure 3.17: Projected Circular Motion – J_2 and Drag Perturbations – Altitude of 350 km – TECSAS Physical Parameters – Gain Matrix (ξ=1, α=1000) – 24 hours

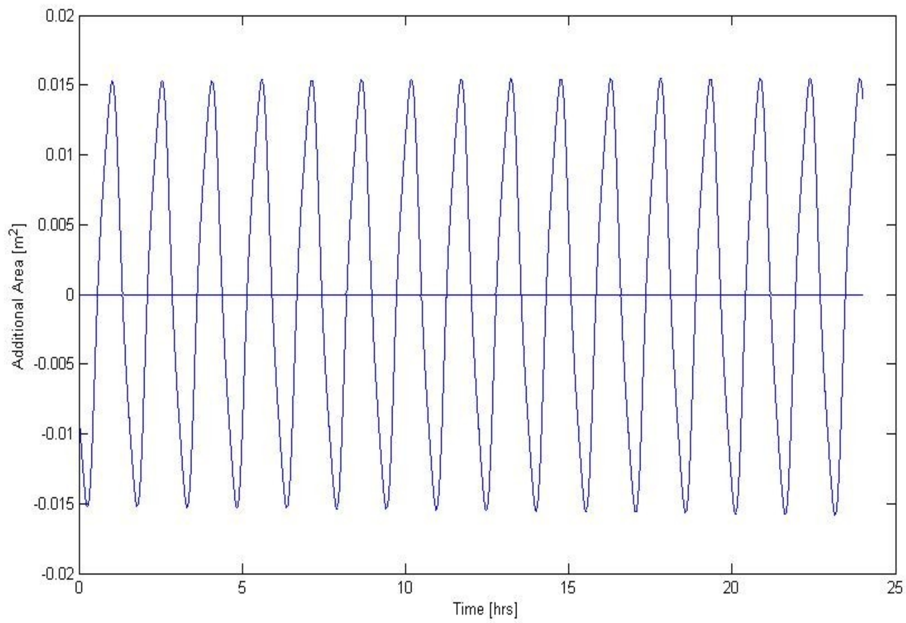

Figure 3.18: Additional Area needed for Control – Altitude of 350 km – TECSAS Physical Parameters – Gain Matrix (ξ =1, α=1000) – 24 hours

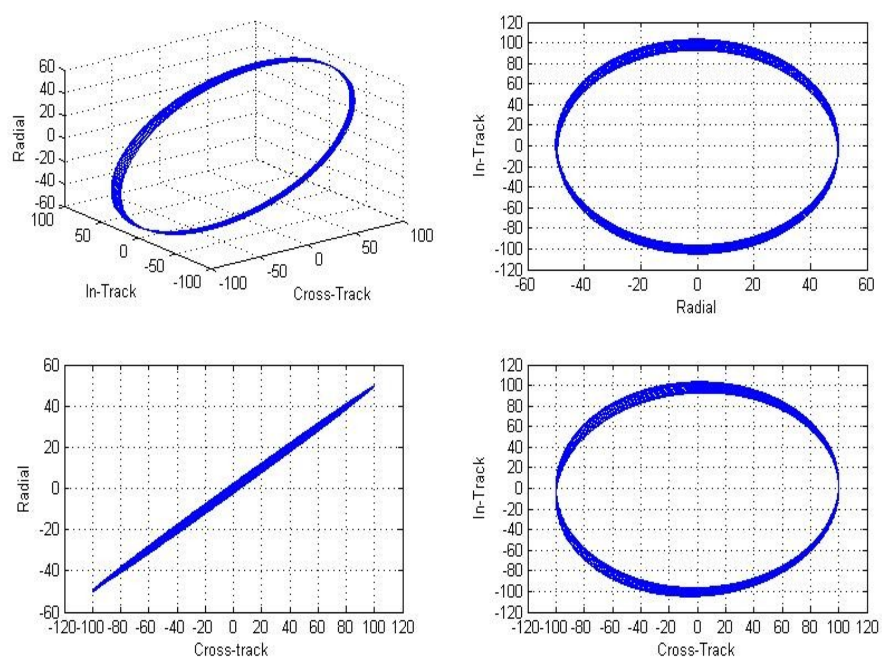

Figure 3.19: Projected Circular Motion – J_2 and Drag Perturbations – Altitude of 250 km – TECSAS Physical Parameters – 24 hours – Gain Matrix (ζ=1, α=300)

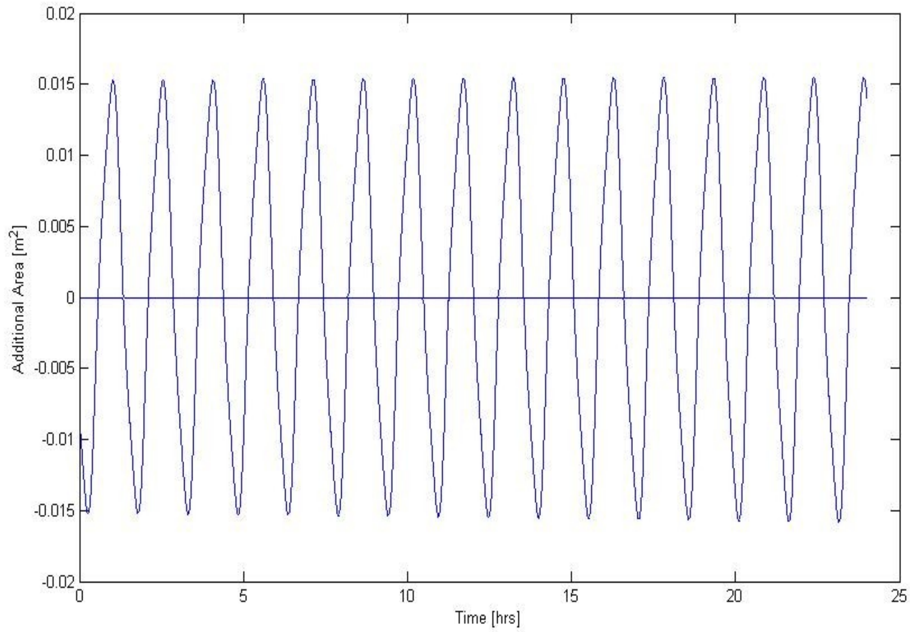

Figure 3.20: Additional Area needed for Control – Altitude of 250 km – TECSAS Physical Parameters – Gain Matrix (ξ =1, α=150) – 24 hours

3.4.2 Results for JC2Sat

The gain matrix will also be tested using the JC2Sat physical parameters. Again, the implementation of a differential atmospheric drag control via a gain matrix improves the quality of the formation and mitigates most of the drift (Figs. 3.21 and 3.23). The area needed to perform this control is again very reasonable (Figs. 3.22 and 3.24).

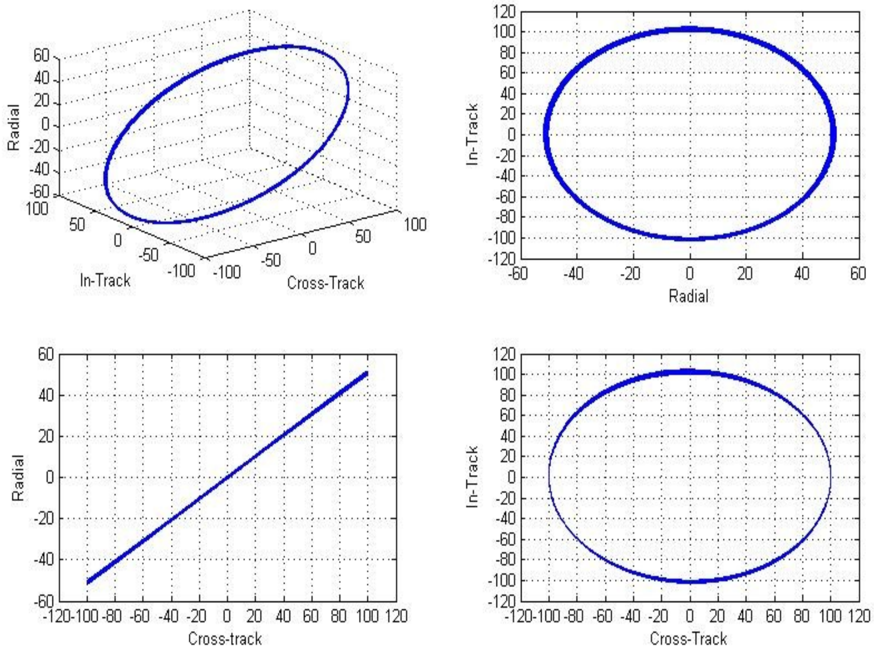

Figure 3.21: Projected Circular Motion – J_2 and Drag Perturbations – Altitude of 350 km – JC2Sat Physical Parameters – Gain Matrix (ξ=1, α=1000) – 24 hours

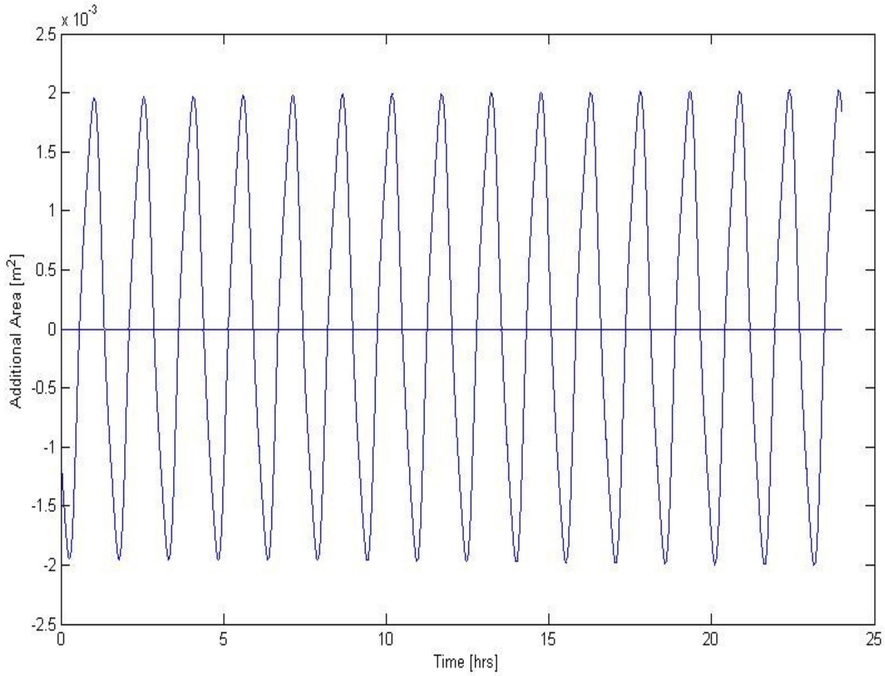

Figure 3.22: Additional Area needed for Control – Altitude of 350 km – JC2Sat Physical Parameters – Gain Matrix (ξ =1, α=1000) – 24 hours

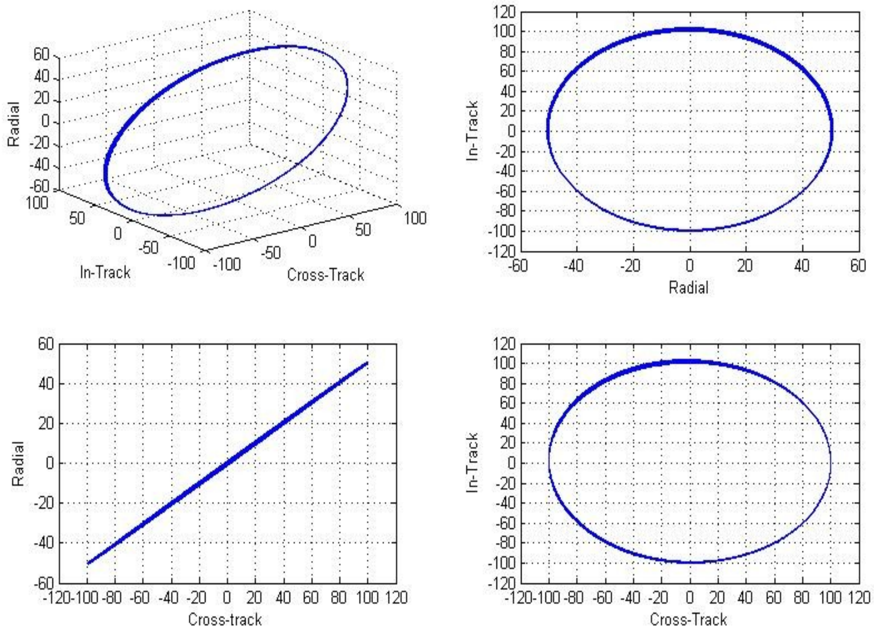

Figure 3.23: Projected Circular Motion – J_2 and Drag Perturbations – Altitude of 250 km – JC2Sat Physical Parameters – 24 hours – Gain Matrix (ζ=1, α=1000)

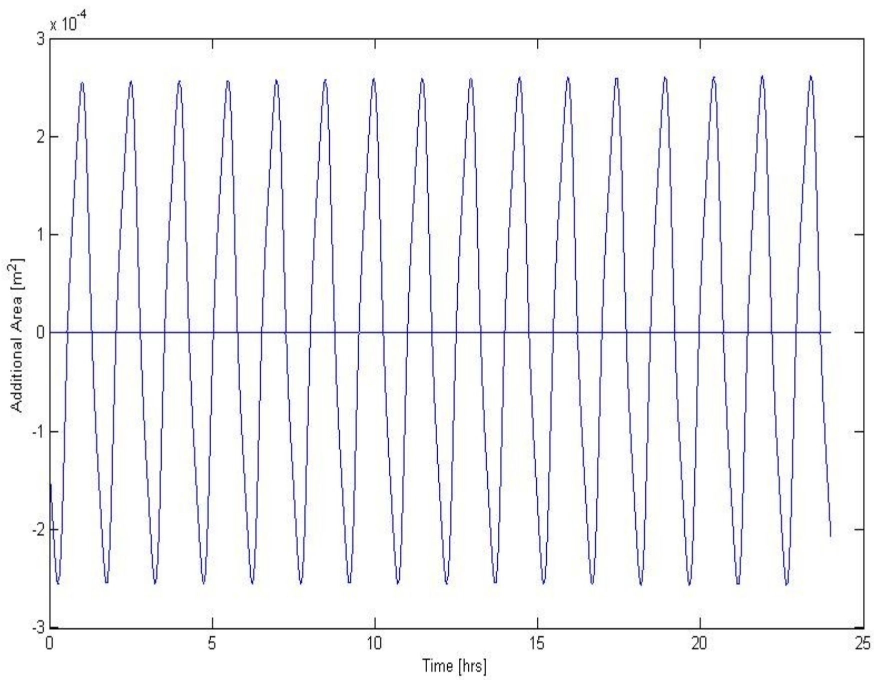

Figure 3.24: Additional Area needed for Control – Altitude of 250 km – JC2Sat Physical Parameters – Gain Matrix (ξ =1, α=1000) – 24 hours

Chapter 4 – Relative Motion Equations for Elliptical Orbits

In this chapter, we will analyse the relative motion between two spacecraft flying in formation when they are placed in an elliptical orbit around the Earth. Through this analysis, we wish to obtain a set of linear differential equations that will account for the J_2 perturbations and the atmospheric drag similar to the equations obtained in the second chapter. They will, however, need to be valid for orbits with a certain eccentricity.

4.1 Relative Motion Equations

In this section, the relative motion equations for the elliptical case will be presented. Since the set of equations developed by Sedwick and Schweighart are only valid for circular reference orbits, another set of equations is needed as starting point. The set of equations used is the linearized general relative motion equations which are valid for any eccentricity. They are given by Schaub and Junkins (2003) as:

$$\begin{aligned}
\ddot{x} - 2\dot{\theta}\dot{y} - \ddot{\theta}y - \left(\dot{\theta}^2 + \frac{2\mu}{r_{ref}^3}\right)x &= \Delta a_{J_2,x} + \Delta a_{Drag,x} \\
\ddot{y} + 2\dot{\theta}\dot{x} - \ddot{\theta}x - \left(\dot{\theta}^2 - \frac{\mu}{r_{ref}^3}\right)y &= \Delta a_{J_2,y} + \Delta a_{Drag,y} \qquad (4.1) \\
\ddot{z} + \frac{\mu}{r_{ref}^3}z &= \Delta a_{J_2,z} + \Delta a_{Drag,z}
\end{aligned}$$

where $\dot{\theta}$ is the instantaneous angular rate of the hill frame and r_{ref} is the instantaneous radial distance taken from the middle of the Earth. The differential accelarations due to the J_2 perturbations and atmospheric drag are denoted by

Δa_{J_2} and $+\Delta a_{Drag}$ respectively. These equations will be simplified in the following sections of this chapter.

4.1.1 Elliptical Reference Orbit

The set of equations just presented (4.1) describes the motion of a deputy spacecraft relative to a virtual chief spacecraft placed in an elliptical reference orbit in presence of J_2 perturbations and atmospheric drag. If the effects of those same perturbations on the reference orbit are not taken into account, a secular drift between the deputy and virtual chief would arise. This would, in turn, reduce the time frame for which the equations are valid.

To avoid this problem and to account for these perturbations, one can use Gauss' Planetary Equations. This set of equations allows us to model the effects of both conservative perturbations forces, such as the ones arising from the oblateness of the Earth, and non-conservative forces, such as atmospheric drag. The set is comprised of six differential equations that can propagate the orbital elements of the reference orbit (Battin, 1987):

$$\begin{gathered}
\frac{da}{dt} = \frac{2a^2}{h}\left[e \sin f\, a_x + \frac{p}{r_{ref}} a_y\right] \\
\frac{di}{dt} = \frac{r_{ref}\cos\theta}{h} a_z \\
\frac{d\Omega}{dt} = \frac{r_{ref}\sin\theta}{h\sin i} a_z \\
\frac{de}{dt} = \frac{1}{h}\left[p \sin f\, a_x + \left[\left(p + r_{ref}\right)\cos f + r_{ref} e\right] a_y\right] \\
\frac{d\omega}{dt} = \frac{1}{he}\left[-p\cos f\, a_x + \left(p + r_{ref}\right)\sin f\, a_y\right] - \frac{r_{ref}\sin\theta\cos i}{h\sin i} a_z \\
\frac{dM}{dt} = n + \frac{\sqrt{1-e^2}}{he}\left[\left(p\cos f - 2r_{ref} e\right) a_x - \left(p + r_{ref}\right)\sin f\, a_y\right]
\end{gathered} \tag{4.2}$$

where h is the magnitude of the specific angular moment vector of the reference orbit and p is the semi-latus rectum. These two parameters, along with r_{ref}, can be defined with the orbital elements as:

$$p = a(1 - e^2) \tag{4.3}$$

$$h = \sqrt{\mu a(1 - e^2)} \tag{4.4}$$

$$r_{ref} = \frac{a(1 - e^2)}{1 + e\cos f} \tag{4.5}$$

The a_x, a_y and a_z terms represent the accelerations due to the perturbations in the radial, in-track and cross-track directions respectively.

To solve the equations above, the true anomaly f is required. It can be obtained as long as we know the eccentric anomaly E and the eccentricity from the identity:

$$\tan\frac{f}{2} = \sqrt{\frac{1 + e}{1 - e}}\tan\frac{E}{2} \tag{4.6}$$

To obtain the eccentric anomaly, one can use the following identity:

$$M = E - e\sin E \tag{4.7}$$

which can be solved numerically through iterative methods such as the one proposed by Vallado (2007) in Algorithms 2 and 6.

4.1.2 Small Eccentricity Assumption

In order to simplify the analysis, we will assume the reference orbit to have a small eccentricity. In other words, we will assume higher than first order eccentricity terms to be negligible when compared to numbers of the order of 1. Using this assumption, some of the previously defined parameters can be simplified. The semi-latus rectum defined in Eq. (4.3) becomes:

$$p = a(1 - e^2) \approx a \tag{4.8}$$

Similarly, the specific angular moment becomes:

$$h = \sqrt{\mu a(1 - e^2)} \approx \sqrt{\mu a} = \sqrt{(n^2 a^3) a} = n a^2 \tag{4.9}$$

During the upcoming analysis powers of r_{ref} are common. Fortunately, they can be simplified using the small eccentricity assumption in conjunction with a binomial expansion:

$$r_{ref}^k = \left(\frac{a(1 - e^2)}{1 + e\cos f}\right)^k \approx a^k (1 + e\cos f)^{-k} \approx a^k (1 - ke\cos f) \tag{4.10}$$

The same assumption will be made for $\widehat{\omega}_e$, since it is also of a very small magnitude.

4.1.3 J₂ Perturbation Forces

In this section the acceleration due to the J_2 perturbations needed to propagate the reference orbit will be presented. This acceleration is given by Schweighart and Sedwick (2002) and is expressed in the Hill frame as:

$$\mathbf{a}_{J_2} = \begin{bmatrix} a_{J_2,x} \\ a_{J_2,y} \\ a_{J_2,z} \end{bmatrix} = -\frac{3}{2}\frac{J_2 \mu R_e^2}{r_{ref}^4} \begin{bmatrix} 1 - 3\sin^2 i \sin^2\theta \\ 2\sin^2 i \sin\theta\cos\theta \\ 2\sin i\cos i\sin\theta \end{bmatrix} \tag{4.11}$$

This expression can be simplified using the small eccentricity assumption and Eq. (4.10). The resulting simplified expression is:

$$\mathbf{a}_{J_2} = -\frac{3}{2}\frac{J_2 \mu R_e^2}{a^4}(1 + 4e\cos f) \begin{bmatrix} 1 - 3\sin^2 i \sin^2\theta \\ 2\sin^2 i \sin\theta\cos\theta \\ 2\sin i\cos i\sin\theta \end{bmatrix} \tag{4.12}$$

Finally, we can get its dimensionless counterpart:

$$\hat{\mathbf{a}}_{J_2} = \frac{\mathbf{a}_{J_2}}{n_0^2 d} == -\frac{3}{2}\frac{J_2 \hat{n}^2 R_e^2}{ad}(1 + 4e\cos f)\begin{bmatrix} 1 - 3\sin^2 i \sin^2\theta \\ 2\sin^2 i \sin\theta\cos\theta \\ 2\sin i\cos i\sin\theta \end{bmatrix} \tag{4.13}$$

4.1.4 Atmospheric Drag Perturbation Forces

As stated previously in Eq. (2.8), the acceleration arising from the perturbations in the presence of atmospheric drag is given by:

$$\hat{\mathbf{a}}_{Drag} = -\frac{1}{2}\rho\frac{C_D A}{m} d\|\hat{\mathbf{v}}_{rel}\|\hat{\mathbf{v}}_{rel} \tag{4.14}$$

where $\hat{\mathbf{v}}_{rel}$ is the dimensionless velocity vector of the spacecraft relative to the Earth's rotating atmosphere and is expressed in the Hill frame as (refer to Appendix A):

$$\hat{\mathbf{v}}_{rel} = \frac{1}{n_0 d}\begin{bmatrix} \dot{x} + \dot{r}_{ref} - y(\dot{f} - \omega_e\cos i) - z\omega_e\cos\theta\sin i \\ \dot{y} + (r_{ref} + x)(\dot{f} - \omega_e\cos i) + z\omega_e\sin\theta\sin i \\ \dot{z} + (r_{ref} + x)\omega_e\cos\theta\sin i - y\omega_e\sin\theta\sin i \end{bmatrix} \tag{4.15}$$

Since we are considering the perturbations on a spacecraft placed at the origin of the Hill frame, x, y, z and their derivatives are all set to zero to simplify the above expression and obtain:

$$\hat{\mathbf{v}}_{rel} = \begin{bmatrix} \frac{r'_{ref}}{d} \\ \frac{r_{ref}}{d}(f' - \hat{\omega}_e\cos i) \\ \frac{r_{ref}}{d}\hat{\omega}_e\cos\theta\sin i \end{bmatrix} \tag{4.16}$$

The term f' can be related to the orbital elements through the following relation (Vallado, 2007):

$$f' = \frac{\dot{f}}{n_0} = \frac{h}{n_0 r_{ref}^2} \tag{4.17}$$

Then, r'_{ref} can be obtained using the chain rule:

$$r'_{ref} = \frac{\dot{r}_{ref}}{n_0} = \frac{1}{n_0}\frac{dr_{ref}}{df}\frac{df}{dt} = \frac{1}{n_0}\frac{dr_{ref}}{df}\frac{h}{r_{ref}^2} \tag{4.18}$$

After using the small eccentricity assumption, the two terms can be simplified to:

$$f' = \frac{h}{n_0 r_{ref}^2} \approx \hat{n}(1 + 2e\cos f) \tag{4.19}$$

$$r'_{ref} = \frac{1}{n_0 d}\frac{dr_{ref}}{df}\frac{h}{r_{ref}^2} \approx \hat{n}ae\sin f\,(1 + 2e\cos f) \approx \hat{n}ae\sin f \tag{4.20}$$

Now, $\hat{\mathbf{v}}_{rel}$ can be written as:

$$\hat{\mathbf{v}}_{rel} = \frac{a}{d}\begin{bmatrix} \hat{n}e\sin f \\ \hat{n} + \hat{n}e\cos f - \widehat{\omega}_e\cos i \\ \widehat{\omega}_e\cos\theta\sin i \end{bmatrix} = \frac{a}{d}\begin{bmatrix} v_x \\ v_y \\ v_z \end{bmatrix} \tag{4.21}$$

and $\|\hat{\mathbf{v}}_{rel}\|$ as:

$$\|\hat{\mathbf{v}}_{rel}\| = \frac{a}{d}\sqrt{v_x^2 + v_y^2 + v_z^2} \tag{4.22}$$

Note that v_x^2 and v_z^2 are negligible in front of v_y^2 since v_y^2 is of the order of 1 while v_x^2 and v_z^2 are higher order terms in e and $\widehat{\omega}_e$. Thus, we can state that:

$$\|\hat{\mathbf{v}}_{rel}\| \approx \frac{a}{d}v_y = \frac{a}{d}(\hat{n} + \hat{n}e\cos f - \widehat{\omega}_e\cos i) \tag{4.23}$$

We can now examine each component of the perturbative acceleration due to drag. Let us start with the radial component:

$$\begin{aligned} \hat{a}_{Drag,x} &= -\frac{1}{2}\rho\frac{C_D A}{m}a\|\hat{\mathbf{v}}_{rel}\|v_x \\ \hat{a}_{Drag,x} &= -\frac{1}{2}\frac{1}{\beta}\frac{a}{d}\hat{n}^2 e\sin f \end{aligned} \tag{4.24}$$

where β is the dimensionless ballistic coefficient and is similar to the one defined for the circular case:

$$\beta = \left(\rho \frac{C_D A}{m} a\right)^{-1} \tag{4.25}$$

Similarly, for the in-track component:

$$\begin{aligned} \hat{a}_{Drag,y} &= -\frac{1}{2} \rho \frac{C_D A}{m} a \|\hat{\mathbf{v}}_{rel}\| v_y \\ \hat{a}_{Drag,y} &= -\frac{1}{2} \frac{1}{\beta} \frac{a}{d} \hat{n} (\hat{n} + 2\hat{n} e \cos f - 2\hat{\omega}_e \cos i) \end{aligned} \tag{4.26}$$

Finally, for the cross track component:

$$\begin{aligned} \hat{a}_{Drag,z} &= -\frac{1}{2} \rho \frac{C_D A}{m} a \|\hat{\mathbf{v}}_{rel}\| v_z \\ \hat{a}_{Drag,z} &= -\frac{1}{2} \frac{1}{\beta} \frac{a}{d} \hat{n} \hat{\omega}_e \cos\theta \sin i \end{aligned} \tag{4.27}$$

Combining all the components, we obtain the final expression for the dimensionless perturbative acceleration due to atmospheric drag:

$$\hat{\mathbf{a}}_{Drag} = -\frac{1}{2} \frac{1}{\beta} \frac{a}{d} \hat{n} \begin{bmatrix} \hat{n} e \sin f \\ \hat{n} + 2\hat{n} e \cos f - 2\hat{\omega}_e \cos i \\ \hat{\omega}_e \cos\theta \sin i \end{bmatrix} \tag{4.28}$$

4.1.5 Reference Orbit Propagation

In this section, the final differential equations allowing for the propagation of the orbital elements describing the reference orbit will be presented. To do so, Gauss' planetary equations, Eq. (4.2), will modified to be derivatives with respect to τ and then used in conjunction with the perturbative accelerations previously calculated (Eqs. (4.13) and (4.28)). Modifying Gauss' planetary equation so that they are comprised of derivatives with respect to τ, we obtain:

$$
\begin{aligned}
\frac{da}{d\tau} &= (n_0 d)\frac{2a^2}{h}\left[e\sin f\,\hat{a}_x + \frac{p}{r_{ref}}\hat{a}_y\right] \\
\frac{di}{d\tau} &= (n_0 d)\frac{r_{ref}\cos\theta}{h}\hat{a}_z \\
\frac{d\Omega}{d\tau} &= (n_0 d)\frac{r_{ref}\sin\theta}{h\sin i}\hat{a}_z \\
\frac{de}{d\tau} &= (n_0 d)\frac{1}{h}\left[p\sin f\,\hat{a}_x + \left[\left(p + r_{ref}\right)\cos f + r_{ref}e\right]\hat{a}_y\right] \\
\frac{d\omega}{d\tau} &= (n_0 d)\left\{\frac{1}{he}\left[-p\cos f\,\hat{a}_x + \left(p + r_{ref}\right)\sin f\,\hat{a}_y\right] \right. \\
&\qquad \left. - \frac{r_{ref}\sin\theta\cos i}{h\sin i}\hat{a}_z\right\} \\
\frac{dM}{d\tau} &= \hat{n} + (n_0 d)\left\{\frac{\sqrt{1-e^2}}{he}\left[\left(p\cos f - 2r_{ref}e\right)\hat{a}_x \right.\right. \\
&\qquad \left.\left. - \left(p + r_{ref}\right)\sin f\,\hat{a}_y\right]\right\}
\end{aligned}
\tag{4.29}
$$

They can be simplified by using the small eccentricity assumption:

$$
\begin{aligned}
\frac{da}{d\tau} &= \frac{2d}{\hat{n}}\left[e\sin f\,\hat{a}_x + (1 + e\cos f)\hat{a}_y\right] \\
\frac{di}{d\tau} &= \frac{d(1 - e\cos f)\cos\theta}{\hat{n}a}\hat{a}_z \\
\frac{d\Omega}{d\tau} &= \frac{d(1 - e\cos f)\sin\theta}{\hat{n}a\sin i}\hat{a}_z \\
\frac{de}{d\tau} &= \frac{d}{\hat{n}a}\left[\sin f\,\hat{a}_x + \left[(2 - e\cos f)\cos f + e\right]\hat{a}_y\right] \\
\frac{d\omega}{d\tau} &= \frac{d}{\hat{n}a}\left\{\frac{1}{e}\left[-\cos f\,\hat{a}_x + (2 - e\cos f)\sin f\,\hat{a}_y\right] \right. \\
&\qquad \left. - \frac{(1 - e\cos f)\sin\theta\cos i}{\sin i}\hat{a}_z\right\} \\
\frac{dM}{d\tau} &= \hat{n} + \left\{\frac{d}{\hat{n}ae}\left[(\cos f - 2e)\hat{a}_x - (2 - e\cos f)\sin f\,\hat{a}_y\right]\right\}
\end{aligned}
\tag{4.30}
$$

To further simplify our analysis, we orbit-average these equations. The ensuing equations will ignore the small periodic perturbations, but will capture the larger, more significant, secular drifts. To orbit-average the equations, the method described by Schaub and Junkins (2003) will be used:

$$\begin{gathered}\frac{d\bar{\xi}}{d\tau} = \frac{(1-e^2)^{3/2}}{2\pi}\int_0^{2\pi}(1+e\cos f)^{-2}\frac{d\xi}{d\tau}df \\ \frac{d\bar{\xi}}{d\tau} \approx \frac{1}{2\pi}\int_0^{2\pi}(1-2e\cos f)\frac{d\xi}{d\tau}df\end{gathered} \tag{4.31}$$

where ξ represents any orbital element and the overbar signifies the term has been orbit-averaged. The orbit-averaged expressions for the J_2 perturbations do not need to be calculated as they can be found in the literature (Schaub and Junkins, 2003). Using the small eccentricity assumption on them and making the transition from time to dimensionless time, we obtain:

$$\begin{gathered}\frac{d\bar{a}}{d\tau} = 0 \\ \frac{d\bar{\imath}}{d\tau} = 0 \\ \frac{d\bar{\Omega}}{d\tau} = -\frac{3}{2}J_2\hat{n}\left(\frac{R_e}{a}\right)^2\cos\bar{\imath} \\ \frac{d\bar{e}}{d\tau} = 0 \\ \frac{d\bar{\omega}}{d\tau} = \frac{3}{4}J_2\hat{n}\left(\frac{R_e}{a}\right)^2(5\cos^2\bar{\imath}-1) \\ \frac{d\bar{M}}{d\tau} = \hat{n} + \frac{3}{4}J_2\hat{n}\left(\frac{R_e}{a}\right)^2(3\cos^2\bar{\imath}-1)\end{gathered} \tag{4.32}$$

We now need to get similar expressions for the effects of atmospheric drag. Substituting Eq. (4.28) into Eq. (4.30), we obtain the following expressions:

$$\begin{gathered}\frac{da}{d\tau} \approx -\frac{1}{\beta}a[\hat{n}+3\hat{n}e\cos f - 2\hat{\omega}_e\cos i] \\ \frac{di}{d\tau} \approx -\frac{1}{2}\frac{1}{\beta}\hat{\omega}_e\cos^2\theta\sin i\end{gathered} \tag{4.33}$$

$$\frac{d\Omega}{d\tau} \approx -\frac{1}{2}\frac{1}{\beta}\widehat{\omega}_e \cos\theta \sin\theta$$

$$\frac{de}{d\tau} \approx -\frac{1}{\beta}[\hat{n}e(1+\cos^2 f) + (\hat{n} - 2\widehat{\omega}_e \cos i)\cos f]$$

$$\frac{d\omega}{d\tau} \approx -\frac{1}{\beta}\frac{1}{e}\sin f\,[\hat{n} + \hat{n}e\cos f - 2\widehat{\omega}_e \cos i]$$

$$\frac{dM}{d\tau} \approx \hat{n} + \frac{1}{\beta}\frac{1}{e}\sin f\,[\hat{n} + \hat{n}e\cos f - 2\widehat{\omega}_e \cos i]$$

which can be orbit-averaged using the expression previously introduced in Eq. (4.31):

$$\begin{aligned}
\frac{d\bar{a}}{d\tau} &\approx -\frac{1}{\beta}\bar{a}[\hat{n} - 2\widehat{\omega}_e \cos\bar{\imath}] \\
\frac{d\bar{\imath}}{d\tau} &\approx -\frac{1}{4}\frac{1}{\beta}\widehat{\omega}_e \sin\bar{\imath} \\
\frac{d\bar{\Omega}}{d\tau} &\approx 0 \\
\frac{d\bar{e}}{d\tau} &\approx -\frac{1}{2}\frac{1}{\beta}\hat{n}\bar{e} \\
\frac{d\bar{\omega}}{d\tau} &\approx 0 \\
\frac{dM}{d\tau} &\approx \hat{n}
\end{aligned} \tag{4.34}$$

To obtain the final orbit-averaged expressions describing the motion of a satellite placed in an elliptical orbit perturbed by both the J_2 effects and atmospheric drag, we can combine both set of expressions (4.32 and 4.34):

$$\begin{aligned}
\frac{d\bar{a}}{d\tau} &= -\frac{1}{\beta}\bar{a}[\hat{n} - 2\widehat{\omega}_e \cos\bar{\imath}] \\
\frac{d\bar{\imath}}{d\tau} &= -\frac{1}{4}\frac{1}{\beta}\widehat{\omega}_e \sin\bar{\imath} \\
\frac{d\bar{\Omega}}{d\tau} &= -\frac{3}{2}J_2\hat{n}\left(\frac{R_e}{a}\right)^2 \cos\bar{\imath} \\
\frac{d\bar{e}}{d\tau} &= -\frac{1}{2}\frac{1}{\beta}\hat{n}\bar{e}
\end{aligned} \tag{4.35}$$

$$\frac{d\bar{\omega}}{d\tau} = \frac{3}{4} J_2 \hat{n} \left(\frac{R_e}{a}\right)^2 (5\cos^2 \bar{\imath} - 1)$$

$$\frac{d\bar{M}}{d\tau} = \hat{n} + \frac{3}{4} J_2 \hat{n} \left(\frac{R_e}{a}\right)^2 (3\cos^2 \bar{\imath} - 1)$$

This set of equations will be used later in simulations to describe the motion of the chief spacecraft.

4.2 Relative Perturbations

We have obtained the equations describing the motion of the chief under the effect of aerodynamic drag and J_2 perturbations in the previous section. In this section, we will investigate the effect of those perturbations on the motion of the deputy relative to the chief.

4.2.1 Relative J_2 Perturbations

To obtain the relative acceleration arising in the presence of the J_2 effects, the method proposed by Schweighart and Sedwick (2002) is used. This relative acceleration vector is obtained by multiplying the relative position vector taken in the Hill frame by the gradient of the J_2 potential field:

$$\Delta \mathbf{a}_{J_2} = \nabla \mathbf{J}_2 (r_{ref}) \mathbf{x} \tag{4.36}$$

where the J_2 gradient is given by:

$$\nabla \mathbf{J}_2 = \frac{6\mu J_2 R_e^2}{r_{ref}^5} \begin{bmatrix} 1 - 3\sin^2 i \sin^2 \theta & \sin^2 i \sin 2\theta & \sin 2i \sin \theta \\ \sin^2 i \sin 2\theta & -\frac{1}{4} - \sin^2 i \left(\frac{1}{2} - \frac{7}{4}\sin^2 \theta\right) & -\frac{1}{4}(\sin 2i \cos \theta) \\ \sin 2i \sin \theta & -\frac{1}{4}(\sin 2i \cos \theta) & -\frac{3}{4} + \sin^2 i \left(\frac{1}{2} + \frac{5}{4}\sin^2 \theta\right) \end{bmatrix} \tag{4.37}$$

Similarly to the perturbations analyzed in the previous section, the gradient can be simplified by orbit-averaging it to capture only the secular effects and eliminate the periodic effects. To obtain that simplified version, the following integral is used:

$$\overline{\nabla \mathbf{J}_2} = \frac{1}{2\pi}\int_0^{2\pi} \nabla \mathbf{J}_2 d\theta \tag{4.38}$$

To properly obit-average the gradient, we have to keep in mind that r_{ref} is a function of θ through the previously defined relation:

$$\frac{1}{r_{ref}^5} \approx \frac{1}{a^5}(1 + 5e\cos f) = \frac{1}{a^5}(1 + 5e\cos(\theta - \omega)) \tag{4.39}$$

Keeping this in mind, we can rewrite the integral as:

$$\overline{\nabla \mathbf{J}_2} = n^2\mathbf{Q} + n^2 e\widetilde{\mathbf{Q}} \tag{4.40}$$

where the gradient has been split into two matrices to simplify the analysis. We can now get the value for each component of those matrices. It can be noticed that the **Q** matrix will be a diagonal matrix as all the off-diagonal terms will be zero. Therefore, only the diagonal terms need to be calculated:

$$q_{11} = \frac{3}{2}J_2\left(\frac{R_e}{a}\right)^2(1 + 3\cos 2\mathrm{i}) \tag{4.41}$$

$$q_{22} = -\frac{3}{8}J_2\left(\frac{R_e}{a}\right)^2(1 + 3\cos 2\mathrm{i}) \tag{4.42}$$

$$q_{33} = -\frac{9}{8}J_2\left(\frac{R_e}{a}\right)^2(1 + 3\cos 2\mathrm{i}) \tag{4.43}$$

With the terms calculated we can now define our first matrix to be:

$$\mathbf{Q} = \begin{bmatrix} 4s & 0 & 0 \\ 0 & -s & 0 \\ 0 & 0 & -3s \end{bmatrix} \tag{4.44}$$

where s is a dimensionless parameter similar to the one defined for the circular case by Schweighart and Sedwick (2002):

$$s = \frac{3}{8} J_2 \left(\frac{R_e}{a}\right)^2 (1 + 3\cos 2\mathrm{i}) \tag{4.45}$$

As for the terms of our second matrix, we have:

$$\tilde{q}_{11} = 0 \tag{4.46}$$

$$\tilde{q}_{22} = 0 \tag{4.47}$$

$$\tilde{q}_{33} = 0 \tag{4.48}$$

$$\tilde{q}_{12} = \tilde{q}_{21} = 0 \tag{4.49}$$

$$\tilde{q}_{13} = \tilde{q}_{31} = 15 J_2 \left(\frac{R_e}{a}\right)^2 \sin 2\mathrm{i} \sin \omega \tag{4.50}$$

$$\tilde{q}_{23} = \tilde{q}_{32} = -\frac{15}{4} J_2 \left(\frac{R_e}{a}\right)^2 \sin 2\mathrm{i} \cos \omega \tag{4.51}$$

With these terms, we can now define our second matrix to be:

$$\mathbf{Q} = \begin{bmatrix} 0 & 0 & 4\tilde{s}\sin\omega \\ 0 & 0 & -\tilde{s}\cos\omega \\ 4\tilde{s}\sin\omega & -\tilde{s}\cos\omega & 0 \end{bmatrix} \tag{4.52}$$

where $\tilde{s}$ is a new dimensionless parameter defined as:

$$\tilde{s} = \frac{15}{4} J_2 \left(\frac{R_e}{a}\right)^2 \sin 2\mathrm{i} \tag{4.53}$$

We now have all the elements to obtain the orbit-averaged J_2 gradient:

$$\overline{\nabla \mathbf{J}_2} = n^2 \begin{bmatrix} 4s & 0 & 4e\tilde{s}\sin\omega \\ 0 & -s & -e\tilde{s}\cos\omega \\ 4e\tilde{s}\sin\omega & -e\tilde{s}\cos\omega & -3s \end{bmatrix} \tag{4.54}$$

The dimensionless relative acceleration due to the J_2 perturbations will then be:

$$\Delta\hat{\mathbf{a}}_{J_2} = \frac{1}{n_0^2 d} \Delta\mathbf{a}_{J_2} = \hat{n}^2 \begin{bmatrix} 4s & 0 & 4e\tilde{s}\sin\omega \\ 0 & -s & -e\tilde{s}\cos\omega \\ 4e\tilde{s}\sin\omega & -e\tilde{s}\cos\omega & -3s \end{bmatrix} \begin{bmatrix} \hat{x} \\ \hat{y} \\ \hat{z} \end{bmatrix} \tag{4.55}$$

4.2.2 Relative Drag Perturbations

In this section, we will evaluate the effects of atmospheric drag on the motion of the deputy spacecraft relative to the chief spacecraft. Recall that the acceleration due to atmospheric drag is given by:

$$\mathbf{a}_{Drag} = -\frac{1}{2}\rho\frac{C_D A}{m}\|\mathbf{v}_{rel}\|\mathbf{v}_{rel} \tag{4.56}$$

where is the velocity of the deputy spacecraft relative to the rotating atmosphere as expressed in the Hill frame. Non-dimensionalizing this acceleration term, we obtain:

$$\hat{\mathbf{a}}_{Drag} = \frac{1}{n_0^2 d}\mathbf{a}_{Drag} = -\frac{1}{2}\rho\frac{C_D A}{m}d\|\hat{\mathbf{v}}_{rel}\|\hat{\mathbf{v}}_{rel} \tag{4.55}$$

where the dimensionless velocity $\hat{\mathbf{v}}_{rel}$ is:

$$\hat{\mathbf{v}}_{rel} = \frac{1}{n_0 d}\mathbf{v}_{rel} = \begin{bmatrix} \hat{x}' + \frac{r'_{ref}}{d} - \hat{y}(f' - \widehat{\omega}_e \cos i) - \hat{z}\widehat{\omega}_e \cos\theta \sin i \\ \hat{y}' + \left(\frac{r_{ref}}{d} + \hat{x}\right)(f' - \widehat{\omega}_e \cos i) + \hat{z}\widehat{\omega}_e \sin\theta \sin i \\ \hat{z}' + \left(\frac{r_{ref}}{d} + \hat{x}\right)\widehat{\omega}_e \cos\theta \sin i - \hat{y}\widehat{\omega}_e \sin\theta \sin i \end{bmatrix} \tag{4.56}$$

Similarly to what was done for the circular case, the dimensionless velocity term $\hat{\mathbf{v}}_{rel}$ will be split into two parts. The first part containing the zeroeth order terms in $\hat{x}$, $\hat{y}$, $\hat{z}$, $\hat{x}'$, $\hat{y}'$ and $\hat{z}'$ while the second part holds the first order terms:

$$\hat{\mathbf{v}}_{rel} = \mathbf{v}_0 + \mathbf{v}_1 \tag{4.57}$$

where

$$\mathbf{v}_0 = \begin{bmatrix} \dfrac{r'_{ref}}{d} \\ \dfrac{r_{ref}}{d}(f' - \widehat{\omega}_e \cos i) \\ \dfrac{r_{ref}}{d}\widehat{\omega}_e \cos\theta \sin i \end{bmatrix} \approx \frac{a}{d}\begin{bmatrix} \hat{n} e \sin f \\ \hat{n} + \hat{n} e \cos f - \widehat{\omega}_e \cos i \\ \widehat{\omega}_e \cos\theta \sin i \end{bmatrix} \tag{4.58}$$

$$\begin{gathered} \mathbf{v}_1 = \begin{bmatrix} \hat{x}' - \hat{y}(f' - \widehat{\omega}_e \cos i) - \hat{z}\widehat{\omega}_e \cos\theta \sin i \\ \hat{y}' + \hat{x}(f' - \widehat{\omega}_e \cos i) + \hat{z}\widehat{\omega}_e \sin\theta \sin i \\ \hat{z}' + \hat{x}\widehat{\omega}_e \cos\theta \sin i - \hat{y}\widehat{\omega}_e \sin\theta \sin i \end{bmatrix} \\ \mathbf{v}_1 \approx \begin{bmatrix} \hat{x}' - \hat{y}(\hat{n} + 2\hat{n}e\cos f - \widehat{\omega}_e \cos i) - \hat{z}\widehat{\omega}_e \cos\theta \sin i \\ \hat{y}' + \hat{x}(\hat{n} + 2\hat{n}e\cos f - \widehat{\omega}_e \cos i) + \hat{z}\widehat{\omega}_e \sin\theta \sin i \\ \hat{z}' + \hat{x}\widehat{\omega}_e \cos\theta \sin i - \hat{y}\widehat{\omega}_e \sin\theta \sin i \end{bmatrix} \end{gathered} \tag{4.59}$$

Note that the magnitude of $\mathbf{v}_0$ is significantly larger than that of $\mathbf{v}_1$. We now need to linearize and simplify the following expression:

$$\|\hat{\mathbf{v}}_{rel}\|\hat{\mathbf{v}}_{rel} = \|\mathbf{v}_0 + \mathbf{v}_1\|(\mathbf{v}_0 + \mathbf{v}_1) \tag{4.60}$$

Doing so yield the same results as for the circular case (Eq. (2.47)):

$$\|\mathbf{v}_0 + \mathbf{v}_1\|(\mathbf{v}_0 + \mathbf{v}_1) \approx \|\mathbf{v}_0\|\mathbf{v}_0 + \|\mathbf{v}_0\|\mathbf{v}_1 + \left(\frac{\mathbf{v}_0 . \mathbf{v}_1}{\|\mathbf{v}_0\|}\right)\mathbf{v}_0 \tag{4.61}$$

Let us now look at the value of each term as those will differ from the circular case. We first need to obtain an expression for $\|\mathbf{v}_0\|$:

$$\|\mathbf{v}_0\| = \frac{a}{d}(\hat{n} + \hat{n} e \cos f - \widehat{\omega}_e \cos i) \tag{4.62}$$

With that done, we can obtain the first term in the sum:

$$\|\mathbf{v}_0\|\mathbf{v}_0 = \left(\frac{a}{d}\right)^2 \begin{bmatrix} \hat{n}^2 e \sin f \\ \hat{n}^2 + 2\hat{n}^2 e \cos f - 2\hat{n}\widehat{\omega}_e \cos i \\ \hat{n}\widehat{\omega}_e \cos\theta \sin i \end{bmatrix} \tag{4.63}$$

Similarly to what was done for the relative J_2 perturbations, we will orbit average the terms in the sum to keep only the secular components:

$$\frac{1}{2\pi}\int_0^{2\pi} \|\mathbf{v}_0\|\mathbf{v}_0 d\theta = \left(\frac{a}{d}\right)^2 \begin{bmatrix} 0 \\ \hat{n}^2 - 2\hat{n}\widehat{\omega}_e \cos i \\ 0 \end{bmatrix} \tag{4.64}$$

As for the second term, we obtain:

$$\|\mathbf{v}_0\|\mathbf{v}_1 = \frac{a}{d}(\hat{n} + \hat{n}e\cos f - \widehat{\omega}_e \cos i)\begin{bmatrix}\hat{x}' \\ \hat{y}' \\ \hat{z}'\end{bmatrix} + \frac{a}{d}\begin{bmatrix}-\hat{y}(\hat{n}^2 + 3\hat{n}^2 e\cos f - 2\hat{n}\widehat{\omega}_e \cos i) - \hat{z}\hat{n}\widehat{\omega}_e \cos\theta \sin i \\ (\hat{n}^2 + 3\hat{n}^2 e\cos f - 2\hat{n}\widehat{\omega}_e \cos i) + \hat{z}\hat{n}\widehat{\omega}_e \sin\theta \sin i \\ \hat{x}\hat{n}\widehat{\omega}_e \cos\theta \sin i - \hat{y}\hat{n}\widehat{\omega}_e \sin\theta \sin i\end{bmatrix} \tag{4.65}$$

Orbit-averaging this term results in the following:

$$\frac{1}{2\pi}\int_0^{2\pi}\|\mathbf{v}_0\|\mathbf{v}_1 d\theta = \frac{a}{d}(\hat{n} - \widehat{\omega}_e \cos i)\begin{bmatrix}\hat{x}' \\ \hat{y}' \\ \hat{z}'\end{bmatrix} + \frac{a}{d}\begin{bmatrix}-\hat{y}(\hat{n}^2 - 2\hat{n}\widehat{\omega}_e \cos i) \\ \hat{x}(\hat{n}^2 - 2\hat{n}\widehat{\omega}_e \cos i) \\ 0\end{bmatrix} \tag{4.66}$$

The third term in the sum is more complicated than the first two and will thus be broken up into different segments to simplify its analysis. We will start by each component of the dot product in the numerator. For the x-component, we have:

$$v_{0,x}v_{1,x} = \frac{a}{d}\hat{n}e\sin f\,(\hat{x}' - \hat{y}\hat{n}) \tag{4.67}$$

For the y-component:

$$\begin{aligned} v_{0,y}v_{1,y} = \frac{a}{d}[&\hat{y}'(\hat{n} + \hat{n}e\cos f - \widehat{\omega}_e \cos i) \\ &+ \hat{x}(\hat{n}^2 + 3\hat{n}^2 e\cos f - 2\hat{n}\widehat{\omega}_e \cos i) \\ &+ \hat{z}\hat{n}\widehat{\omega}_e \sin\theta \sin i] \end{aligned} \tag{4.68}$$

For the z-component:

$$v_{0,z}v_{1,z} = \frac{a}{d}\hat{z}'\widehat{\omega}_e \cos\theta \sin i \tag{4.69}$$

We also need to get the inverse of $\|\mathbf{v}_0\|$:

$$\|\mathbf{v}_0\|^{-1} = \frac{d}{a\hat{n}^2}(\hat{n} - e\hat{n}\cos f + \widehat{\omega}_e \cos i) \tag{4.70}$$

We now have all the components to obtain the bracketed part of the third component in Eq. (4.61):

$$\left(\frac{\mathbf{v}_0.\mathbf{v}_1}{\|\mathbf{v}_0\|}\right) = \frac{1}{\hat{n}^2}[\hat{n}^2 e \sin f\,(\hat{x}' - \hat{y}\hat{n}) + \hat{n}^2\hat{y}' \\ + \hat{x}(\hat{n}^3 + 2\hat{n}^3 e\cos f - \hat{n}^2\widehat{\omega}_e \cos i) \\ + \hat{z}\hat{n}^2\widehat{\omega}_e \sin\theta \sin i + \hat{z}'\hat{n}\widehat{\omega}_e \cos\theta \sin i] \tag{4.71}$$

Multiplying this term by the zeroeth order vector to obtain the last part of the sum and orbit-averaging it, we get the following:

$$\frac{1}{2\pi}\int_0^{2\pi}\left(\frac{\mathbf{v}_0.\mathbf{v}_1}{\|\mathbf{v}_0\|}\right)\mathbf{v}_0 d\theta = \frac{a}{d}\begin{bmatrix} 0 \\ \hat{y}'(\hat{n} - \widehat{\omega}_e \cos i) + \hat{x}\hat{n}(\hat{n} - 2\widehat{\omega}_e \cos i) \\ 0 \end{bmatrix} \tag{4.72}$$

Combining all three terms in the sum, we obtain the orbit-averaged dimensionless acceleration due to drag:

$$\hat{\mathbf{a}}_{Drag} = \mathbf{D}_0 + \mathbf{D}_1\hat{\mathbf{x}} + \mathbf{D}_2\hat{\mathbf{x}}' \tag{4.73}$$

where $\mathbf{D}_0$, $\mathbf{D}_1$ and $\mathbf{D}_2$ are given by:

$$\mathbf{D}_0 = -\frac{1}{2}\frac{1}{\beta}\frac{a}{d}\hat{n}\begin{bmatrix} 0 \\ \hat{n} - 2\widehat{\omega}_e \cos i \\ 0 \end{bmatrix} \tag{4.74}$$

$$\mathbf{D}_1 = -\frac{1}{2}\frac{1}{\beta}\hat{n}\begin{bmatrix} 0 & -(\hat{n} - 2\widehat{\omega}_e \cos i) & 0 \\ 2(\hat{n} - 2\widehat{\omega}_e \cos i) & 0 & 0 \\ 0 & 0 & 0 \end{bmatrix} \tag{4.75}$$

$$\mathbf{D}_2 = -\frac{1}{2}\frac{1}{\beta}\begin{bmatrix} (\hat{n} - \widehat{\omega}_e \cos i) & 0 & 0 \\ 0 & 2(\hat{n} - \widehat{\omega}_e \cos i) & 0 \\ 0 & 0 & (\hat{n} - \widehat{\omega}_e \cos i) \end{bmatrix} \tag{4.76}$$

To obtain the acceleration of the deputy relative to the chief we simply need to subtract the acceleration of the chief to that of the deputy. Keeping in mind that the chief remains at the center of the Hill frame, we obtain:

$$\Delta\hat{\mathbf{a}}_{Drag} = -\frac{1}{2}\left(\frac{1}{\beta_D}-\frac{1}{\beta_C}\right)\frac{a}{d}\hat{n}^2\tilde{\sigma}_2\begin{bmatrix}0\\1\\0\end{bmatrix} - \frac{1}{2}\frac{1}{\beta}\hat{n}^2\tilde{\sigma}_2\begin{bmatrix}0 & -1 & 0\\2 & 0 & 0\\0 & 0 & 0\end{bmatrix}\begin{bmatrix}\hat{x}\\\hat{y}\\\hat{z}\end{bmatrix} - \frac{1}{2}\frac{1}{\beta}\hat{n}\tilde{\sigma}_1\begin{bmatrix}1 & 0 & 0\\0 & 2 & 0\\0 & 0 & 1\end{bmatrix}\begin{bmatrix}\hat{x}'\\\hat{y}'\\\hat{z}'\end{bmatrix} \tag{4.77}$$

where

$$\tilde{\sigma}_1 = 1 - \frac{\widehat{\omega}_e}{\hat{n}}\cos i \tag{4.78}$$

$$\tilde{\sigma}_2 = 1 - 2\frac{\widehat{\omega}_e}{\hat{n}}\cos i \tag{4.79}$$

4.3 Final Equations of Motion

In this section, the final equations describing the motion of a deputy spacecraft relative to a chief spacecraft placed on an elliptical orbit will be presented. Those equations account for J_2 perturbations and the effect of atmospheric drag. Although these effects have been orbit-averaged, they capture the secular effects. Similarly, the reference orbit's orbital elements propagation is orbit-averaged to obtain the motion of the chief.

The equations of relative motion placing no constraint on eccentricity have been given earlier in Eq. (4.1). Non-dimensionalizing these equations and using the small eccentricity assumption, we obtain the following dimensionless equations of relative motion:

$$\begin{aligned}&\hat{x}'' - 2\theta'\hat{y}' - \theta''\hat{y} - [(\theta')^2 + 2\hat{n}^2(1 + 3e\cos f)]\hat{x}\\&\qquad = \Delta\hat{a}_{J_2,x} + \Delta\hat{a}_{Drag,x}\\&\hat{y}'' + 2\theta'\hat{x}' - \theta''\hat{x} - [(\theta')^2 - \hat{n}^2(1 + 3e\cos f)]\hat{y}\\&\qquad = \Delta\hat{a}_{J_2,y} + \Delta\hat{a}_{Drag,y}\end{aligned} \tag{4.80}$$

$$\hat{z}'' + \hat{n}^2(1 + 3e\cos f)\hat{z} = \Delta\hat{a}_{J_2,z} + \Delta\hat{a}_{Drag,z}$$

where the first and second derivatives of the true latitude θ are the only undefined terms. We must therefore define those two parameters. The first derivative θ' is the instantaneous rotation rate of the Hill frame and depends on the derivatives of the true anomaly f, the right ascension of ascending node Ω and the argument of perigee ω. In an unperturbed circular orbit, Ω and ω are constant and the true anomaly's derivative becomes the orbital rate n. However, due to the elliptic nature of the reference orbit, f and f' are functions of time and, as previously shown in Eq. (4.35), Ω and ω vary with time due to J_2 effects. To combine the three rates, they must be projected along the z-direction. The f' and ω' vectors are, by definition, aligned with the orbit normal vector. On the other hand, the Ω' vector is normal to the equatorial plane and, thus, points along the Z-direction (refer to Fig. 2.2). Summing the components of all three rates along the cross-track direction, we obtain the following:

$$\theta' = f' + \omega' + \Omega' \cos i \tag{4.81}$$

Using the orbit-averaged rates of Eq. (4.35) to approximate ω' and Ω', the above equations can be rewritten as:

$$\theta' = f' + \frac{d\bar{\omega}}{d\tau} + \frac{d\bar{\Omega}}{d\tau}\cos i \tag{4.82}$$

Part of this equation can be further simplified:

$$\frac{d\bar{\omega}}{d\tau} + \frac{d\bar{\Omega}}{d\tau}\cos i = \frac{3}{8}J_2\hat{n}\left(\frac{R_e}{a}\right)^2(1 + 3\cos 2i) = \hat{n}s \tag{4.83}$$

Such that we get the following expression for the instantaneous rotation rate of the Hill frame:

$$\theta' = f' + \hat{n}s \approx \hat{n}(1 + 2e\cos f + s) \tag{4.84}$$

However, we note that there is an inconsistency here with the Schweighart and Sedwick formulation, since in their formulation this rate is given as:

$$\theta' = \hat{n}(1+s)^{1/2} \tag{4.85}$$

which can be approximated as:

$$\theta' \approx \hat{n}\left(1+\frac{1}{2}s\right) \tag{4.86}$$

while in our formulation, ignoring eccentricity, we have:

$$\theta' \approx \hat{n}(1+s) \tag{4.87}$$

There seems to be a missing $-\frac{1}{2}s$ term in the brackets. This could be due the effect of J_2 perturbations on f' which we haven't analyzed. Assuming that this is indeed the case, we will make the change to Eq. (4.84) to obtain a rate consistent with the Schweighart and Sedwick formulation:

$$\theta' \approx \hat{n}\left(1+2e\cos f+\frac{1}{2}s\right) \tag{4.88}$$

With θ' now defined, we can now determine the two remaining unknowns in the relative motion equations, namely $(\theta')^2$ and θ''. The square of θ' can be simplified using the small eccentricity assumption combined with a binomial expansion to:

$$(\theta')^2 \approx \hat{n}^2(1+4e\cos f+s) \tag{4.89}$$

Obtaining θ'' is slightly more complicated however. It first requires us to use the chain rule:

$$\theta'' = \frac{d}{d\tau}\theta' \approx \frac{d}{d\tau}\left[\hat{n}\left(1+2e\cos f+\frac{1}{2}s\right)\right] \tag{4.90}$$

$$\theta'' \approx -\frac{3}{2}\hat{n}\frac{1}{a}\frac{da}{d\tau}\left(1 + 2e\cos f + \frac{1}{2}s\right) + \hat{n}\left(2\frac{de}{d\tau}\cos f - 2e\frac{df}{d\tau}\sin f + \frac{1}{2}\frac{ds}{d\tau}\right)$$

Substituting the orbit-averaged derivatives and simplifying the resulting terms leads to the following expression:

$$\theta'' \approx \hat{n}^2\left[\frac{3}{2}\frac{1}{\beta_C}\left(1 + \frac{4}{3}e\cos f - 2\frac{\widehat{\omega}_e}{\hat{n}}\cos i + \frac{1}{2}s\right) - 2e\cos f\right] \tag{4.91}$$

Looking at the term in the parentheses multiplying the inverse of the ballistic coefficient is highly similar to the $\tilde{\sigma}_2$ previously defined. The difference lies in the orbit-averaging operation that was done earlier to define that term. To remain consistent and for the added precision, we will redefine the previously defined term as:

$$\tilde{\sigma}_1 = 1 + \frac{2}{3}e\cos f - \frac{\widehat{\omega}_e}{\hat{n}}\cos i \tag{4.92}$$

$$\tilde{\sigma}_2 = 1 + \frac{4}{3}e\cos f - 2\frac{\widehat{\omega}_e}{\hat{n}}\cos i \tag{4.93}$$

We now have all the terms defined for the dimensionless relative motion equations, which are given in matrix form as:

$$\mathbf{M}_e\hat{\mathbf{x}}'' + \mathbf{C}_e\hat{\mathbf{x}}' + \mathbf{K}_e\hat{\mathbf{x}} = \mathbf{f}_e \tag{4.94}$$

where the generalized inertia matrix $\mathbf{M}_e$, positive definite damping matrix $\mathbf{C}_e$, stiffness matrix $\mathbf{K}_e$ and forcing function $\mathbf{f}_e$ are given by:

$$\mathbf{M}_e = \begin{bmatrix} 1 & 0 & 0 \\ 0 & 1 & 0 \\ 0 & 0 & 1 \end{bmatrix} = \mathbf{I} \tag{4.95}$$

$$\mathbf{C}_e = \hat{n}\begin{bmatrix} \frac{1}{2}\frac{1}{\beta_D}\tilde{\sigma}_1 & -2\left(1+2e\cos f+\frac{1}{2}s\right) & 0 \\ 2\left(1+2e\cos f+\frac{1}{2}s\right) & \frac{1}{\beta_D}\tilde{\sigma}_1 & 0 \\ 0 & 0 & \frac{1}{2}\frac{1}{\beta_D}\tilde{\sigma}_1 \end{bmatrix} \tag{4.96}$$

$$\mathbf{K}_e = \hat{n}^2\begin{bmatrix} -(3+10e\cos f+5s) & -\frac{\theta''}{\hat{n}^2}-\frac{1}{2}\frac{1}{\beta_D}\tilde{\sigma}_2 & -4e\tilde{s}\sin\omega \\ -\frac{\theta''}{\hat{n}^2}+\frac{1}{\beta_D}\tilde{\sigma}_2 & -e\cos f & e\tilde{s}\cos\omega \\ -4e\tilde{s}\sin\omega & e\tilde{s}\cos\omega & 1+3e\cos f+3s \end{bmatrix} \tag{4.97}$$

$$\mathbf{f}_e = -\frac{1}{2}\left(\frac{1}{\beta_D}-\frac{1}{\beta_C}\right)\frac{a}{d}\hat{n}^2\tilde{\sigma}_2\begin{bmatrix}0\\1\\0\end{bmatrix} \tag{4.98}$$

To make sure the resulting matrices are consistent with the ones from the Scweighart and Sedwick equations, the matrices $\mathbf{C}_e$ and $\mathbf{K}_e$ will be reformulated in terms of c:

$$\mathbf{C}_e = \hat{n}\begin{bmatrix} \frac{1}{2}\frac{1}{\beta_D}\tilde{\sigma}_1 & -2(c+2e\cos f) & 0 \\ 2(c+2e\cos f) & \frac{1}{\beta_D}\tilde{\sigma}_1 & 0 \\ 0 & 0 & \frac{1}{2}\frac{1}{\beta_D}\tilde{\sigma}_1 \end{bmatrix} \tag{4.99}$$

$$\mathbf{K}_e = \hat{n}^2\begin{bmatrix} -(5c^2-2+10e\cos f) & -\frac{\theta''}{\hat{n}^2}-\frac{1}{2}\frac{1}{\beta_D}\tilde{\sigma}_2 & -4e\tilde{s}\sin\omega \\ -\frac{\theta''}{\hat{n}^2}+\frac{1}{\beta_D}\tilde{\sigma}_2 & -e\cos f & e\tilde{s}\cos\omega \\ -4e\tilde{s}\sin\omega & e\tilde{s}\cos\omega & 3c^2-2+3e\cos f \end{bmatrix} \tag{4.100}$$

As expected, setting the drag and eccentricity terms to zero, we go back to the Schweighart and Sedwick equations. Finally, the equations can be written is state-space from as:

$$\mathbf{X}' = \mathbf{A}_e\mathbf{X} + \mathbf{W}_e \tag{4.101}$$

where

$$\mathbf{X} = \begin{bmatrix} \mathbf{x} \\ \mathbf{x}' \end{bmatrix} \tag{4.102}$$

$$\mathbf{A}_e = \begin{bmatrix} \mathbf{0}_{3\times3} & \mathbf{M}_e \\ -\mathbf{K}_e & -\mathbf{C}_e \end{bmatrix} \tag{4.103}$$

$$\mathbf{W}_e = \begin{bmatrix} \mathbf{0}_{3\times1} \\ \mathbf{f}_e \end{bmatrix} \tag{4.104}$$

In the matrices the terms including a $\tilde{\sigma}$ or a β refer to the characterize the effects of drag while the ones that include a $\tilde{s}$ or a s refer to J_2 effects. When calculating the dimensionless ballistic coefficients, it is very important to calculate the local atmospheric density for both spacecraft as they will not be the same, primarily due to the eccentric nature of the orbit leading to different altitudes for both.

4.4 Control Schemes

In this section, two different methods of performing formation maintenance in elliptic orbits will be presented. In both cases differential atmospheric drag will be used as means of control.

4.4.1 Energy Controller

The controller presented in this section is based on the works of Kumar, Alfred Ng, Yoshihara and De Ruiter (2007). In their work, they have developed a PID controller capable of performing formation maintenance for formation placed in circular orbits. This PID controller used the difference between the spacecrafts' energy and their desired energy to determine the area change needed to maintain the desired formation. We wish to see if this method can be applied to formation placed in orbits of small eccentricity.

The control law given by Kumar, Alfred Ng, Yoshihara and De Ruiter is as follows:

$$\delta A = K_P \delta E + K_I \int \delta E d\tau + K_D \frac{d\delta E}{d\tau} \tag{4.105}$$

where δA is the change in area needed, δE is the difference in energy and K_P, K_I and K_D are control gains. If we consider the state of the two spacecraft in the Hill frame centered on the chief, it becomes apparent that the chief's energy can be seen as always being equal to its desired energy. Therefore, only the deputy spacecraft's energy will be compared to its desired energy. The energy of a spacecraft is given by:

$$E = \frac{1}{2} v^2 - \frac{\mu}{r} \tag{4.106}$$

where v is its absolute velocity and r its distance from the center of the Earth and are given by:

$$r = \left\| \mathbf{r}_{ref} + \mathbf{R}_{Hill \to ECI} \mathbf{x} \right\| \tag{4.107}$$

$$v = \left\| \mathbf{v}_{ref} + \mathbf{R}_{Hill \to ECI} \dot{\mathbf{x}} + \dot{\mathbf{R}}_{Hill \to ECI} \mathbf{x} \right\| \tag{4.108}$$

The absolute velocity of the Hill frame and the rotation matrix $\mathbf{R}_{Hill \to ECI}$ are defined as:

$$\mathbf{v}_{ref} = \sqrt{\frac{\mu}{r_{ref}}} \begin{bmatrix} -c_\Omega s_\theta - s_\Omega c_i c_\theta \\ -s_\Omega s_\theta + c_\Omega c_i c_\theta \\ s_i s_\theta \end{bmatrix} \tag{4.109}$$

$$\mathbf{R}_{Hill \to ECI} = \begin{bmatrix} c_\theta c_\Omega - s_\theta c_i s_\Omega & -s_\theta c_\Omega - c_\theta c_i s_\Omega & s_i s_\Omega \\ c_\theta s_\Omega - s_\theta c_i c_\Omega & -s_\theta s_\Omega - c_\theta c_i c_\Omega & -s_i c_\Omega \\ s_\theta s_i & c_\theta s_i & c_i \end{bmatrix} \tag{4.110}$$

where c and s denote the sine and cosine functions of the angle given as subscript. The dimensionless time derivative of $\mathbf{R}_{Hill \to ECI}$ can be obtained as we know the derivative for all the angles of the matrix. Using these equations, it is now possible to obtain the value of δE at any time. From there, $\int \delta E d\tau$ and $\frac{d\delta E}{d\tau}$

can be obtained numerically and, thus, δA can be determined for a specified set of control gains.

4.4.2 Floquet-Lyapunov Controller

The control scheme presented in this section is based on Floquet-Lyapunov theory and a control method proposed by Lee and Balas (1999). Similarly to the circular case the elliptical system cannot be controlled in the cross-track direction through differential atmospheric drag. For this reason, we will limit our analysis to the in-plane case. To control the in plane motion via aerodynamic drag, we need to have a system of the form:

$$\mathbf{X}'(\tau) = \mathbf{A}_e(\tau)\mathbf{X}(\tau) + \mathbf{B}(\tau)u(\tau) \tag{4.111}$$

where the control input $u(\tau)$ is a function of the projected areas of both chief and deputy spacecraft. Note that the matrix $\mathbf{A}_e$ in equation differs from the one in Eq. (4.103) as it is now 4x4 matrix instead of a 6x6 matrix. Obtaining the desired form can be done by rewriting the forcing function $\mathbf{f}_e$ of Eq. (4.98) as:

$$\mathbf{f_e} = \alpha(\Delta\tilde{A})\begin{bmatrix}0\\1\end{bmatrix} \tag{4.112}$$

where

$$\alpha = -\frac{1}{2}\frac{C_D}{m}\frac{a^2}{d}\hat{n}^2\tilde{\sigma}_2 \tag{4.113}$$

$$\Delta\tilde{A} = (\rho_D A_D - \rho_C A_C) \tag{4.114}$$

Then $\mathbf{B}(\tau)$ and $u(\tau)$ can be given as:

$$\mathbf{B}(\tau) = [0 \quad 0 \quad 0 \quad \alpha]^T \tag{4.115}$$

$$u(\tau) = \Delta\tilde{A} \tag{4.116}$$

A major difference between the equations of motion for the circular case and the ones for elliptical case becomes apparent when looking at the damping and stiffness matrices. In the circular case these two matrices are constant, but in the elliptical case those matrices become periodically time-varying. In fact, both matrices $\mathbf{A}_e(\tau)$ and $\mathbf{B}(\tau)$ are periodically time-varying. Regular time invariant methods of control are thus inappropriate in dealing with this system. One way of controlling the system is use Floquet-Lyapunov theory in conjunction with a controller proposed by Lee and Balas (1992). The first step is to apply the Floquet-Lyapunov transformation to our system. This transformation is given as:

$$\mathbf{X}(\tau) = \mathbf{L}(\tau)\mathbf{Z}(\tau) \tag{4.117}$$

This transformation leads to the following system:

$$\mathbf{Z}'(\tau) = \widetilde{\mathbf{A}}\mathbf{Z}(\tau) + \widetilde{\mathbf{B}}(\tau)u(\tau) \tag{4.118}$$

This new system is similar in form to that of Eq. (4.111), but the key difference lies in the fact that the $\widetilde{\mathbf{A}}$ matrix is constant instead of periodically time-varying. The $\widetilde{\mathbf{B}}(\tau)$ matrix, however, while different from the $\mathbf{B}(\tau)$ matrix, is still periodically time-varying. The $\widetilde{\mathbf{A}}$ and $\widetilde{\mathbf{B}}(\tau)$ matrices are defined as:

$$\widetilde{\mathbf{A}} = \mathbf{L}^{-\mathbf{1}}(\tau)\mathbf{A}(\tau)\mathbf{L}(\tau) - \mathbf{L}^{-\mathbf{1}}(\tau)\mathbf{L}'(\tau) \tag{4.119}$$

$$\widetilde{\mathbf{B}}(\tau) = \mathbf{L}^{-\mathbf{1}}(\tau)\mathbf{B}(\tau) \tag{4.120}$$

The periodically time-varying matrix $\mathbf{L}(\tau)$ can be determined from if we know the system's state transition matrix. Obtaining the state transition matrix is not a problem since there exist multiple methods to obtain it numerically such as the ones described by Friedmann, Hammond and Woo (1977). From Floquet-Lyapunov theory, we know that:

$$\mathbf{\Phi}(\tau, 0) = \mathbf{L}(\tau)\exp(\tau\mathbf{F}) \tag{4.121}$$

Since our system is T_A-periodic, we can say that $\mathbf{L}(T_A) = \mathbf{L}(0) = \mathbf{I}$, such that $\mathbf{F}$ can be obtained by solving:

$$\mathbf{\Phi}(T_A, 0) = \exp(T_A\mathbf{F}) \tag{4.122}$$

$\mathbf{L}(\tau)$ is then given by:

$$\mathbf{L}(\tau) = \mathbf{\Phi}(\tau, 0)\exp(-\tau\mathbf{F}) \tag{4.123}$$

Now, if we consider the ideal system where $\widetilde{\mathbf{B}}$ is a constant column vector:

$$\mathbf{Z}^{*\prime}(\tau) = \widetilde{\mathbf{A}}\mathbf{Z}^*(\tau) + \widetilde{\mathbf{B}}u^*(\tau) \tag{4.124}$$

We can obtain a constant gain matrix $\widetilde{\mathbf{G}}$ that will stabilize this ideal system through the feedback law:

$$u^*(\tau) = \widetilde{\mathbf{G}}\mathbf{Z}^*(\tau) \tag{4.125}$$

If we define the error in the signal that will be given to feedback law as:

$$\mathbf{E}^*(\tau) = \mathbf{Z}(\tau) - \mathbf{Z}^*(\tau) \tag{4.126}$$

then we can obtain the error between the system in Eq. (4.112) and the ideal system as:

$$\begin{gathered}\mathbf{E}^{*\prime}(\tau) = \mathbf{Z}'(\tau) - \mathbf{Z}^{*\prime}(\tau) = \left[\widetilde{\mathbf{A}}\mathbf{Z}(\tau) + \widetilde{\mathbf{B}}(\tau)u(\tau)\right] - \left[\widetilde{\mathbf{A}}\mathbf{Z}^*(\tau) + \widetilde{\mathbf{B}}u^*(\tau)\right] \\ \mathbf{E}^{*\prime}(\tau) = \left(\widetilde{\mathbf{A}} + \widetilde{\mathbf{B}}\widetilde{\mathbf{G}}\right)\mathbf{E}^*(\tau) + \left[\widetilde{\mathbf{B}}(\tau)u(\tau) - \widetilde{\mathbf{B}}\widetilde{\mathbf{G}}\mathbf{Z}(\tau)\right]\end{gathered} \tag{4.127}$$

In order for the error system to be stable the second term in Eq. (4.127) must be equal to zero. This leads to:

$$u(\tau) = \widetilde{\mathbf{B}}^{\#}(\tau)\widetilde{\mathbf{B}}\widetilde{\mathbf{G}}\mathbf{Z}(\tau) = \widetilde{\mathbf{G}}(\tau)\mathbf{Z}(\tau) = \widetilde{\mathbf{G}}(\tau)\mathbf{L}^{-1}(\tau)\mathbf{X}(\tau) \tag{4.128}$$

where $\widetilde{\mathbf{B}}^{\#}(\tau)$ is the Moore-Penrose pseudoinverse satisfying $\widetilde{\mathbf{B}}^{\#}(\tau)\widetilde{\mathbf{B}}(\tau) = \mathbf{I}$. It can be obtained as:

$$\widetilde{\mathbf{B}}^{\#}(\tau) = \left[\widetilde{\mathbf{B}}^{T}(\tau)\widetilde{\mathbf{B}}(\tau)\right]^{-\mathbf{1}}\widetilde{\mathbf{B}}^{T}(\tau) \tag{4.129}$$

If we use $\mathrm{X}(\mathrm{t})$ in the control law given in Eq. (4.128), the deputy will be driven towards the chief's position at the center of the Hill frame. To maintain the formation, we need to replace $\mathrm{X}(\mathrm{t})$ by $\mathrm{X}_e(\mathrm{t})$, which is the error in the deputy's relative position with respect to the chief.

$$\mathbf{X}_e(t) = \mathbf{X}(t) - \mathbf{X}_d(t) \tag{4.130}$$

Here, $\mathrm{X}_{\boldsymbol{d}}(\mathrm{t})$ is the desired position of the deputy and depends on the formation that is to be achieved.

Chapter 5 – Numerical Simulations for Elliptical Reference Orbits

In this section, numerical simulations based on the equations of motion presented in Chapter 4 will be presented. The first set of simulations will be for circular reference orbits, in order to compare them with the ones presented in Chapter 3 and thus validate the new set of equations. The second set of simulations will demonstrate the effect of eccentricity on a formation. The final three sets of simulations will show the effectiveness of the three controllers proposed to perform formation maintenance.

5.1 Uncontrolled Projected Circular Formation

The desired motion of the deputy relative to the chief is given by Vaddi and Vadali (2003) as:

$$\begin{aligned}
x_d &= \frac{d}{2}\sin(nct+\alpha) \\
y_d &= d\cos(nct+\alpha) \\
z_d &= d\sin(nct+\alpha) \\
\dot{x}_d &= \frac{dnc}{2}\cos(nct+\alpha) \\
\dot{y}_d &= -dnc\sin(nct+\alpha) \\
\dot{z}_d &= dnc\cos(nct+\alpha)
\end{aligned} \tag{5.1}$$

where α is the initial phase angle in the y- z plane. Setting this term to zero and non-dimensionalizing the set of equations, the following set of equation is obtained:

$$
\begin{aligned}
x_d &= \frac{1}{2}\sin(\hat{n}c\tau) \\
y_d &= \cos(\hat{n}c\tau) \\
z_d &= \sin(\hat{n}c\tau) \\
\dot{x}_d &= \frac{\hat{n}c}{2}\cos(\hat{n}c\tau) \\
\dot{y}_d &= -\hat{n}c\sin(\hat{n}c\tau) \\
\dot{z}_d &= \hat{n}c\cos(\hat{n}c\tau)
\end{aligned}
\tag{5.2}
$$

Setting the dimensionless time to zero we obtain the following initial conditions for this type of formation:

$$
\begin{aligned}
\hat{x}_0 &= 0 \\
\hat{y}_0 &= 1 \\
\hat{z}_0 &= 0 \\
\hat{x}_0' &= \frac{c}{2} \\
\hat{y}_0' &= 0 \\
\hat{z}_0' &= c
\end{aligned}
\tag{5.3}
$$

5.1.1 Comparison of Results for Circular Orbits

A small comparative study between the elliptical model and the circular model was undertaken using the TECSAS physical parameters. In theory, the results obtained for both models should be the same when simulating for a circular orbit and identical initial reference orbit parameters (Table 3.3).

The first simulation was performed for a reference orbit placed at an altitude of 450 km (Fig 5.1). The results obtained are very similar to those of Chapter 3. The in-plane motion is still unaffected and therefore identical. However, there is a slight difference in the cross-track motion as the drift obtained seems to be large than that obtained in Chapter 3.

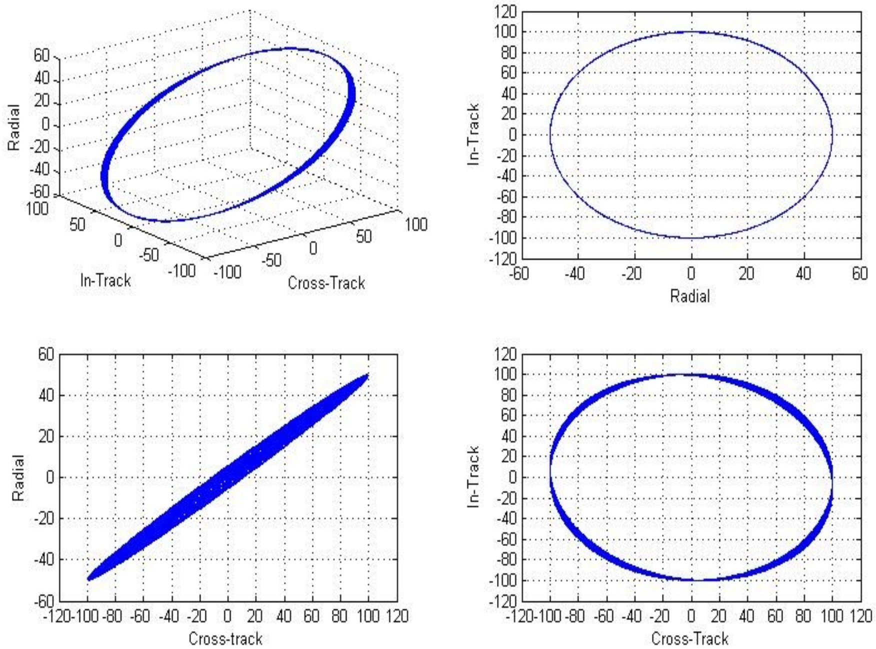

Figure 5.1: Projected Circular Motion – J_2 and Drag Perturbations – Altitude of 450 km – TECSAS Physical Parameters – Uncontrolled – 24 hours

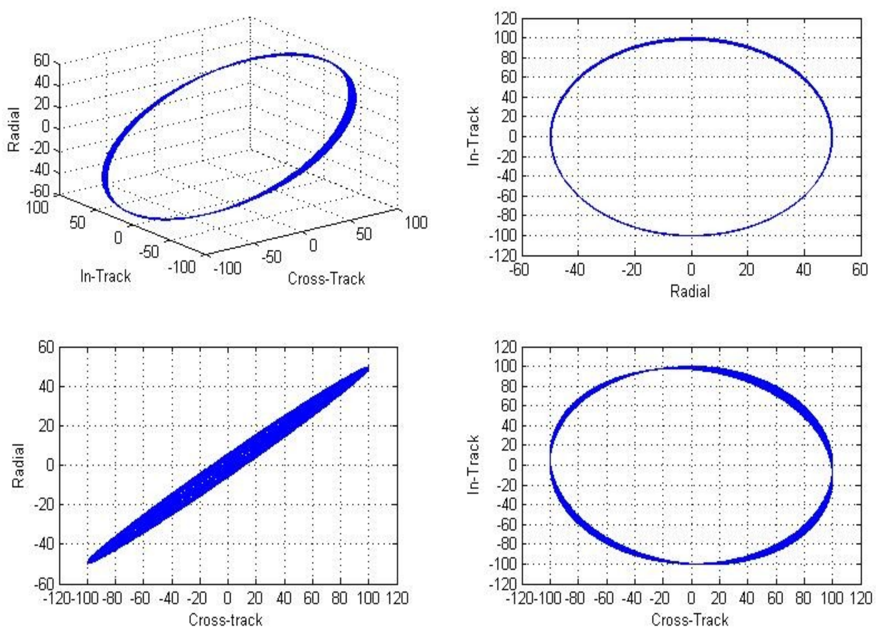

Figure 5.2: Projected Circular Motion – J_2 and Drag Perturbations – Altitude of 350 km – TECSAS Physical Parameters – Uncontrolled – 24 hours

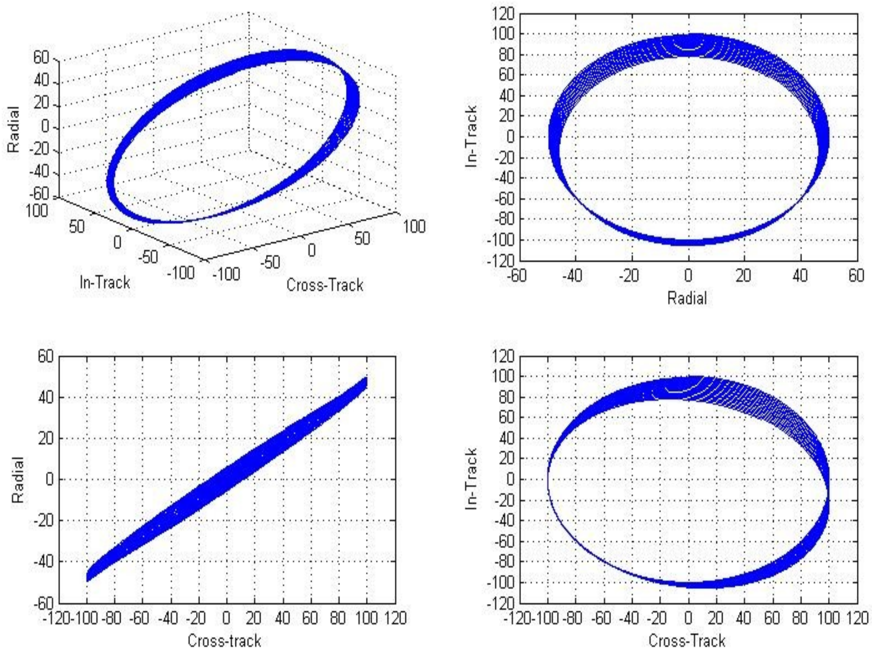

Figure 5.3: Projected Circular Motion – J_2 and Drag Perturbations – Altitude of 250 km – TECSAS Physical Parameters – Uncontrolled – 24 hours

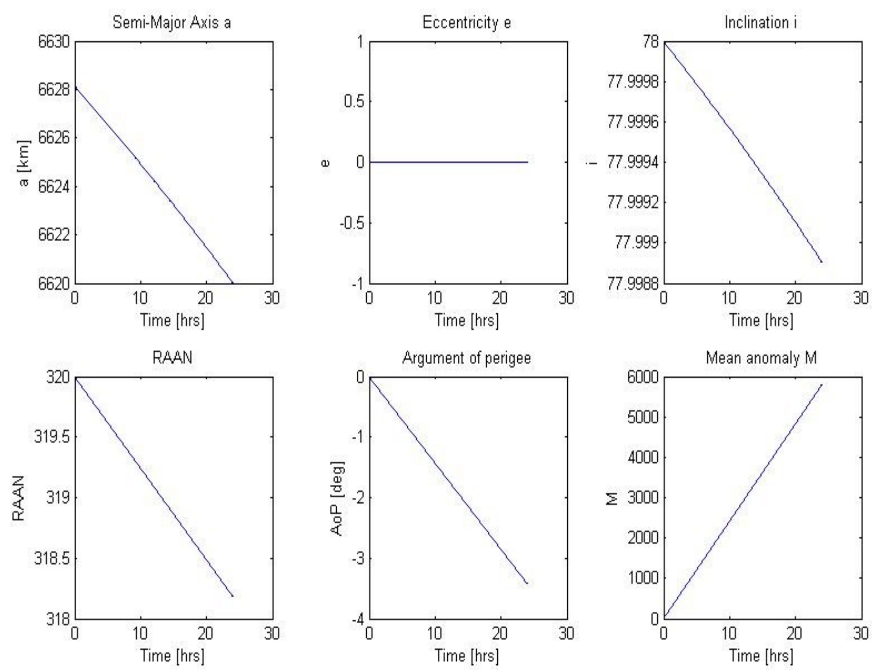

Figure 5.4: Drift of Orbital Elements – J_2 and Drag Perturbations – Altitude of 250 km – TECSAS Physical Parameters – Uncontrolled – 24 hours

The second simulation (Fig 5.2) result also shows an overestimation of the cross-track drift. However, at this altitude a difference in the in-plane motion become apparent as well. While the damping is still present, the in-track drift predicted here is smaller than what had been predicted in Chapter 3. The result for an altitude of 250 km (Fig 5.3) confirms that, while the results are similar, there is a slight overestimation of the cross-track drift and a small underestimation of the in-track drift. Finally, Fig. 5.4 shows the drift of the reference orbit's orbital elements over 24 hours for an initial altitude of 250 km.

5.1.2 Results for Elliptical Orbits

To evaluate the impact that eccentricity has on a formation, a few simulations were performed for different altitudes and values of eccentricities. The TECSAS physical parameters were again used along with the following initial reference orbit parameters:

Elliptical Reference Orbit Parameters		
Parameter	**Value**	**Units**
ω	0	[deg]
i	78	[deg]
Ω	320	[deg]
M	0	[deg]

Table 5.1: Initial Reference Orbit Parameters

The first set of simulations is for an eccentricity of 10^{-6}. Comparing Figs. 5.5 and 5.6 with Figs. 5.2 and 5.3, it is clear that such a low eccentricity had no significant effect on the relative motion. However, increasing the eccentricity to 10^{-5} yields different results. An in-track drift becomes noticeable and this drift is of the order of those caused by the J_2 perturbations and atmospheric drag.

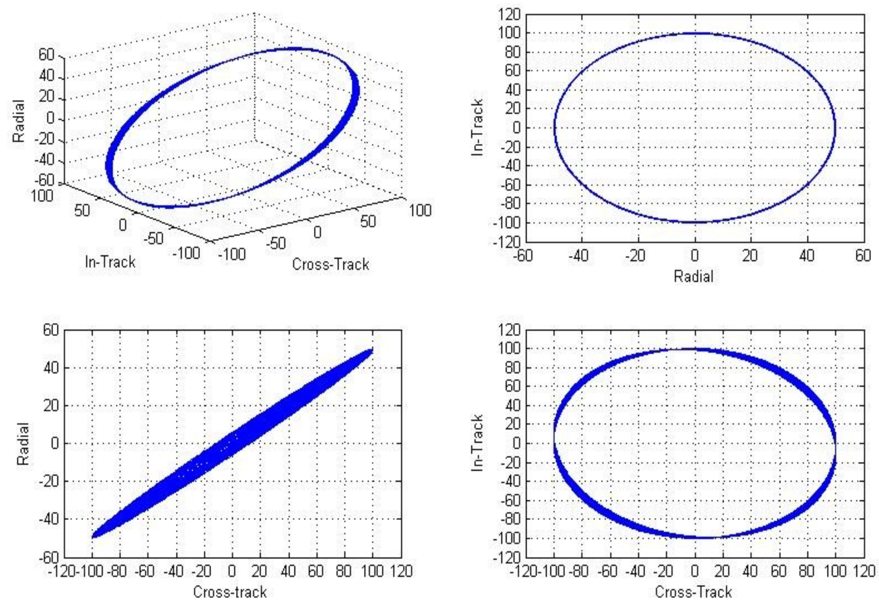

Figure 5.5: Projected Circular Motion – J_2 and Drag Perturbations – Perigee Altitude of 350 km – $e = 10^{-6}$ – TECSAS Physical Parameters – Uncontrolled – 24 hours

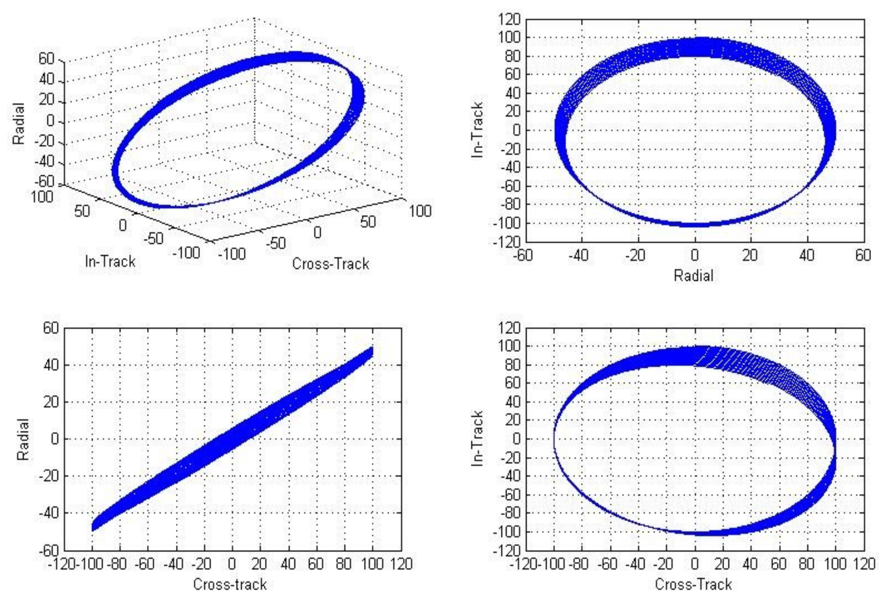

Figure 5.6: Projected Circular Motion – J_2 and Drag Perturbations – Perigee Altitude of 250 km – $e = 10^{-6}$ – TECSAS Physical Parameters – Uncontrolled – 24 hours

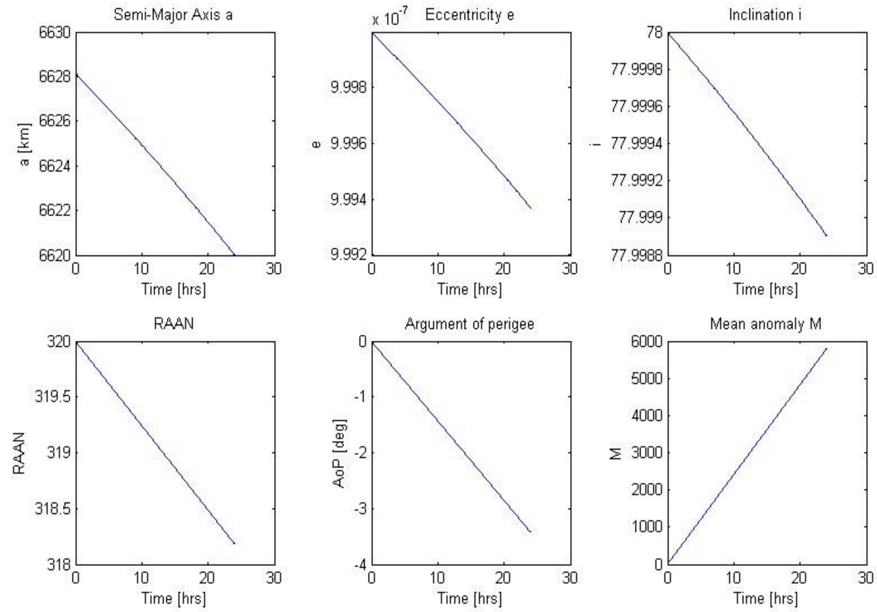

Figure 5.7: Drift of Orbital Elements – J_2 and Drag Perturbations –Perigee Altitude of 250 km – e = 10^{-6} – TECSAS Physical Parameters – Uncontrolled – 24 hours

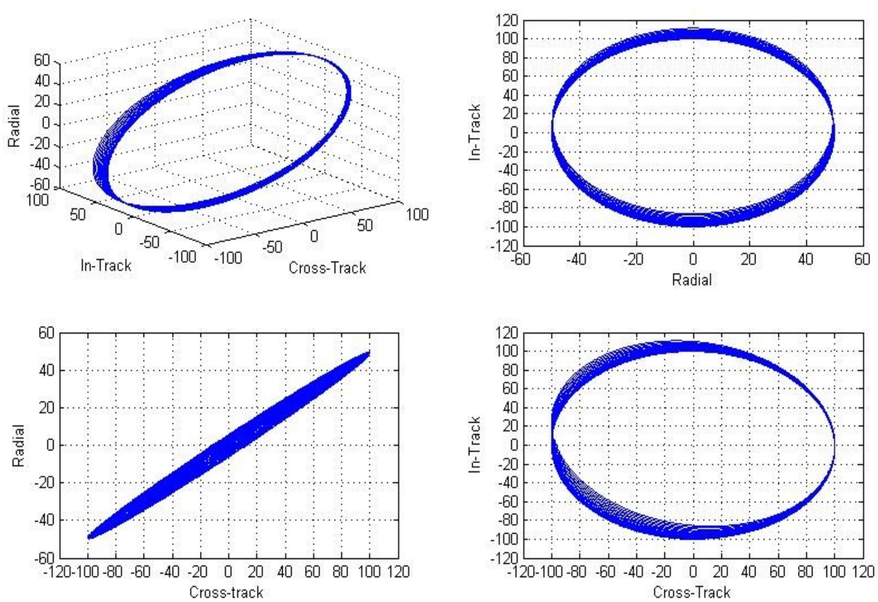

Figure 5.8: Projected Circular Motion – J_2 and Drag Perturbations – Perigee Altitude of 350 km – e = 10^{-5} – TECSAS Physical Parameters – Uncontrolled – 24 hours

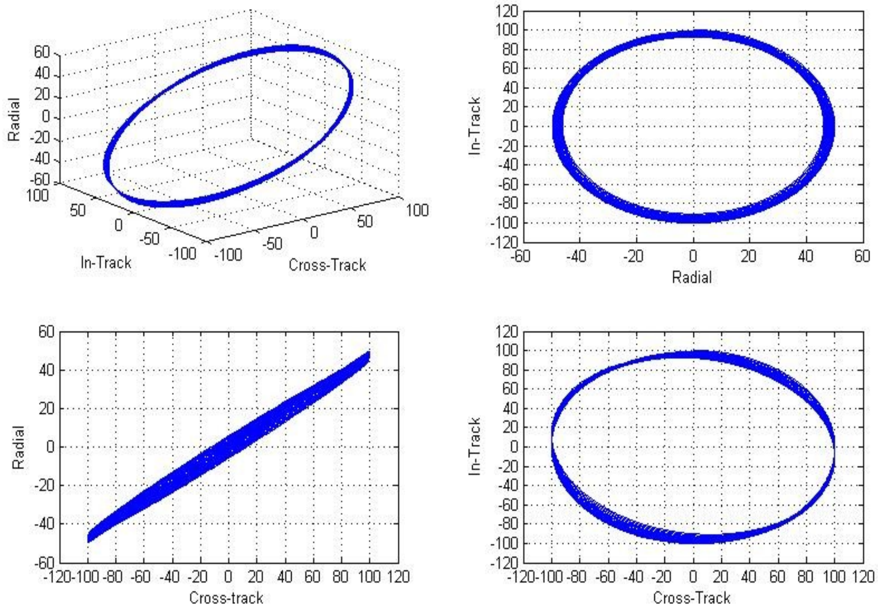

Figure 5.9: Projected Circular Motion – J_2 and Drag Perturbations – Perigee Altitude of 250 km – e = 10^{-5} – TECSAS Physical Parameters – Uncontrolled – 24 hours

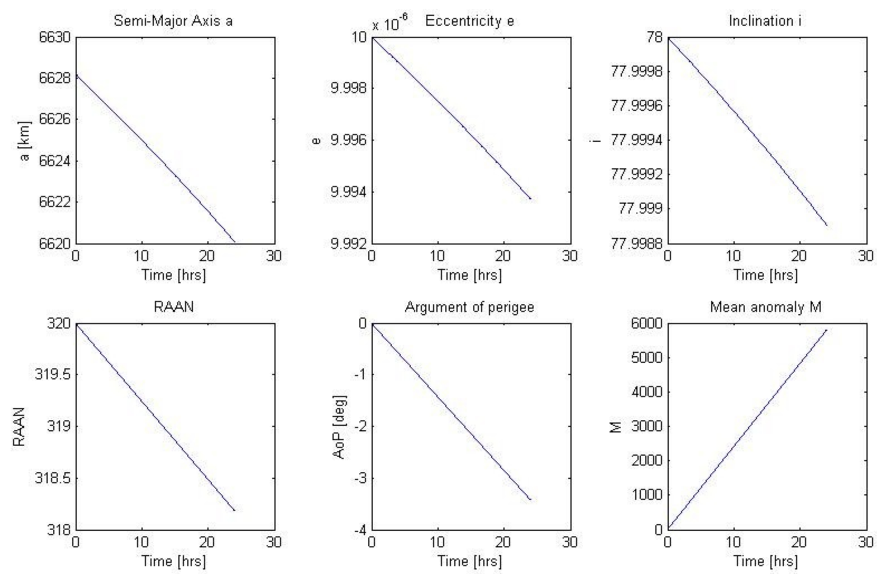

Figure 5.10: Drift of Orbital Elements – J_2 and Drag Perturbations –Perigee Altitude of 250 km – e = 10^{-5} – TECSAS Physical Parameters – Uncontrolled – 24 hours

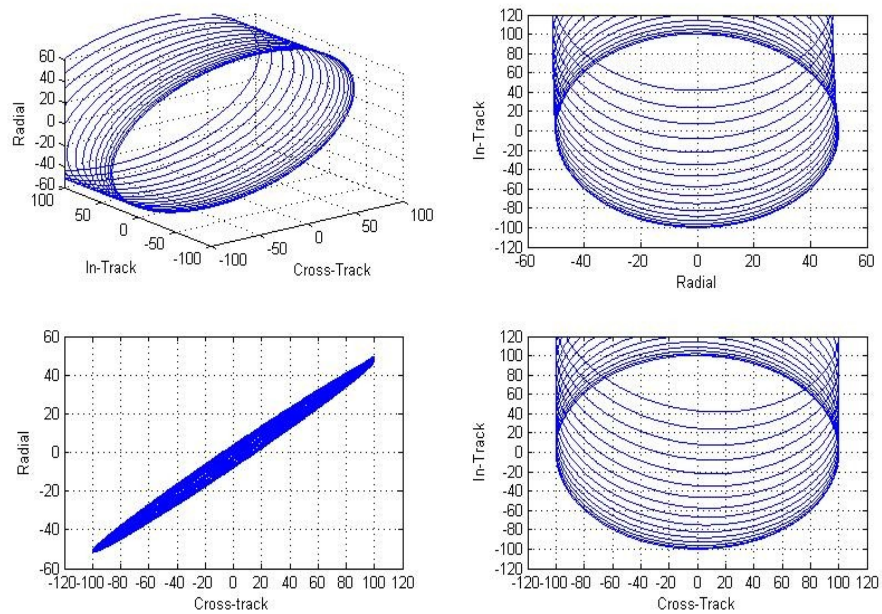

Figure 5.11: Projected Circular Motion – J_2 and Drag Perturbations – Perigee Altitude of 350 km – e = 10^{-4} – TECSAS Physical Parameters – Uncontrolled – 24 hours

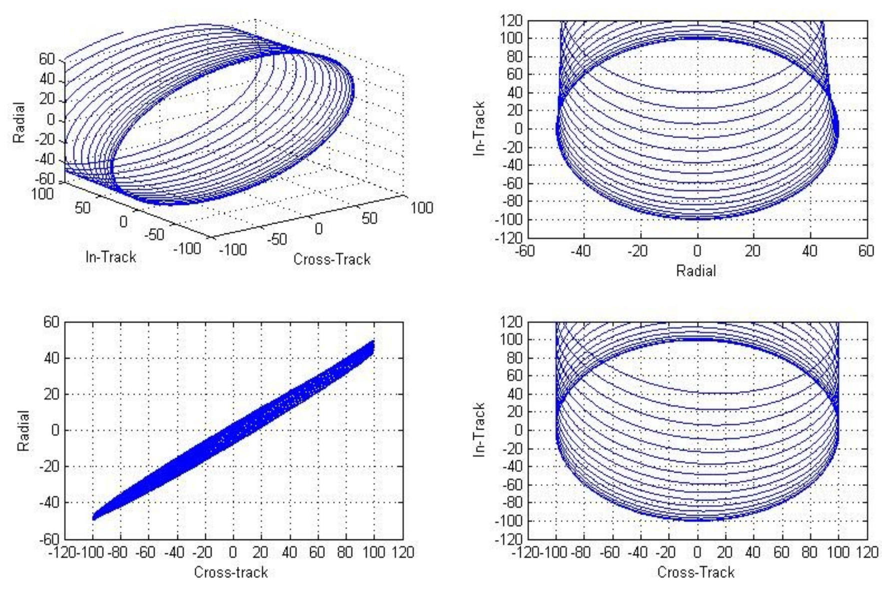

Figure 5.12: Projected Circular Motion – J_2 and Drag Perturbations – Perigee Altitude of 250 km – e = 10^{-4} – TECSAS Physical Parameters – Uncontrolled – 24 hours

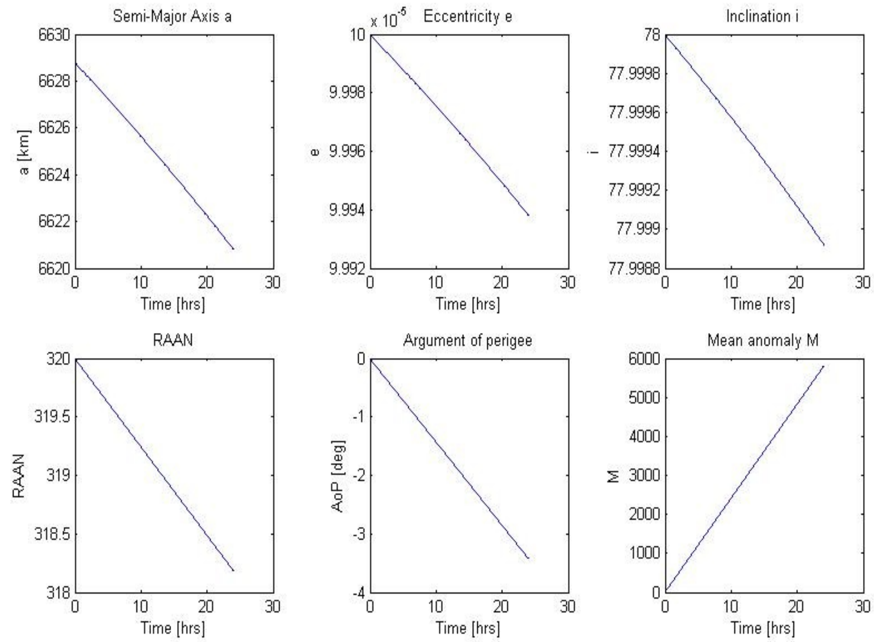

Figure 5.13: Projected Circular Motion – J_2 and Drag Perturbations –Perigee Altitude of 250 km – e = 10^{-4} – TECSAS Physical Parameters – Uncontrolled – Drift of Orbital Elements – 24 hours

The final set of simulation is for eccentricities of 10^{-4}. At this higher eccentricity the magnitude of the in-track drift increases to the point where it now trumps the effects of the perturbation forces and the difference in the motion for different altitudes is barely noticeable (Figs. 5.11 and 5.12). Figs. 5.7, 5.10 and 5.13 show the drift of the reference orbit's orbital element over a period of 24 hours at an altitude of 250 km for different eccentricities.

5.2 Uncontrolled In-track Formation

In this section, the effect of eccentricity on an in-track formation will be analyzed. The same parameters as for the projected circular analysis will be used. The desired relative motion is given by Sabol et al. (2001). Non-dimensionalizing, these equations become:

$$
\begin{aligned}
x_d &= 0 \\
y_d &= 1 \\
z_d &= -\frac{\widehat{\omega}_e}{\hat{n}c}\sin i\cos(\hat{n}c\tau) \\
\dot{x}_d &= 0 \\
\dot{y}_d &= 0 \\
\dot{z}_d &= \widehat{\omega}_e \sin i \sin(\hat{n}c\tau)
\end{aligned}
\tag{5.4}
$$

Setting the dimensionless to zero, we obtain the following initial conditions:

$$
\begin{aligned}
x_d &= 0 \\
y_d &= 1 \\
z_d &= -\frac{\widehat{\omega}_e}{\hat{n}c}\sin i \\
\dot{x}_d &= 0 \\
\dot{y}_d &= 0 \\
\dot{z}_d &= 0
\end{aligned}
\tag{5.5}
$$

5.2.1 Comparison for Circular Orbits

In this section, a small comparative analysis between the results obtained in Chapter 3 and the results given by the elliptical model will be undertaken. The first two simulations were performed for formation orbiting the Earth at altitude of 450 km and 350km (Fig. 5.14 – 5.15). The results are similar to those obtained in Chapter 3 as the drifts in the in-track and radial directions are so small that they can be neglected. However, for the next altitude (Fig. 5.16), significant differences between the results obtained with the elliptical model and the circular model become apparent. The in-track and radial drifts predicted with the elliptical model are much smaller in magnitude.

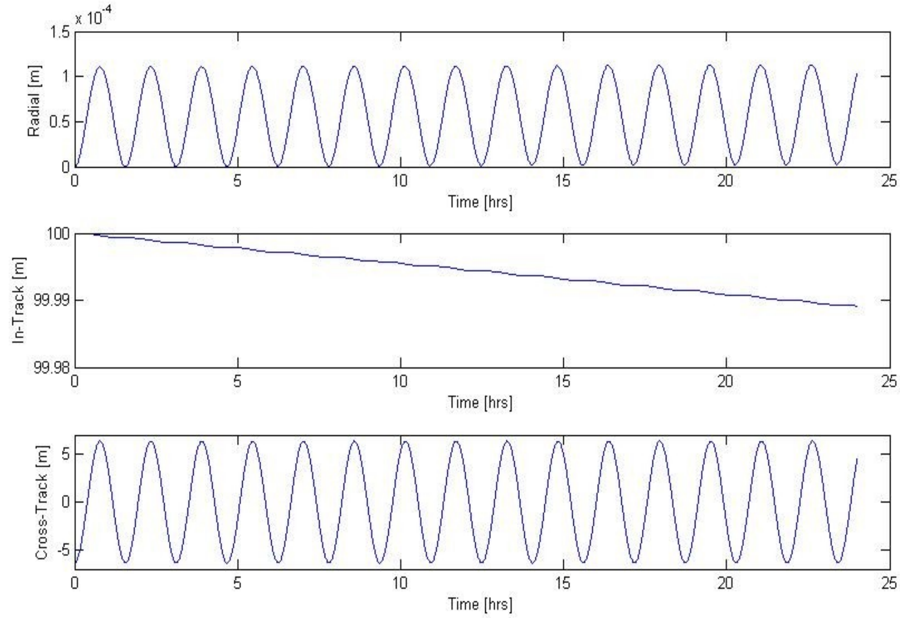

Figure 5.14: In-track Motion – J_2 and Drag Perturbations – Altitude of 450 km – TECSAS Physical Parameters – Uncontrolled – 24 hours

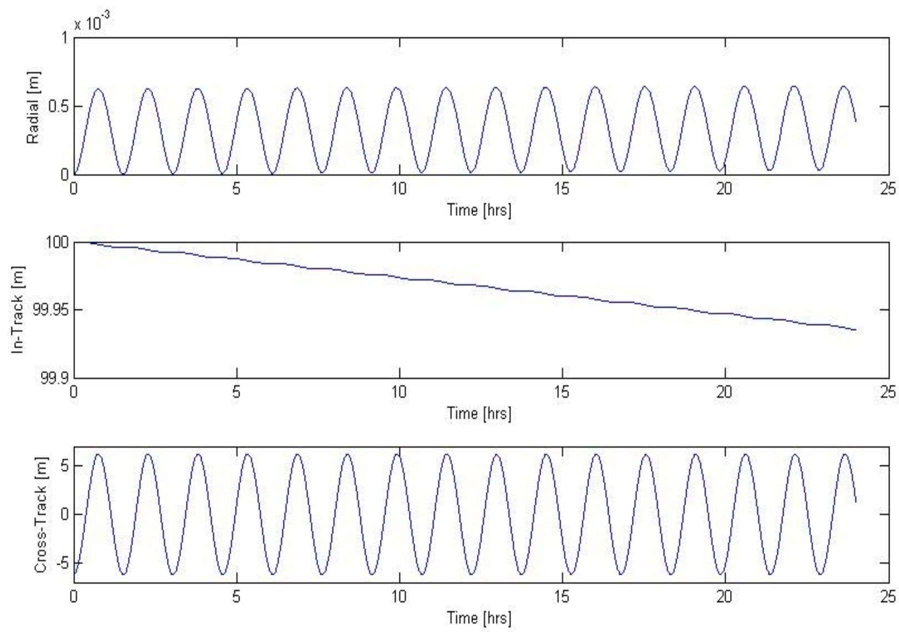

Figure 5.15: In-track Motion – J_2 and Drag Perturbations – Altitude of 350 km – TECSAS Physical Parameters – Uncontrolled – 24 hours

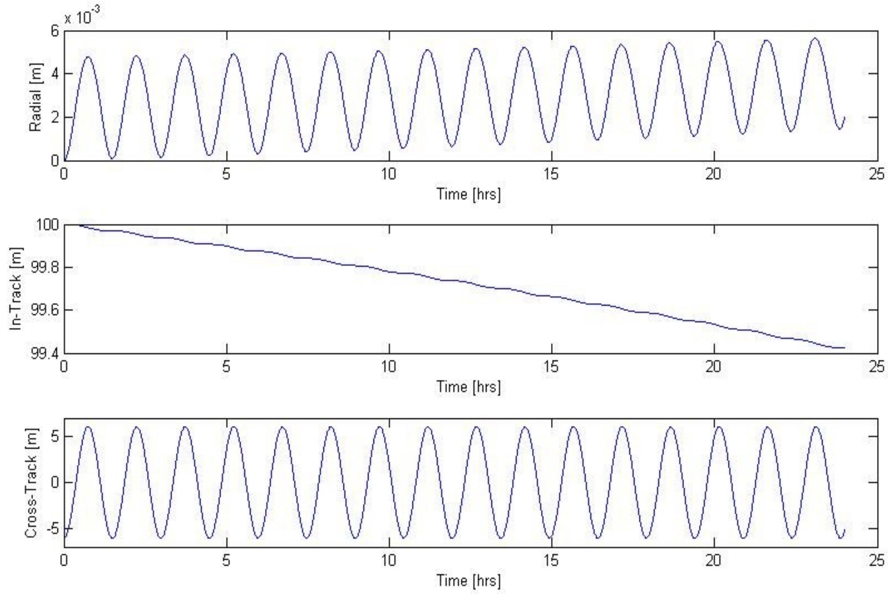

Figure 5.16: In-track Motion – J_2 and Drag Perturbations – Altitude of 250 km – TECSAS Physical Parameters – Uncontrolled – 24 hours

5.2.2 Results for Elliptical Orbits

Although the results obtained for the in-track formation using the elliptical model do not match those using the circular model, a preliminary analysis of the effects of eccentricity on an in-track formation will be conducted. This analysis will use the same parameters as for the one for the projected circular formation (Section 5.2.1). For the first three simulations (Figs. 5.17, 5.18 and 5.19), the eccentricity seems to low to have an effect on the formation. However, as the eccentricity is increased (Fig. 5.20) a small drift in the radial direction appears along with a significant drift in the direction.

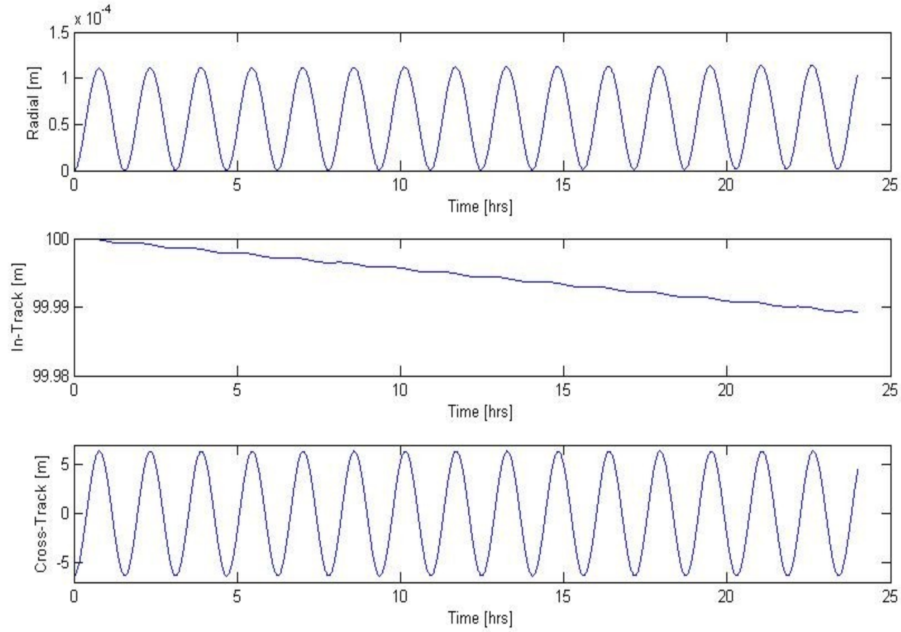

Figure 5.17: In-track Motion – J_2 and Drag Perturbations – Perigee Altitude of 450 km – e = 10^{-6} – TECSAS Physical Parameters – Uncontrolled – 24 hours

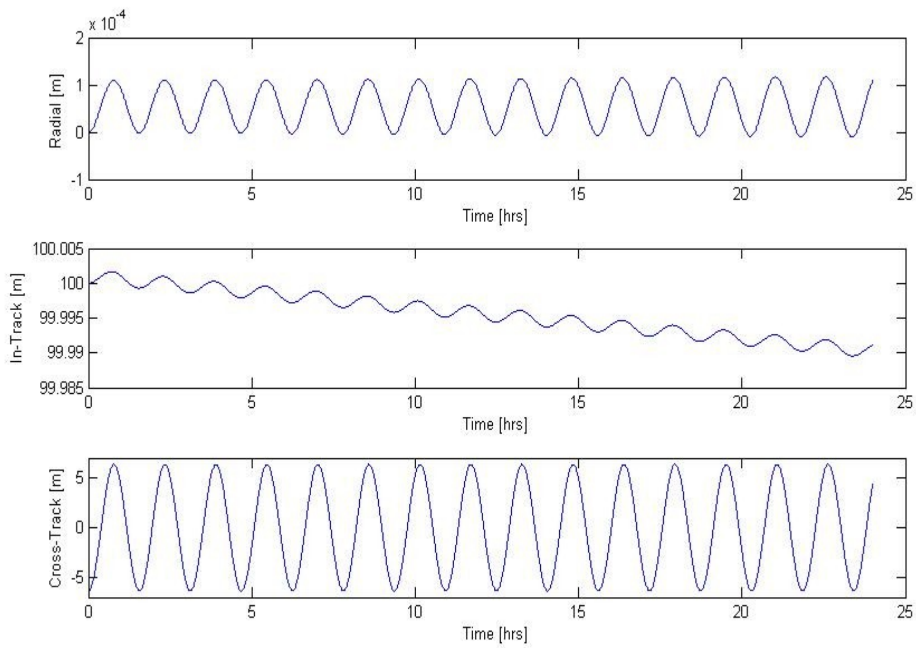

Figure 5.18: In-track Motion – J_2 and Drag Perturbations – Perigee Altitude of 450 km – e = 10^{-5} – TECSAS Physical Parameters – Uncontrolled – 24 hours

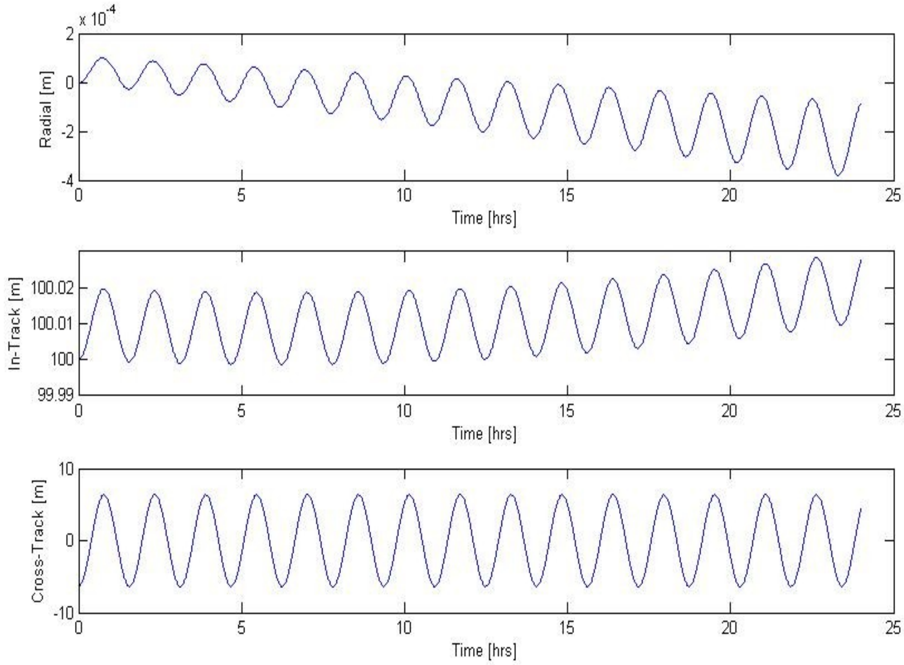

Figure 5.19: In-track Motion – J_2 and Drag Perturbations – Perigee Altitude of 450 km – e = 10^{-4} – TECSAS Physical Parameters – Uncontrolled – 24 hours

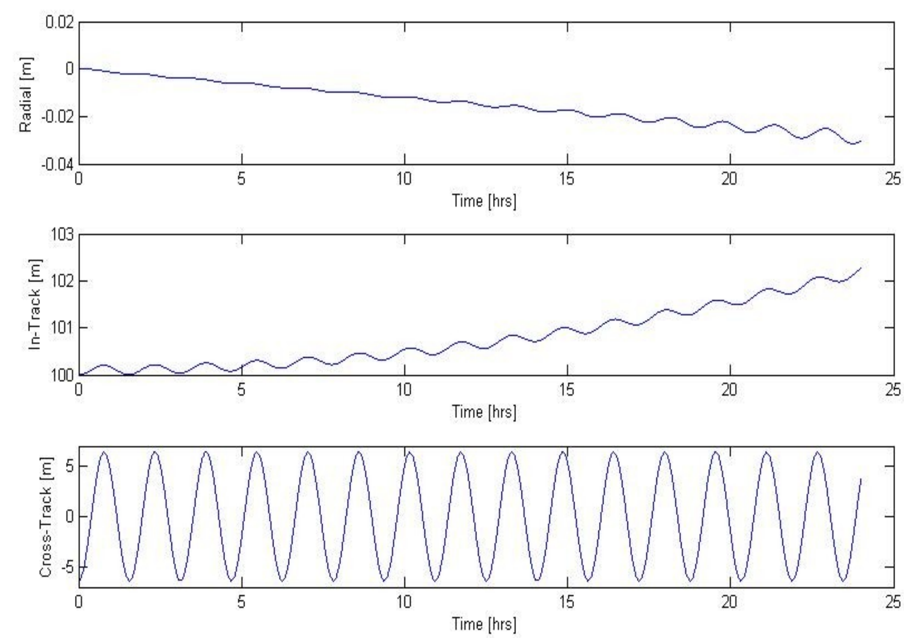

Figure 5.20: In-track Motion – J_2 and Drag Perturbations – Perigee Altitude of 250 km – e = 10^{-3} – TECSAS Physical Parameters – Uncontrolled – 24 hours

Something interesting to note is that the drift caused by eccentricity acts in the direction opposite to the one cause by atmospheric drag. It could therefore be possible to find, for a given orbit perigee altitude, an eccentricity that would negate the drift cause by atmospheric drag.

5.3 Effectiveness of Formation Maintenance Schemes

In this section the formation maintenance schemes proposed in this thesis will be put to the test. Throughout this thesis, three different schemes have been proposed: the gain matrix developed in Chapter 2, the controller based on energy presented in Chapter 4 and the Floquet-Lyapunov controller also presented in Chapter 4. To gage their effectiveness, they will be tested on projected circular formations of different eccentricities and altitudes. These eccentricities and altitudes are the same as the ones tested in section 5.2.2 for the uncontrolled case.

5.3.1 Results for the Gain Matrix

In this section, the effectiveness of the gain matrix developed in Chapter 2 will be put to the test in the context of elliptical orbits. The first set of result is for an eccentricity of 10^{-5}. It seems that the eccentricity is low enough for the gain matrix to manage to control the relative motion fairly well (Fig. 5.21). However, the control input need to perform the formation is clearly unbounded and will, with time, grow too large in magnitude to be admissible (Fig. 5.22).

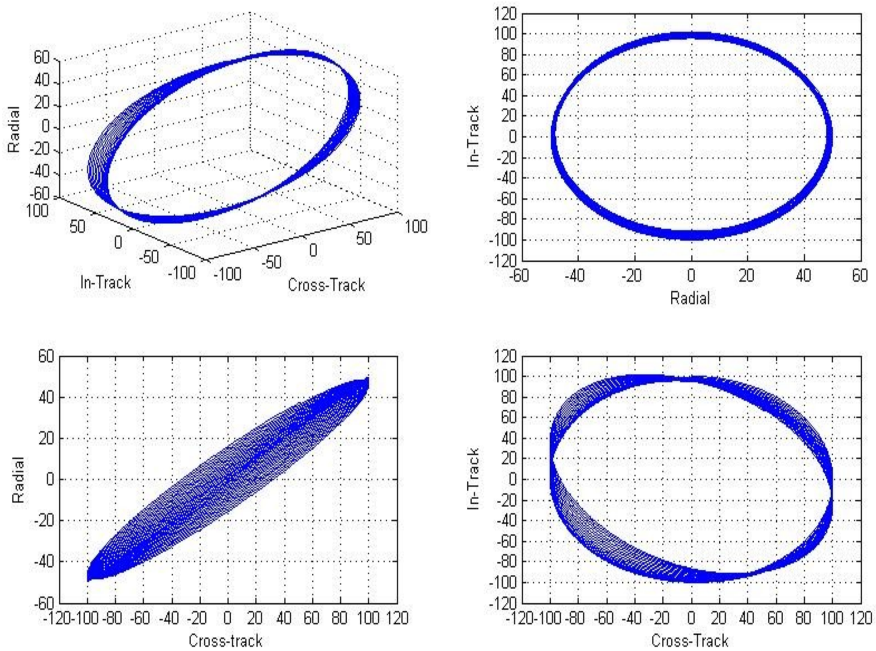

Figure 5.21: Projected Circular Motion – J_2 and Drag Perturbations – Perigee Altitude of 250 km – e = 10^{-5} – TECSAS Physical Parameters – Gain Matrix (ξ=1, α=150) – 24 hours

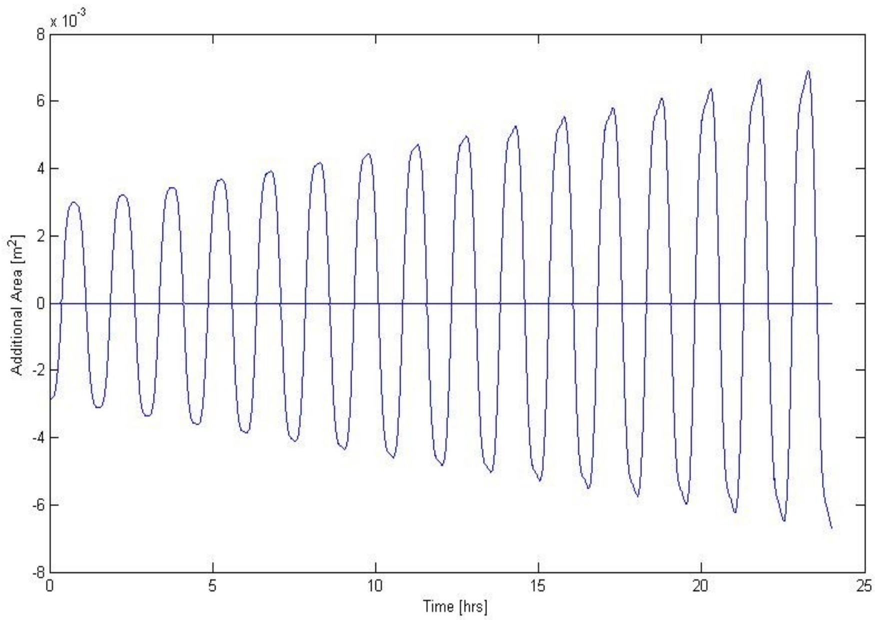

Figure 5.22: Additional Area needed for Control – Perigee Altitude of 250 km – e=10^{-5} – TECSAS Physical Parameters – Gain Matrix (ξ =1, α=150) – 24 hours

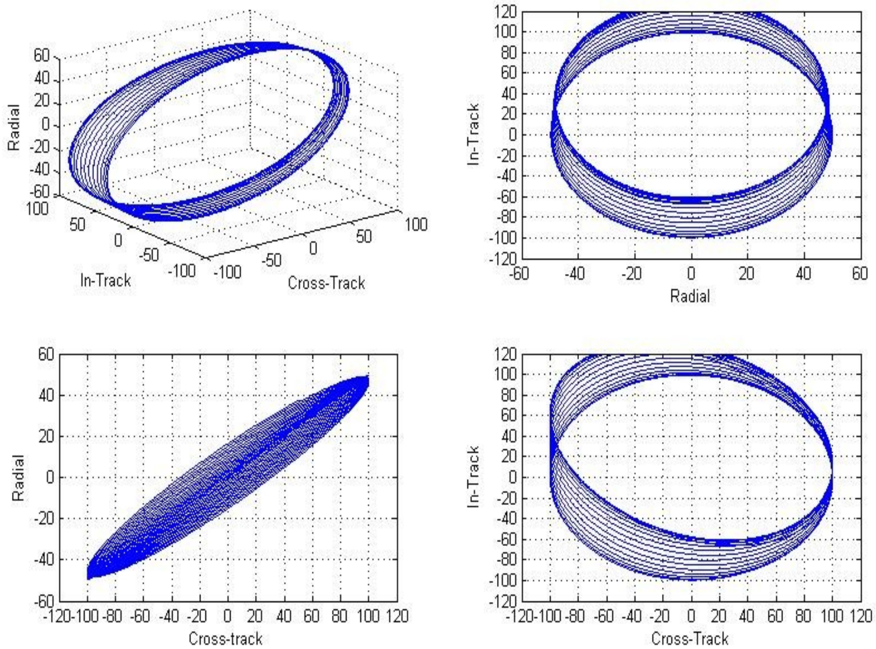

Figure 5.23: Projected Circular Motion – J_2 and Drag Perturbations – Perigee Altitude of 250 km – e = 10^{-4} – TECSAS Physical Parameters – Gain Matrix (ξ=1, α=150) – 24 hours

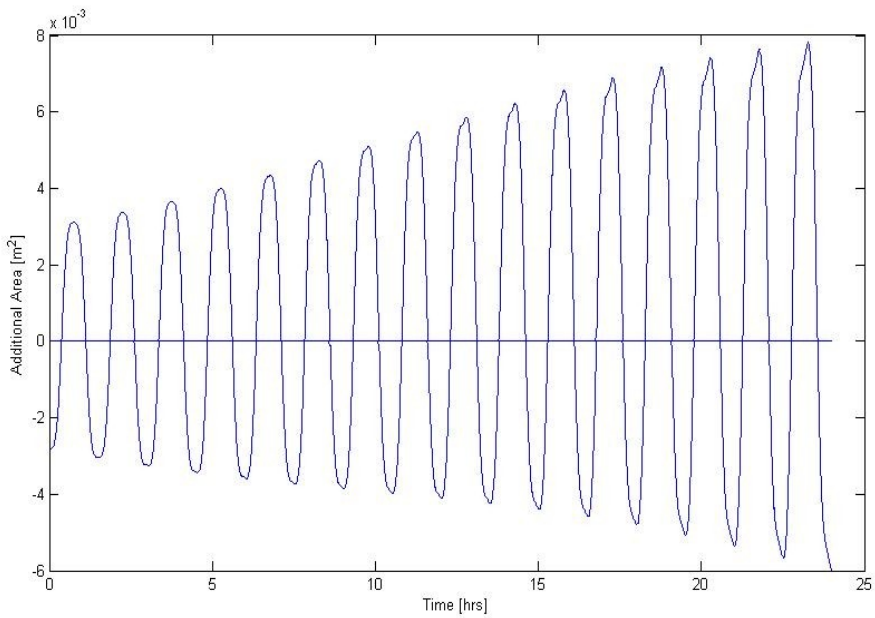

Figure 5.24: Additional Area needed for Control – Perigee Altitude of 250 km – e=10^{-4} – TECSAS Physical Parameters – Gain Matrix (ξ =1, α=1000) – 24 hours

The second set of result is for an eccentricity of 10^{-4}. Now that the eccentricity has been increased, the shortcomings of the gain matrix developed in Chapter 2 become more apparent. The control input required to perform formation maintenance is still unbounded (Fig. 5.24) and, furthermore, the control scheme is not very effective at performing said formation maintenance as there is still quite a lot of visible drift (Fig 5.23). This was to be expected as a time invariant method cannot effectively perform control on a time-varying system. Note that in Figs 5.22 and 5.24, a positive value indicates area added to the chief while a negative value indicates area added to the deputy.

5.3.2 Results for the Energy Controller

The next control scheme to be tested is the control scheme based on the energy of the spacecraft proposed by Kumar, Ng, Yoshihara and De Ruiter and presented in Section 4.4.1. The first set of results is for a perigee altitude of 350 km and an eccentricity of 10^{-5}. The first thing to notice is that in-plane motion is identical to the desired relative motion (Fig. 5.25) and in that aspect the formation maintenance scheme is acting exactly as desired. Furthermore, the control input (Fig. 5.26) is bounded and the maximum area required for control is very small in comparison to the satellite's baseline area. The control scheme is therefore performing well in that regard as well.The second set of results is for the same eccentricity, but the perigee atltitude has been lowered to 250 km. Again, the in-plane relative motion is the desired one (Fig. 5.27). The additional area needed for formation maintenance is much lower than for the formation at 350 km of altitude at perigee (Fig. 5.28). This was to be expected since the atmospheric density is lower at higher altitudes. As such, the additional area required is well within acceptable bounds.

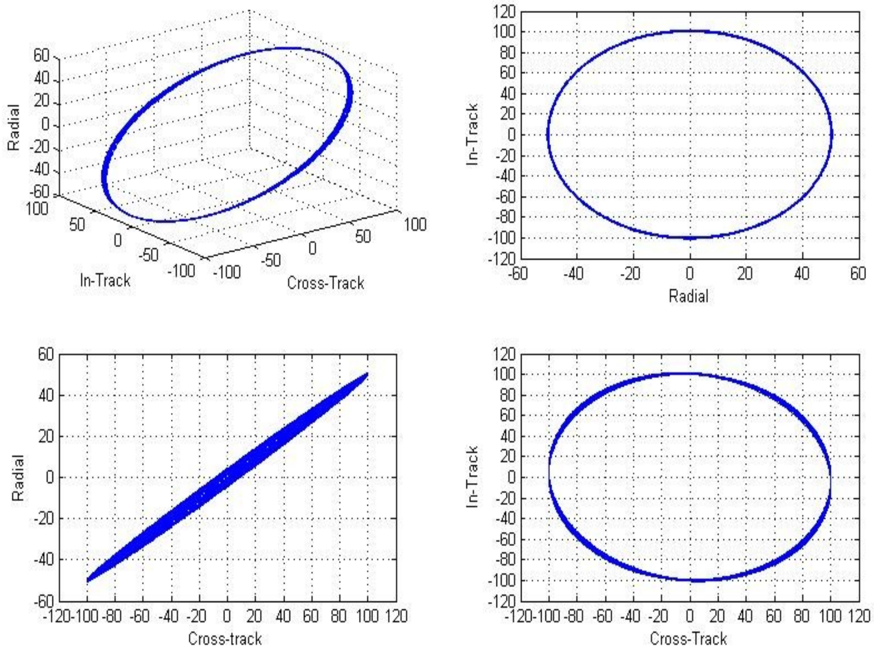

Figure 5.25: Projected Circular Motion – J_2 and Drag Perturbations – Perigee Altitude of 350 km – e = 10^{-5} – TECSAS Physical Parameters – Energy PID ($K_p = 5 \times 10^{-18}$, $K_d = 0$, $K_i = 5 \times 10^{-16}$) –c24 hours

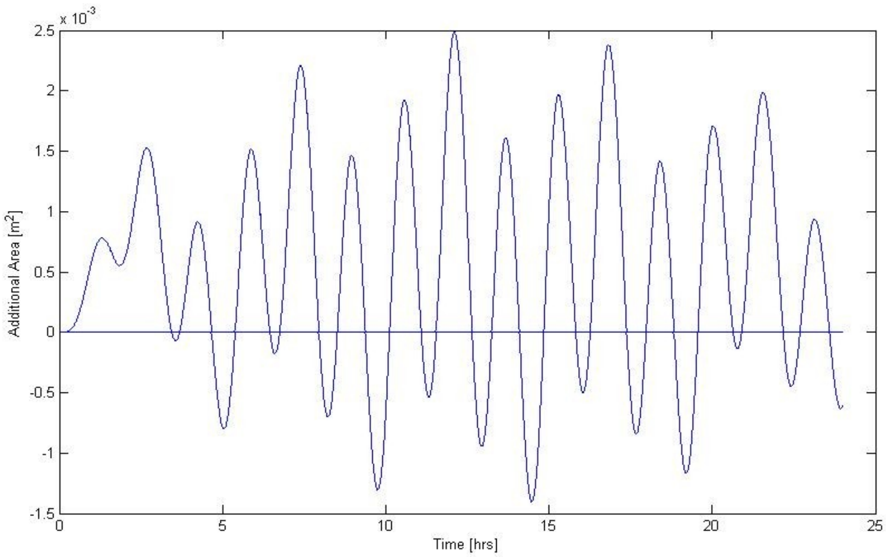

Figure 5.26: Additional Area needed for Control – Perigee Altitude of 350 km – e=10^{-5} – TECSAS Physical Parameters – Energy PID ($K_p = 5 \times 10^{-18}$, $K_d = 0$, $K_i = 5 \times 10^{-16}$) – 24 hours

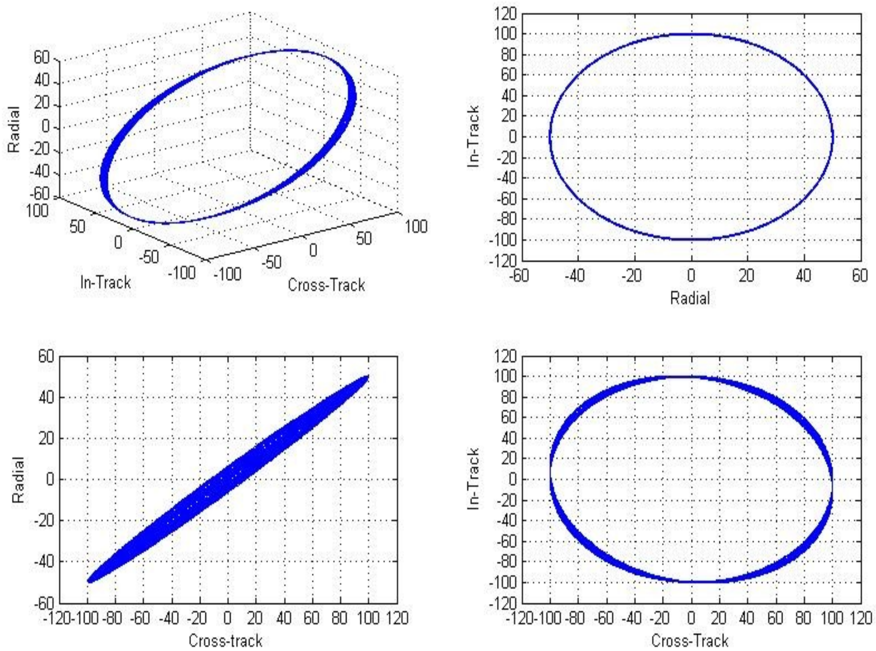

Figure 5.27: Projected Circular Motion – J_2 and Drag Perturbations – Perigee Altitude of 250 km – e = 10^{-5} – TECSAS Physical Parameters – Energy PID ($K_p = 5 \times 10^{-18}$, $K_d = 0$, $K_i = 5 \times 10^{-17}$) – 24 hours

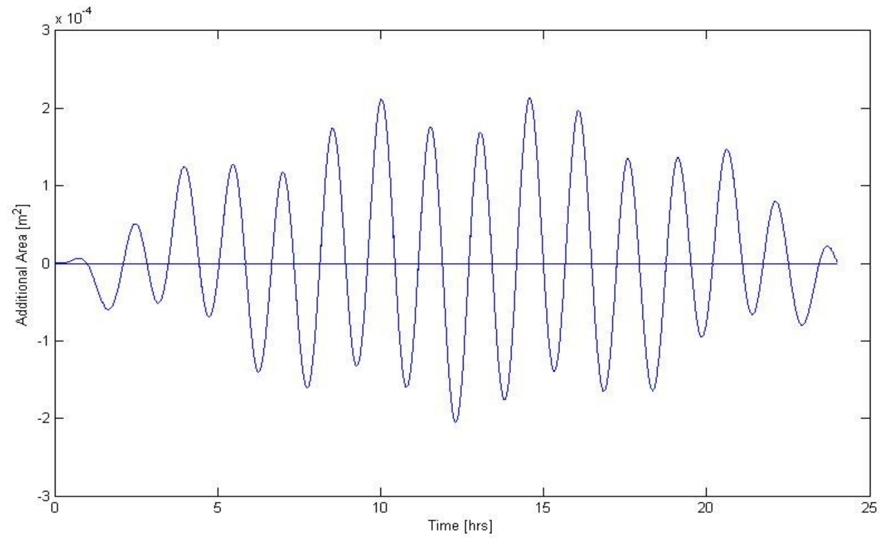

Figure 5.28: Additional Area needed for Control – Perigee Altitude of 250 km – e=10^{-5} – TECSAS Physical Parameters – Energy PID ($K_p = 5 \times 10^{-18}$, $K_d = 0$, $K_i = 5 \times 10^{-17}$) – 24 hours

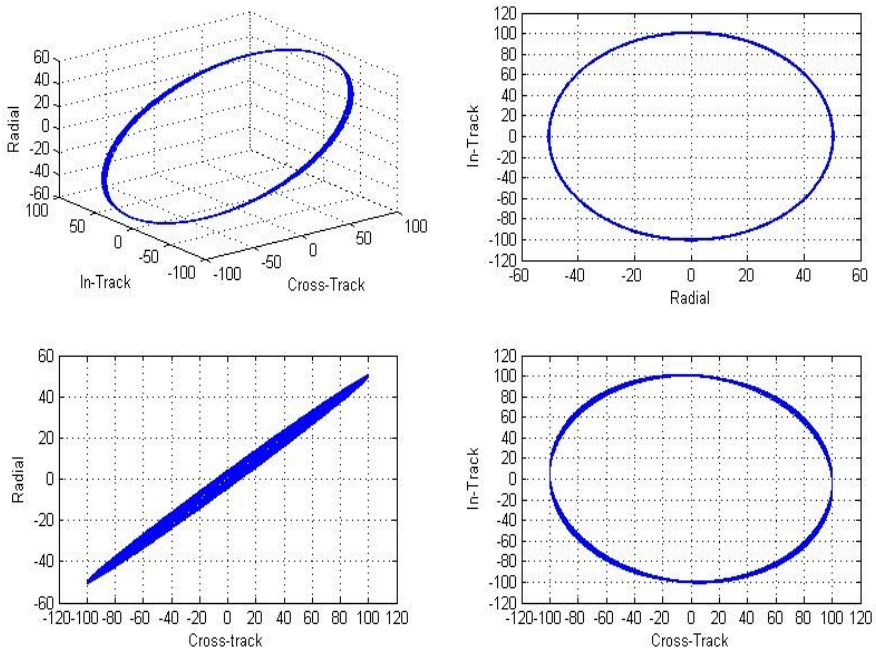

Figure 5.29: Projected Circular Motion – J_2 and Drag Perturbations – Perigee Altitude of 350 km – e = 10^{-4} – TECSAS Physical Parameters – Energy PID ($K_p = 5 \times 10^{-18}$, $K_d = 0$, $K_i = 5 \times 10^{-16}$) – 24 hours

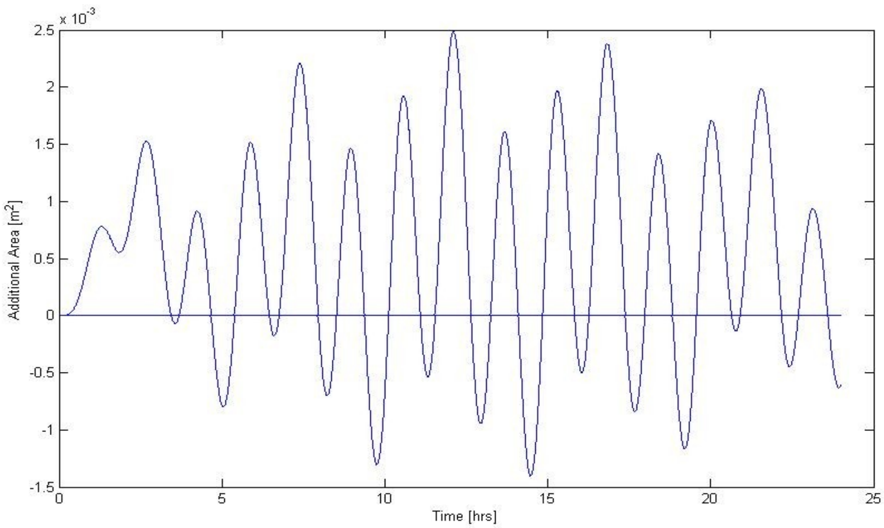

Figure 5.30: Additional Area needed for Control – Perigee Altitude of 350 km – e=10^{-4} – TECSAS Physical Parameters – Energy PID ($K_p = 5 \times 10^{-18}$, $K_d = 0$, $K_i = 5 \times 10^{-16}$) – 24 hours

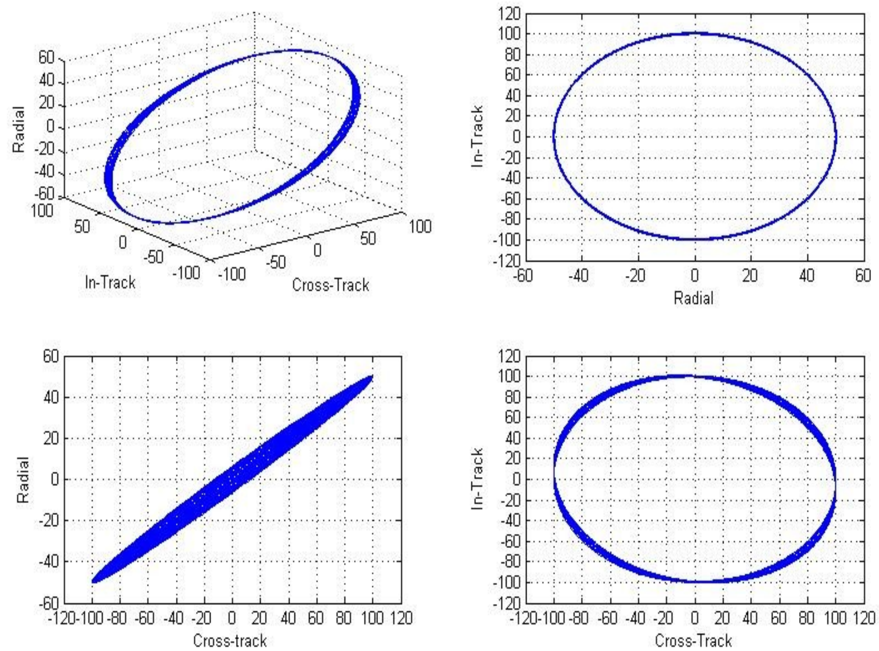

Figure 5.31: Projected Circular Motion – J_2 and Drag Perturbations – Perigee Altitude of 250 km – e = 10^{-4} – TECSAS Physical Parameters – Energy PID ($K_p = 5 \times 10^{-18}$, $K_d = 0$, $K_i = 5 \times 10^{-17}$) – 24 hours

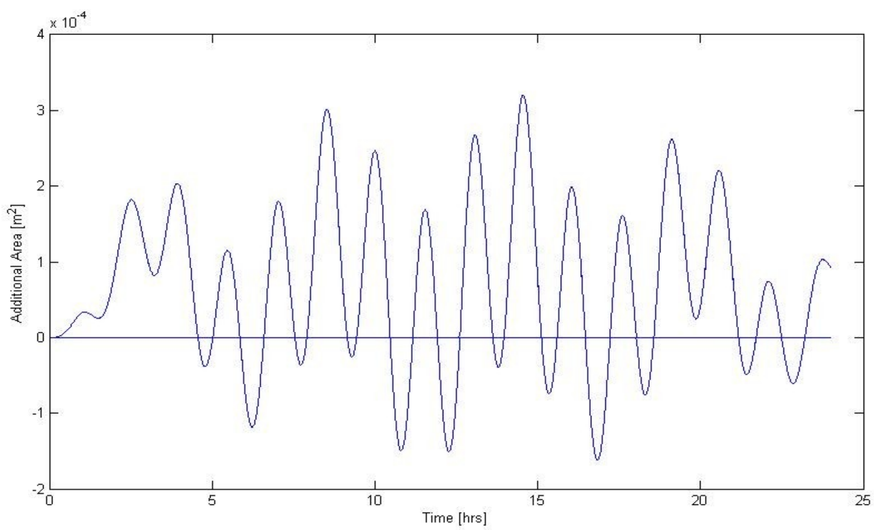

Figure 5.32: Additional Area needed for Control – Perigee Altitude of 250 km – e=10^{-4} – TECSAS Physical Parameters – Energy PID ($K_p = 5 \times 10^{-18}$, $K_d = 0$, $K_i = 5 \times 10^{-17}$) – 24 hours

The third set of results was for an altitude at perigee of 350 km and an eccentricity of 10^{-4}. Similarly to the previous 2 simulations, the in-track motion is exactly as desired (Fig. 5.29). Additionally, the control input is still bounded and much smaller than the baseline area (Fig 5.30). The final set of results is again proving the effectiveness of this controller as the in-plane formation is maintained for the same eccentricity but lower altitude (Fig. 5.31) and the control input is bounded (Fig. 5.32). Although the control gains are very small, it is important to note that they must be this small in order to keep the formation.

5.3.3 Results for the Floquet-Lyapunov Controller

The final formation maintenance scheme to be tested is the one based on Floquet-Lyapunov theory which was presented in Section 4.4.2. The parameters used in these simulations were the same as the ones in Section 5.1.3. For the first set of simulations, the control input (Fig. 5.34) differs greatly from the one from the energy controller, both in magnitude and overall shape. Nonetheless the desired in-plane relative motion is achieved (Fig. 5.33) and the control input is bounded. The same can be said for the second set of simulation (Figs. 5.35 and 5.36). As expected the additional area needed to perform formation maintenance is lower in this case since the altitude has been lowered.

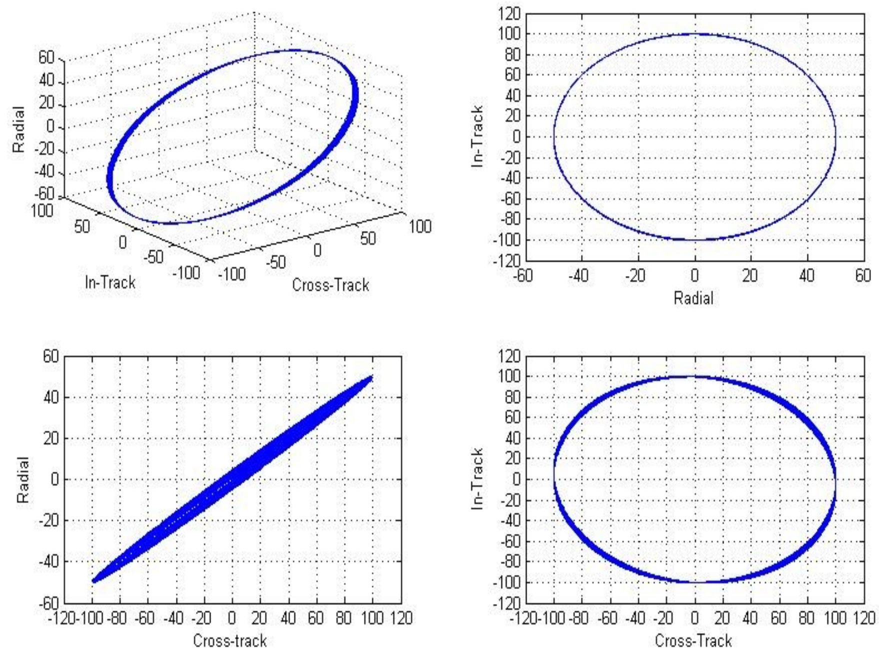

Figure 5.33: Projected Circular Motion – J_2 and Drag Perturbations – Perigee Altitude of 350 km – e = 10^{-5} – TECSAS Physical Parameters – Floquet-Lyapunov Controller – 24 hours

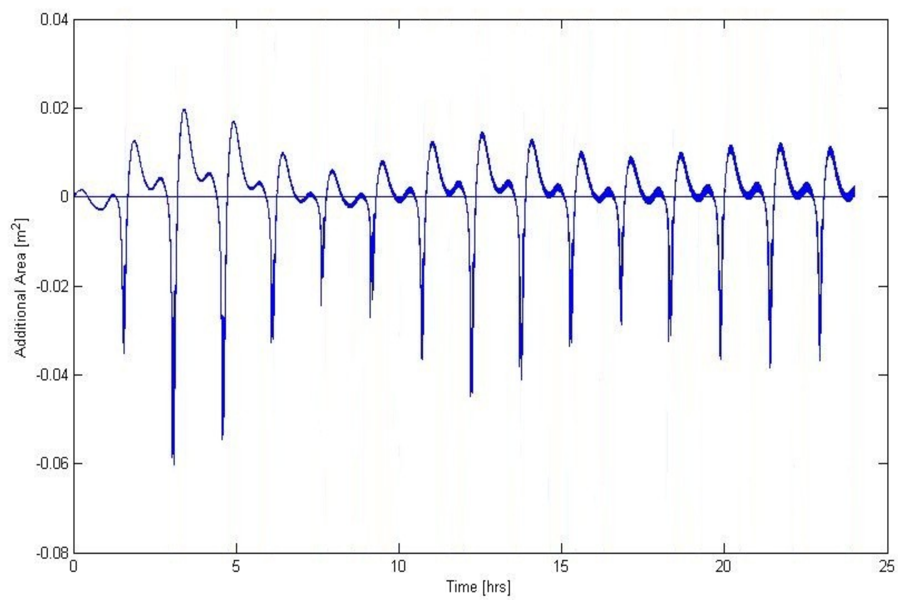

Figure 5.34: Additional Area needed for Control – Perigee Altitude of 350 km – e=10^{-5} – TECSAS Physical Parameters – Floquet-Lyapunov Controller – 24 hours

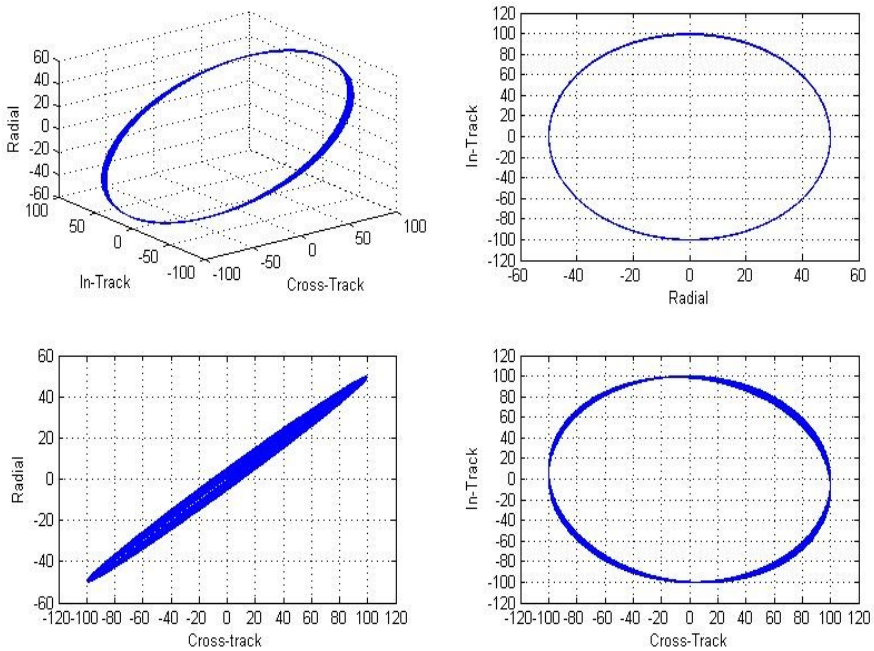

Figure 5.35: Projected Circular Motion – J_2 and Drag Perturbations – Perigee Altitude of 250 km – e = 10^{-5} – TECSAS Physical Parameters – Floquet-Lyapunov Controller – 24 hours

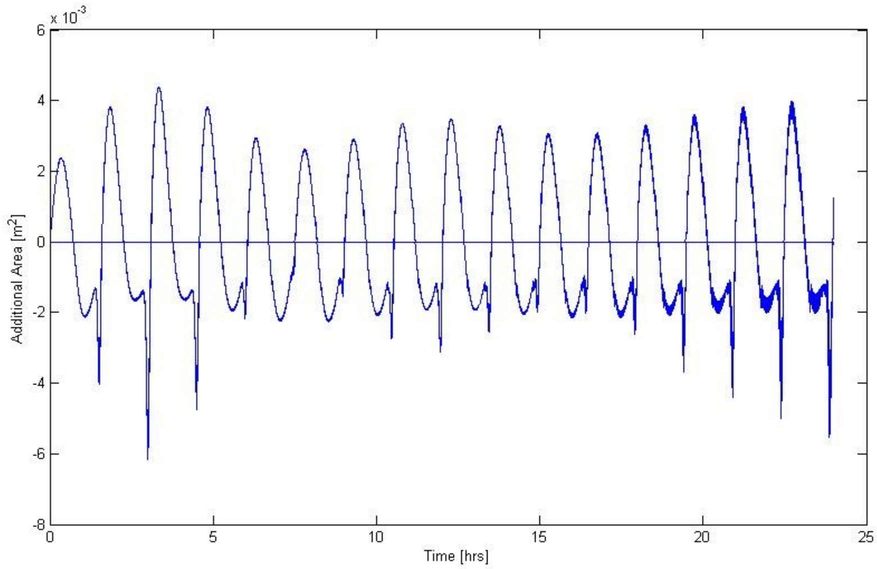

Figure 5.36: Additional Area needed for Control – Perigee Altitude of 250 km – e=10^{-5} – TECSAS Physical Parameters – Floquet-Lyapunov Controller – 24 hours

In the third and fourth set of simulations, the additional area required for formation maintenance is till bounded and within acceptable values (Figs. 5.38 and 5.40). However, while the in-plane motion is very close to the one desired, there seems to be some reduction of the in-plane ellipse (Figs. 5.37 and 5.39). This effect seems to be magnified at the lower altitude of 250 km. This could be due to the gain matrix $\widetilde{\mathbf{G}}$ chosen not being the ideal one. It is possible that with a different matrix $\widetilde{\mathbf{G}}$, the desired in-plane motion could be achieved, but that might require a vigorous method for finding. Unfortunately we do not have one at the moment.

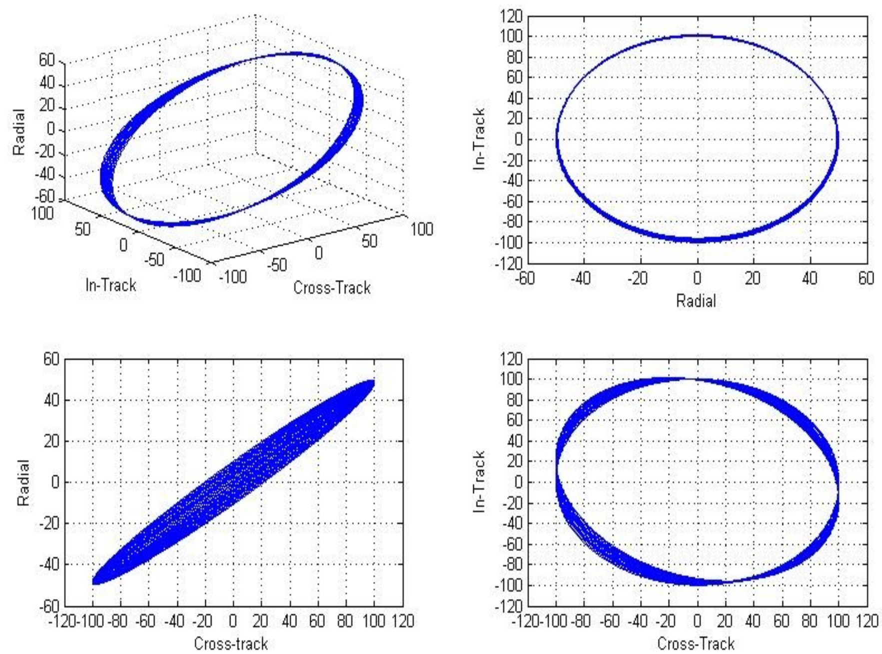

Figure 5.37: Projected Circular Motion – J_2 and Drag Perturbations – Perigee Altitude of 350 km – e = 10^{-4} – TECSAS Physical Parameters – Floquet-Lyapunov Controller – 24 hours

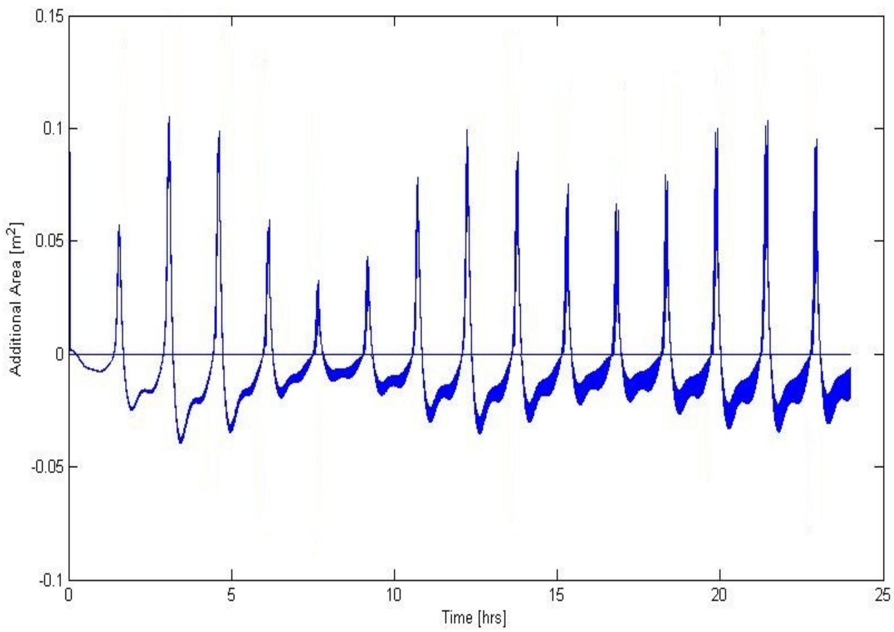

Figure 5.38: Additional Area needed for Control – Perigee Altitude of 350 km – e=10^{-4} – TECSAS Physical Parameters – Floquet-Lyapunov Controller – 24 hours

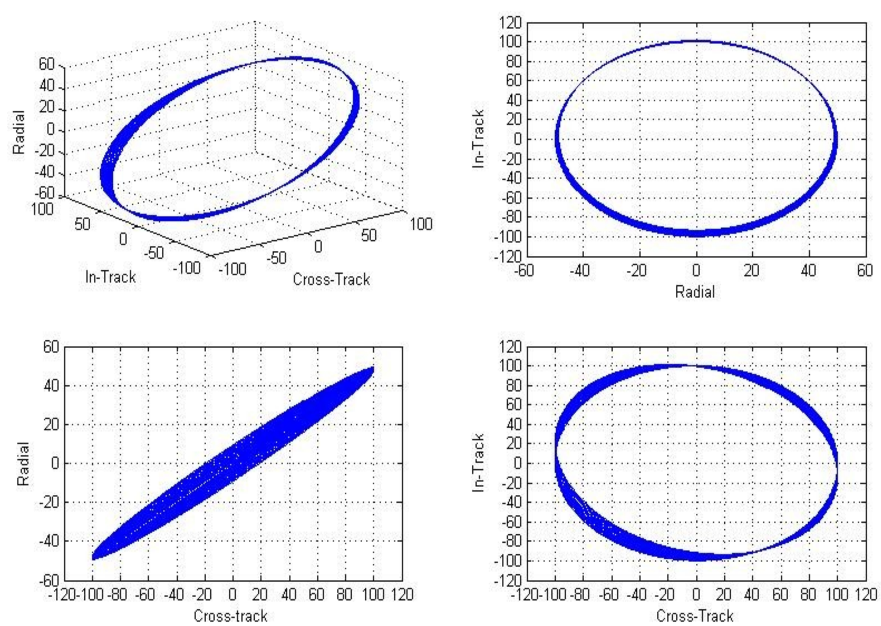

Figure 5.39: Projected Circular Motion – J_2 and Drag Perturbations – Perigee Altitude of 250 km – e = 10^{-4} – TECSAS Physical Parameters – Floquet-Lyapunov Controller – 24 hours

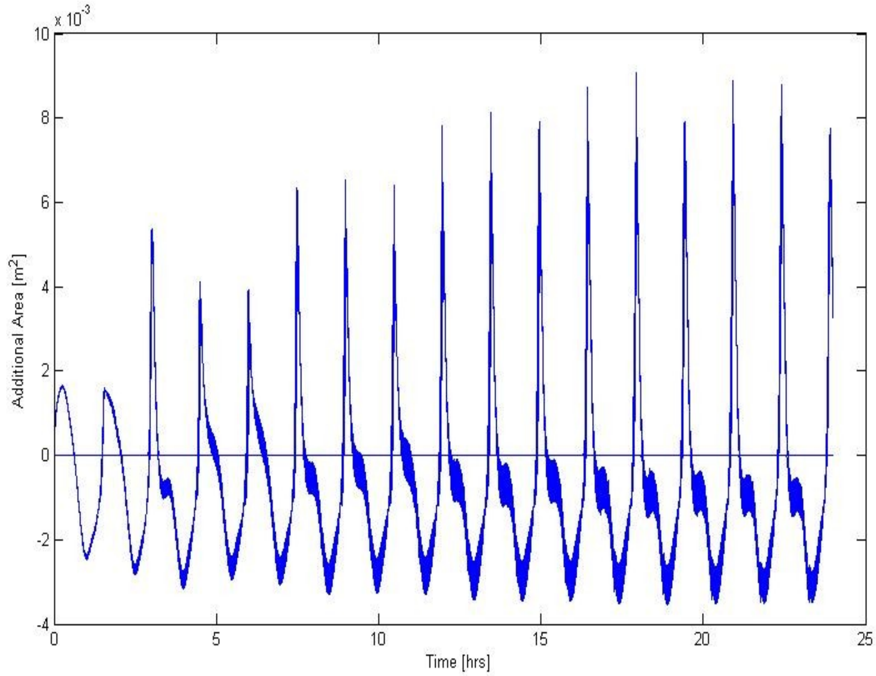

Figure 5.40: Additional Area needed for Control – Perigee Altitude of 250 km – e=10^{-4} – TECSAS Physical Parameters – Floquet-Lyapunov Controller – 24 hours

It should be noted that, since differential drag does not allow for control in the cross-track directions, an additional controller would be required to have control over the relative motion in all directions. Since, the cross-track motion is uncoupled for the motion in the x- y plane, it is possible to add this additional controller without interfering with the in-plane motion already controlled. To demonstrate this a simple bang bang controller using thrusters was added to the Floquet-Lyapunov controller for the case shown in Fig. 5.37. This controller makes sure that the radius of the projected circle is always within a set tolerance and applies a thrust accordingly either in the positive or negative cross-track direction (Fig. 5.42). The resulting motion can be seen in Fig. 5.41. Note that the in-plane motion remains unchanged while the cross-track motion has been corrected.

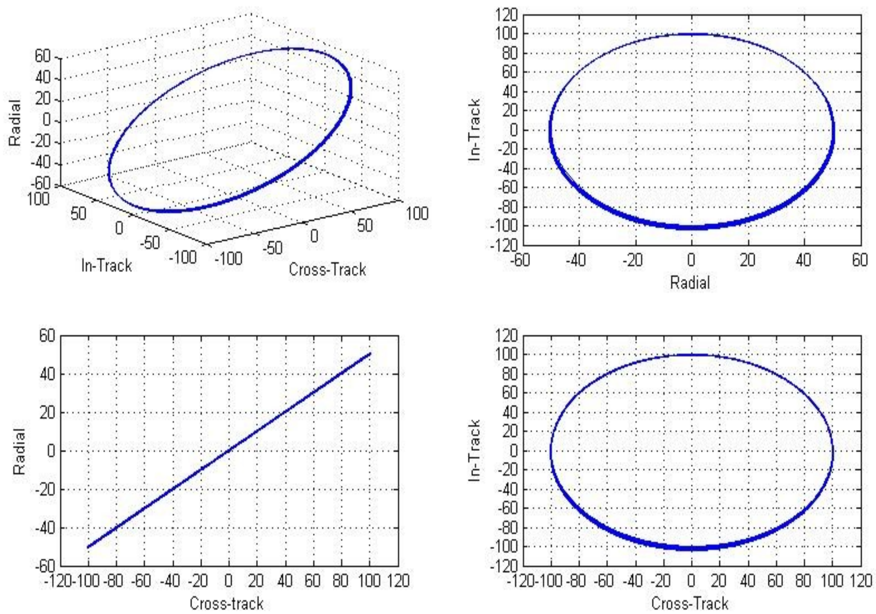

Figure 5.41: Projected Circular Motion – J_2 and Drag Perturbations – Perigee Altitude of 350 km – e = 10^{-4} – TECSAS Physical Parameters – Floquet-Lyapunov Controller and Cross-track Thrust – 24 hours

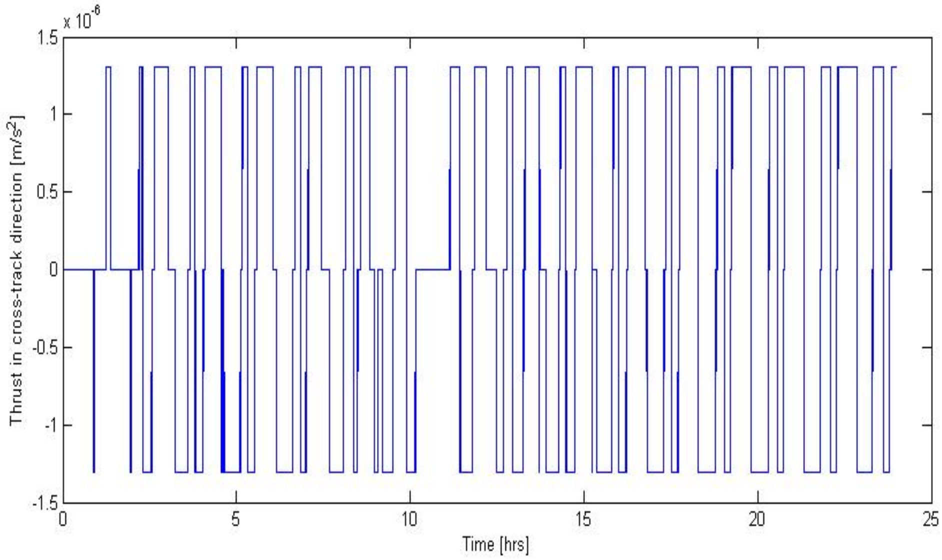

Figure 5.42: Cross-track Thrust input – Perigee Altitude of 350 km – e=10^{-4} – TECSAS Physical Parameters – 24 hours

Chapter 6 – Conclusions

6.1 Summary of the Thesis

In this thesis the effectiveness of using differential atmospheric drag as a means of formation maintenance was investigated. In the first chapter, a literature review was presented. This literature review focused on satellite formation flying in the presence of atmospheric drag, on use of differential drag as means of control and on control of periodically time-varying systems.

In Chapter 2, the dimensionless equations of motion for the circular case in presence of atmospheric drag and J_2 perturbations were developed. To do so, first, the different coordinate frames needed for orbit and relative motion description were presented. Next, the expression describing the effects of atmospheric drag in the Hill frame was introduced. This expression was linearized using binomial series expansion. The effects of drag were then included in the Schweighart and Sedwick model, which was then non-dimensionalized using newly defined dimensionless terms for position, velocity, time and other dimensionless parameters. This allowed for the presentation of a set of linearized equations describing the relative motion of a spacecraft relative to a reference orbit under the effects of both atmospheric drag and J_2 perturbations. Finally, a stability analysis where the control input was related to the satellite's projected was performed on the system.

In Chapter 3, numerous simulation results based on the equations developed in Chapter 2 were presented. Two different sets of spacecraft physical parameters were used for this study: TECSAS and JC2Sat. The first series of simulations were done for a projected circular formation orbiting the Earth at altitudes ranging from 250 to 500 km. It was concluded that the main effects of drag on this type of formation was to induce a drift in the in-track direction and to cause shrinkage of the in-plane ellipse. The J_2 perturbations seemed to mainly cause a drift in the cross-track direction. Next, a series of simulation were performed for an in-track formation. The main effects of atmospheric drag on this type of formation seemed to be a drift in the in-track and radial directions. Finally, the effectiveness of the gain matrix developed in Chapter 2 at performing formation maintenance was put to the test. Although, it significantly improved the relative motion, it did not entirely eliminate the drifts. It was suggested that this might be due to the optimal gain matrix being hard to obtain.

The equations of motion valid for the elliptical case were presented in Chapter 4. In order to simplify the formulation, the orbit's eccentricity was assumed to be small. For this model the chief spacecraft was placed on the reference orbit. Therefore, the reference orbit had to be propagated through time. To do so Gauss' planetary equations, which allow the propagation of the orbital elements through time while accounting for the perturbative forces, were used. The resulting six equations were then simplified using the small eccentricity assumption and by orbit-averaging them to capture solely the secular drifts. Next, the effects of the perturbative forces on the deputy relative to the chief are presented. They two are then linearized and orbit-averaged and included in the equations of relative motion to obtain the model used for the elliptical case. Next, two formation maintenance scheme are presented. The first one, is a PID controller which bases its control law on the energy of the deputy satellite, while the second one is based on Floquet Lyapunov theory and uses relative position and velocity as feedback.

Finally, Chapter 5 present simulation results for the elliptical case. Unlike Chapter 3, only one set of physical parameters were used, namely TECSAS'. The analysis starts by comparing the results obtained for a projected circular formation placed on a circular orbit using the model developed in Chapter 3 with the circular model of Chapter 2. From the simulation results, there seems to be slight overestimation of the cross-track drift and a small under-estimation of the in-track drift. Still, the results are very close to those obtained in Chapter 3. Following this comparative study, simulation results demonstrating the effects of eccentricity on this type of formation are presented. The main effect is a significant in-track drift which increases rapidly as eccentric increases. Next, simulation results for an in-track formation place on a circular orbit are provided. The conclusion of this study is that the elliptical model predicts much smaller in-track and radial drifts. Finally the effectiveness of the gain matrix developed in Chapter 2, of the Energy PID controller and of the Floquet-Lyapunov controller at performing formation maintenance on an elliptical orbit is tested. As expected the gain matrix developed for the circular case in unable to perform formation maintenance. The relative motion when controlled is significantly better, but not always satisfactory. Furthermore, the area needed to perform this control is unbounded and increases rapidly with time. The energy controller, on the other hand, performs very well as the relative motion is almost indistinguishable from the desired relative motion and the additional area needed to perform formation maintenance is bounded and small enough to be implemented. The Floquet-Lyapunov controller also performs very well as it significantly improves the relative motion and the additional area needed to perform control is bounded and small in comparison with the baseline projected area. In some cases the gain matrix $\widetilde{\mathbf{G}}$ needed for this controller is hard to find and might explain some slight deviation from the desired motion. This is the big advantage that the energy controller holds on the Floquet-Lyapunov controller as only three gains need to be specified.

6.2 Recommendations for Future Work

The next step would have to be the validation of the model developed in Chapter 4. The discrepancies between the results obtained for circular orbits using this model and the circular model of Chapter 2 need to be investigated further, especially for the in-track formation. It would also be interesting to see up to what eccentricities this model can be deemed acceptable.

More work is needed for the Floquet-Lyapunov controller to be perfected. The main problem with this controller now lies in the matrix $\widetilde{\mathbf{G}}$. This matrix has a large impact on the behaviour of the system after the feedback control is implemented, yet, right now, we have to resort to trial and error to find this matrix. The method used in this thesis was to provide different matrices **Q** and **R** to the LQR solver implemented in MATLAB© until the results were deemed acceptable. A more robust way of finding this matrix should be developed.

As mentioned in Chapter 5, the drift caused by eccentricity acts and the drift cause by atmospheric drag (if no control is applied) work in opposite directions. This suggests that for a given perigee altitude, it might be possible to find an eccentricity that would negate the drift cause by atmospheric drag. It might be interesting to further investigate this.

Appendix A – Velocity Relative to Rotating Atmosphere

In this appendix, the expression in the Hill frame for the velocity of a spacecraft relative to the rotating atmosphere will be determined. This velocity $\mathbf{v}_{rel}$, crucial to obtaining the drag force acting on a spacecraft, is given in the ECI frame by (Vallado, 2007):

$$\mathbf{v}_{rel} = \mathbf{v} - \boldsymbol{\omega}_e \times \mathbf{r} \tag{A.1}$$

where $\mathbf{r}$ and $\mathbf{v}$ are the absolute position and velocity of the spacecraft expressed in the ECI frame while $\boldsymbol{\omega}_e$is the angular velocity vector of the Earth. This vector is purely in the Z-direction of the ECI frame and has a magnitude of 7.2921150×10^{-5} rad/s.

To obtain $\mathbf{v}_{rel}$ in the Hill frame, all the elements of Eq. (A.1) need to be expressed in the Hill-frame. The absolute position vector is obtained in the Hill frame as:

$$\mathbf{r} = \mathbf{r}_{ref} + \mathbf{x} = \begin{bmatrix}(r_{ref} + x) & y & z\end{bmatrix}^T \tag{A.2}$$

where r_{ref} is the instantaneous distance of the Hill frame from the center of the Earth. The absolute velocity vector is expresses in the Hill frame as:

$$\mathbf{v} = \mathbf{v}_{ref} + \dot{\mathbf{x}} + \dot{\mathbf{f}} \times \mathbf{x} \tag{A.3}$$

where $\mathbf{v}_{ref}$ is the velocity vector of the Hill frame with respect to the center of the Earth expressed in the Hill frame and $\dot{\mathbf{f}}$ is the orbital rate vector of the reference orbit expressed in the Hill frame as well. These vectors are defined as:

$$\mathbf{v}_{ref} = \begin{bmatrix}\dot{r}_{ref} & r_{ref}\dot{f} & 0\end{bmatrix}^T \tag{A.4}$$

$$\dot{\mathbf{f}} = [0 \quad 0 \quad \dot{f}]^T \tag{A.5}$$

This leads to the following expression for the absolute velocity vector:

$$\mathbf{v} = \begin{bmatrix} \dot{x} + \dot{r}_{ref} - \dot{f}y \\ \dot{y} + r_{ref}\dot{f} + \dot{f}x \\ \dot{z} \end{bmatrix} \tag{A.6}$$

The last term from Eq. (A.1) that needs to be expressed in the Hill frame is the angular velocity vector of the Earth $\boldsymbol{\omega}_e$. To do so, a transformation matrix is needed. There is a known transformation to go from the ECI frame to the Perifocal coordinate system (PQW). This transformation is given by the 3-1-3 Euler sequence (Chobotov, 2002):

$$\mathbf{r}_{PQW} = \mathbf{R}_3(\omega)\mathbf{R}_1(i)\mathbf{R}_3(\Omega)\mathbf{r}_{ECI} \tag{A.7}$$

The origin of the Perifocal frame is the center of the Earth and thus one of the focal points of the orbit. The P-axis points toward the perigee, the W-axis is normal the orbital plane and the Q-axis completes the right-hand system.

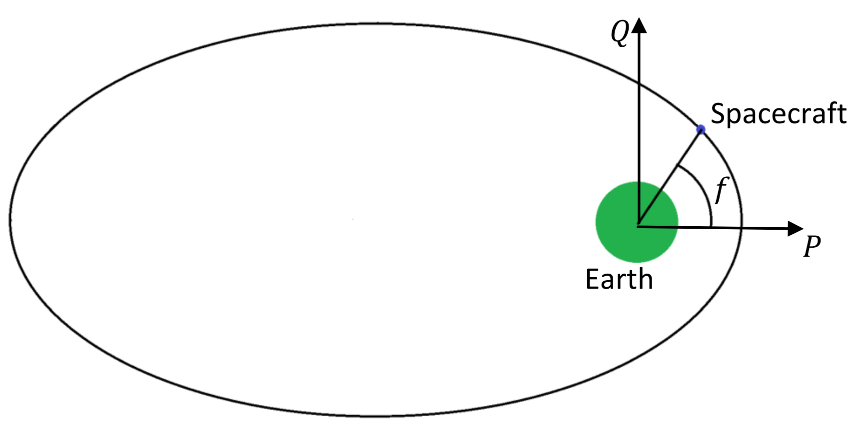

Figure A.1: Orbital Plane View of the PQW Coordinate Frame

To go from the PQW to the Hill frame we, therefore, need to apply a rotation around the orbit-normal of an angle equal to the true anomaly f. The complete sequence to go from the ECI frame to the Hill frame is thus:

$$\mathbf{r}_{Hill} = \mathbf{R}_3(f)\mathbf{R}_3(\omega)\mathbf{R}_1(i)\mathbf{R}_3(\Omega)\mathbf{r}_{ECI}$$

$$\mathbf{r}_{Hill} = \mathbf{R}_3(f+\omega)\mathbf{R}_1(i)\mathbf{R}_3(\Omega)\mathbf{r}_{ECI} \tag{A.8}$$

$$\mathbf{r}_{Hill} = \mathbf{R}_3(\theta)\mathbf{R}_1(i)\mathbf{R}_3(\Omega)\mathbf{r}_{ECI}$$

where $\mathbf{R}_1$ and $\mathbf{R}_3$ are canonical rotation matrices defined as:

$$\mathbf{R}_1(\varphi) = \begin{bmatrix} 1 & 0 & 0 \\ 0 & \cos\varphi & \sin\varphi \\ 0 & -\sin\varphi & \cos\varphi \end{bmatrix} \tag{A.9}$$

$$\mathbf{R}_3(\varphi) = \begin{bmatrix} \cos\varphi & \sin\varphi & 0 \\ -\sin\varphi & \cos\varphi & 0 \\ 0 & 0 & 1 \end{bmatrix} \tag{A.10}$$

for an arbitrary angle φ. Performing the multiplication of the three rotation matrix, the following transformation matrix is obtained:

$$\mathbf{R}_{ECI\rightarrow Hill} = \begin{bmatrix} c_\theta c_\Omega - s_\theta c_i s_\Omega & c_\theta s_\Omega + s_\theta c_i c_\Omega & s_\theta s_i \\ -s_\theta c_\Omega - c_\theta c_i s_\Omega & -s_\theta s_\Omega + c_\theta c_i c_\Omega & c_\theta s_i \\ s_i s_\Omega & -s_i c_\Omega & c_i \end{bmatrix} \tag{A.11}$$

where c and s denote the sine and cosine functions of the angle given as subscript.

The vector $\boldsymbol{\omega}_e$ can now be expressed in the Hill frame by using the transformation matrix defined in Eq. (A.11). This results in the following vector:

$$\boldsymbol{\omega}_e = \omega_e \begin{bmatrix} \sin\theta\sin i \\ \cos\theta\sin i \\ \cos i \end{bmatrix} \tag{A.12}$$

Performing the cross-product of the vectors $\boldsymbol{\omega}_e$ and $\mathbf{r}$ then results in:

$$\boldsymbol{\omega}_e \times \mathbf{r} = \omega_e \begin{bmatrix} z\cos\theta\sin i - y\cos i \\ \left(r_{ref} + x\right)\cos i - z\sin\theta\sin i \\ y\sin\theta\sin i - \left(r_{ref} + x\right)\cos\theta\sin i \end{bmatrix} \tag{A.13}$$

The final expression in the Hill frame for the velocity of a spacecraft relative to the rotating atmosphere is thus given as:

$$\mathbf{v}_{rel} = \begin{bmatrix} \dot{x} + \dot{r}_{ref} - y\left(\dot{f} - \omega_e \cos i\right) - z\omega_e \cos\theta \sin i \\ \dot{y} + \left(r_{ref} + x\right)\left(\dot{f} - \omega_e \cos i\right) + z\omega_e \sin\theta \sin i \\ \dot{z} + \left(r_{ref} + x\right)\omega_e \cos\theta \sin i - y\,\omega_e \sin\theta \sin i \end{bmatrix} \qquad \text{(A.14)}$$

If the reference orbit is circular and the Schweighart and Sedwick formulation is used, this expression can be simplified to:

$$\mathbf{v}_{rel} = \begin{bmatrix} \dot{x} - y(nc - \omega_e \cos i) - z\omega_e \cos\theta \sin i \\ \dot{y} + \left(r_{ref} + x\right)(nc - \omega_e \cos i) + z\omega_e \sin\theta \sin i \\ \dot{z} + \left(r_{ref} + x\right)\omega_e \cos\theta \sin i - y\,\omega_e \sin\theta \sin i \end{bmatrix} \qquad \text{(A.15)}$$

since the radius of the orbit will remain constant and the rate of change of the true anomaly will be simplified to nc.

Appendix B – Schweighart and Sedwick Equations

In this appendix, the formulation developed by Schweighart and Sedwick (2002) will be presented along with the parameters included in their equations. These equations valid for J_2 perturbed circular orbits are given by:

$$\begin{aligned}\ddot{x} - 2(nc)\dot{y} - (5c^2 - 2)n^2 x = -3n^2 J_2\left(R_e^2/r_{ref}\right) \\ \times\left\{\frac{1}{2} - \left[3\sin^2 i_{ref}\sin^2(kt)/2\right] - \left[\left(1 + 3\cos 2i_{ref}\right)/8\right]\right\}\end{aligned} \tag{B.1}$$

$$\ddot{y} + 2(nc)\dot{x} = -3n^2 J_2\left(R_e^2/r_{ref}\right)\sin^2 i_{ref}\sin(kt)\cos(kt) \tag{B.2}$$

$$\ddot{z} + q^2 z = 2lq\cos(qt + \varphi) \tag{B.3}$$

These equations are expressed in the Hill frame. The J_2 term is the Earth's second spherical harmonic and has a value of 1.08263×10^{-3}, R_e is the Earth's mean equatorial radius, r_{ref} is the radius of the circular reference orbit, i_{ref} is the reference orbit's inclination, t is the time, φ is the initial phasing angle for the cross-track motion and n is the mean orbital rate which is defined as:

$$n = \sqrt{\frac{\mu}{{r_{ref}}^3}} \tag{B.4}$$

where μ is the gravitational parameter of the Earth. The other terms are specific to the Schweighart and Sedwick formulation.

The c term in the formulation is introduced to account for the effect of the J_2 perturbation on the mean orbital rate and can thus be seen as a corrective term which reduces to one when J_2 is set to zero. It is given as:

$$c = \sqrt{1 + s} \tag{B.5}$$

where

$$s = \frac{3}{8} J_2 \left(\frac{R_e}{r_{ref}}\right)^2 \left(1 + 3\cos 2i_{ref}\right) \tag{B.6}$$

The k term is there in order to correct the nodal drift caused by the J_2 perturbations and is defined as:

$$k = nc + \frac{3}{2} J_2 n \left(\frac{R_e}{r_{ref}}\right)^2 \cos^2 i_{ref} \tag{B.7}$$

The last two terms, l and q, are there to properly model to cross-track motion under J_2 perturbations. They are defined as:

$$q = nc - (\cos\gamma_0 \sin\gamma_0 \cot\Delta\Omega_0 - \sin^2\gamma_0 \cos i_{sat1})\left(\dot{\Omega}_{sat1} - \dot{\Omega}_{sat2}\right) - \dot{\Omega}_{sat1} \cos i_{sat1} \tag{B.8}$$

$$l = -r_{ref} \frac{\sin i_{sat1} \sin i_{sat2} \sin\Delta\Omega_0}{\sin\Phi_0} \left(\dot{\Omega}_{sat1} - \dot{\Omega}_{sat2}\right) \tag{B.9}$$

where

$$i_{sat1} = i_{sat2} + \frac{\Delta\dot{z}_0}{k r_{ref}} \tag{B.10}$$

$$\dot{\Omega}_{sat1} = -\frac{3}{2} J_2 n \left(\frac{R_e}{r_{ref}}\right)^2 \cos^2 i_{sat1} \tag{B.11}$$

$$\dot{\Omega}_{sat2} = -\frac{3}{2} J_2 n \left(\frac{R_e}{r_{ref}}\right)^2 \cos^2 i_{sat2} \tag{B.12}$$

$$\Delta\Omega_0 = \frac{\Delta z_0}{r_{ref} \sin i_{ref}} \tag{B.13}$$

$$\gamma_0 = \cot^{-1}\left[\frac{\cot i_{sat2} \sin i_{sat1} - \cos i_{sat1} \cos\Delta\Omega_0}{\sin\Delta\Omega_0}\right] \tag{B.14}$$

$$\Phi_0 = \cos^{-1}[\cos i_{sat1} \cos i_{sat2} + \sin i_{sat1} \sin i_{sat2} \cos\Delta\Omega_0] \tag{B.15}$$

The i_{sat1} and i_{sat2} terms correspond to the inclinations of the deputy and chief spacecrafts respectively. Since we are placing the chief spacecraft on the reference orbit, we can state that:

$$i_{sat2} = i_{ref} \tag{B.16}$$

Schweighart and Sedwick also present the initial condition needed to remove secular motion or constant offset terms. They are given as:

$$\dot{x}_0 = \frac{1}{2} y_0 n \left(\frac{1 - s}{\sqrt{1 + s}} \right) \tag{B.17}$$

$$\dot{y}_0 = -2 x_0 n \sqrt{1 + s} + \frac{3}{4} n^2 J_2 \frac{R_e^2}{r_{ref}} \sin^2 i_{ref} \tag{B.18}$$

Due to the J_2 perturbation, the orbital elements will change with time. Schweighart and Sedwick therefore had to provide the expression for those changing orbital elements with respect to time:

$$i(t) = i_{ref} - \frac{3}{2} \left(\frac{n}{k} \right) J_2 \left(\frac{R_e}{r_{ref}} \right)^2 \cos i_{ref} \sin i_{ref} \sin^2 kt \tag{B.19}$$

$$\Omega(t) = \Omega_{ref} - t \frac{3}{2} n J_2 \left(\frac{R_e}{r_{ref}} \right)^2 \cos i_{ref} \tag{B.20}$$

$$\theta(t) = kt \tag{B.21}$$

Finally, the instantaneous position vector of the reference orbit expressed in the ECI frame can be determined using the above expressions for the orbital elements as:

$$\mathbf{r}_{ref} = r_{ref} \begin{bmatrix} \cos \Omega \cos \theta - \sin \Omega \sin \theta \cos i \\ \sin \Omega \cos \theta + \cos \Omega \sin \theta \cos i \\ \sin \theta \sin i \end{bmatrix} \tag{B.22}$$

Appendix C – Atmospheric Density Model

In this appendix, the model used to obtain the instantaneous local density in the vicinity of each spacecraft will be presented. This model is very important to obtain accurate values for the local density as it will impact the atmospheric drag forces acting on each spacecraft. The model used in this thesis is the CIRA-72 semi-theoretical model (Vallado, 2007) and assumes that the atmospheric density decays exponentially with increasing altitude:

$$\rho = \rho_0 \exp\left[-\frac{h_{ellp} - h_0}{H}\right] \tag{A.1}$$

where ρ_0 is the nominal atmospheric density at a base altitude h_0 of a given altitude range and H is called scaled height for this given altitude range. These values can be found in table C.1 for any value of altitude of the spacecraft above the ellipsoid Earth, h_{ellp} and a representation of this value is given in Fig. C.1.

Altitude h_{ellp} [km]	Base Altitude h_0 [km]	Nominal Density ρ_0 [kg/m^3]	Scale Height H [km]	Altitude h_{ellp} [km]	Base Altitude h_0 [km]	Nominal Density ρ_0 [kg/m^3]	Scale Height H [km]
0-25	0	1.225	7.249	150-180	150	2.070	22.523
25-30	25	3.899×10^{-2}	6.349	180-200	180	5.464×10^{-10}	29.740
30-40	30	1.774×10^{-2}	6.682	200-250	200	2.789×10^{-10}	37.105
40-50	40	3.972×10^{-3}	7.554	250-300	250	7.248×10^{-11}	45.546
50-60	50	1.057×10^{-3}	8.382	300-350	300	2.418×10^{-11}	53.628
60-70	60	3.206×10^{-4}	7.714	350-400	350	9.518×10^{-12}	53.298

70-80	70	8.770×10^{-5}	6.549	400-450	400	3.725×10^{-12}	58.515
80-90	80	1.905×10^{-5}	5.799	450-500	450	1.585×10^{-12}	60.828
90-100	90	3.396×10^{-6}	5.382	500-600	500	6.967×10^{-13}	63.822
100-110	100	5.297×10^{-7}	5.877	600-700	600	1.454×10^{-13}	71.835
110-120	110	9.661×10^{-8}	7.263	700-800	700	3.614×10^{-14}	88.667
120-130	120	2.438×10^{-8}	9.473	800-900	800	1.170×10^{-14}	124.64
130-140	130	8.484×10^{-9}	12.636	900-1000	900	5.245×10^{-15}	181.05
140-150	140	3.845×10^{-9}	16.149	1000 +	1000	3.019×10^{-15}	268.00

Table C.1: Exponential Atmospheric Model (Vallado, 2007)

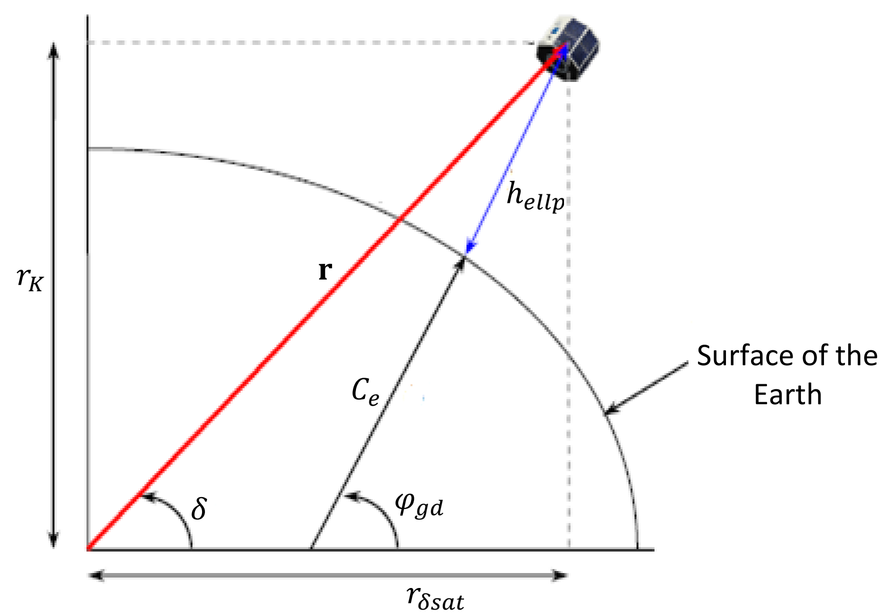

Figure C.1: Model of Ellipsoid Earth

To obtain the height of a spacecraft above the ellipsoid model of the Earth, algorithm 12 of Vallado (2007) is used. The algorithm requires the knowledge of the position vector in the ECI frame, though. The position vector of a spacecraft in the ECI frame is obtained from its position vector in the Hill frame as follows:

$$\mathbf{r}_{ECI} = [r_I \quad r_J \quad r_K]^T = \mathbf{r}_{ref} + \mathbf{R}_{Hill \to ECI}\mathbf{x} \tag{A.2}$$

where $\mathbf{r}_{ECI}$ is the position vector of the spacecraft expressed in the ECI frame, $\mathbf{r}_{ref}$ is the position vector of the reference orbit expressed in the ECI frame, $\mathbf{x}$ is the position vector of the spacecraft expressed in the Hill frame and $\mathbf{R}_{Hill \to ECI}$ is the transformation matrix that changes Hill coordinates into ECI coordinates. The $\mathbf{R}_{ECI \to Hill}$ matrix has already been defined in appendix A. To obtain the $\mathbf{R}_{Hill \to ECI}$ matrix, the inverse of the $\mathbf{R}_{ECI \to Hill}$ must be calculated. Since we know that this matrix is a rotation matrix, which is an orthogonal matrix, its inverse will be its transpose. Therefore, $\mathbf{R}_{Hill \to ECI}$ can be obtained as:

$$\begin{gathered}\mathbf{R}_{Hill \to ECI} = \mathbf{R}_{ECI \to Hill}^T \\ \mathbf{R}_{Hill \to ECI} = \begin{bmatrix} c_\theta c_\Omega - s_\theta c_i s_\Omega & -s_\theta c_\Omega - c_\theta c_i s_\Omega & s_i s_\Omega \\ c_\theta s_\Omega + s_\theta c_i c_\Omega & -s_\theta s_\Omega + c_\theta c_i c_\Omega & -s_i c_\Omega \\ s_\theta s_i & c_\theta s_i & c_i \end{bmatrix}\end{gathered} \tag{A.3}$$

where c and s denote the sine and cosine functions of the angle given as subscript.

Having the position vector expressed in the ECI frame, algorithm 12 of Vallado (2007) can be now be presented. The first step is to get the projection of the spacecraft's position vector onto the equatorial plane:

$$r_{\delta sat} = \sqrt{r_I + r_J} \tag{A.4}$$

Using this value, we can obtain the angle δ shown in Fig. C.1 as:

$$\delta = \tan^{-1}\left(\frac{r_K}{r_{\delta sat}}\right) \tag{A.5}$$

To obtain the radius of curvature in the meridian $C_e$and the geodetic latitude φ_{gd}, an iterative scheme is required:

$$C_e = \frac{R_e}{\sqrt{1 + e_e^2 \sin^2 \varphi_{gd}}} \tag{A.6}$$

$$\tan \varphi_{gd} = \frac{r_K + C_e e_e^2 \sin \varphi_{gd}}{r_{\delta sat}} \tag{A.7}$$

where R_e is the mean equatorial radius of the Earth and e_e is the eccentricity of the Earth which has a value of approximately 0.081819. To perform this iterative scheme, an initial guess is required. A good initial guess is to have φ_{gd} be equal to the angle δ. The iterative scheme can then be performed until a desired tolerance is reached:

$$\left|\varphi_{gd,new} - \varphi_{gd,old}\right| \leq Tolerance \tag{A.8}$$

Finally, the height above the ellipsoidal Earth can be obtained as:

$$h_{ellp} = \frac{r_{\delta sat}}{\cos \varphi_{gd}} - C_e \tag{A.9}$$

Although this algorithm does not take into consideration the curvilinear nature of the Hill frame coordinates, it is still a valid method if the distances calculated in the Hill frame are small when compared to the distance of the Hill frame from the center of the Earth. It is therefore reasonable to use this method for the purposes of this thesis.

References

Battin, R. H., (1987) "*An Introduction to the Mathematics and Methods of Astrodynamics"*, New-York, NY: American Institute of Aeronautics and Astronautics

Bevilacqua, R., & Romano, M., (2008) "Rendezvous Maneuvers of Multiple Spacecraft Using Differential Drag Under J_2 Perturbations", *Journal of Guidance, Control and Dynamics*, Vol. 31, No. 6, pp. 1595-1607.

Blake, C., (2008) "*Dynamics and Control of Satellite Formations Using a Quasi-Rigid Body Formulation*", McGill, Montreal, Quebec.

Calico, R. A., & Wiesel, W. E., (1984) "Control of Time-Periodic Systems", *Journal of Guidance, Control and Dynamics*, Vol. 7, No. 6, pp. 671-676.

Carter, T., & Humi, M., (2002a) "Rendezvous Equations in a Central-Force Field with Linear Drag", *Journal of Guidance, Control and Dynamics*, Vol. 25, No. 1, pp. 74-79.

Carter, T., & Humi, M., (2002b) "Clohessy-Wilthire Equations Modified to Include Quadratic Drag", *Journal of Guidance, Control and Dynamics*, Vol. 25, No. 6, pp. 1595-1607.

Chobotov, V. A., (2002) "*Orbital Mechanics*, *Third Edition*", Reston, Virginia: AIAA Education Series.

Clohessy, W. H., & Wiltshire, R. S., (1960) "Terminal Guidance System for Satellite Rendezvous", *Journal of the Aerospace Sciences*, Vol. 27, No. 9, pp. 653-658.

Fourcade, J., (2004) "Mission Analysis and Orbit Control of Interferometric Wheel Formation Flying", Paper presented at the Proceedings of the 18th Internation Symposium on Space Flight Dynamics (ESA SP-548), Munich.

Franconeri, J., (2003) "Use of Differential Drag as a Satellite Constellation Stationkeeping Strategy", http://ccar.colorado.edu/asen5050/projects/projects_2003/franconeri/

Friedmann, P., Hammond, C. E. & Woo, T.-H., (1977) "Efficient Numerical Treatment of Periodic Systems with Application Stability Problems", International Journal for Numerical Methods in Engineering, Vol. 11, pp. 1117-1136.

Hajovsky, B. B., (2007) "*Satellite Formation Control Using Atmospheric Drag*", Air Force Institute of Technology, Ohio.

Hamel, J.-F., & de Lafontaine, J., (2007) "Linearized Dynamics of Formation Flying Spacecraft on J_2-Perturbed Elliptical Orbit", *Journal of Guidance, Control and Dynamics*, Vol. 30, No. 6, pp. 1649-1658.

Hill, G. W., (1878) "Researches in Lunar Theory", *American Journal of Mathematics*, Vol. 1, No. 1, pp. 5-26.

Jigang, H., & Yulin, Z., (2006) "Application of Phase-Plane Method in the Co-Plane Formation Maintenance of Formation Flying Satellites", *Proceedings of the 25th Chinese Control Conference*, pp. 1900-1904.

Kabamba, P. T., (1986) "Monodromy Eigenvalue Assignment in Linear Periodic Systems", *IEEE Transactions on Automatic Control*, Vol. AC-31, No. 10, pp. 950-952.

Kano, H., & Nishimura, T., (1985) "Controllability, Stabilizability, and Matrix Riccati Equations for Periodic Systems", *IEEE Transactions on Automatic Control*, Vol. AC-30, No. 11, pp. 1129-1131.

Kechichian, J. A., (1998) “Motion in General Elliptic Orbit with Respect to a Dragging and Precessing Coordinate Frame”, *The Journal of the Astronautical Sciences*, Vol. 46, No. 1, pp. 25-45.

Kumar, B. S., Ng, A., Yoshihara, K., & De Ruiter, A., (2007), “Differential Drag as a Means of Spacecraft Formation Control”, Paper presented at the IEEE Aerospace Conference.

Kumar, K. D., Bang, H. C., & Tahk, M. J., (2007), “Satellite Formation Flying Using Along-Track Thrust”, *Acta Astronautica*, Vol. 61, pp. 553-564.

Landry, M. A., (2005) “*Rendezvous and Formation Flying*”, McGill, Montreal, Quebec.

Lee, Y. J., & Balas, M. J., (1999) “Controller Design of Periodic Time-Varying Systems via Time-Invariant Methods”, *Journal of Guidance, Control and Dynamics*, Vol. 22, No. 3, pp. 486-488.

Leonard, C. L., (1986) “Formationkeeping of Spacecraft via Differential Drag”, Unpublished MSc., Massachusetts Institute of Technology, Boston, Massachusetts.

Leonard, C. L., Hollister, W.H., & Bergman, E.V., (1989) “Orbital Formationkeeping with Differential Drag”, *Journal of Guidance, Control and Dynamics*, Vol. 12, pp. 108-113.

Mishne, D., (2004) “Formation Control of Satellites Subject to Drag Variations and J_2 perturbations”, *Journal of Guidance, Control and Dynamics*, Vol. 27, No. 4, pp. 685-692.

Montagnier, P., Spiteri, R. J., & Angeles, J., (2004) “The Control of Linear Time-Periodic Systems using Floquet-Lyapunov Theory”, *International Journal of Control*, Vol. 77, No. 5, pp. 472-490.

Schaub, H., (2004) “Relative Orbit Geometry Through Classical Orbital Element Differences”, *Journal of Guidance, Control and Dynamics*, Vol. 27, No. 5, pp. 839-848.

Schaub, H. & Alfriend, K. T., (2002) “Hybrid Cartesian and Orbit Element Feedback Law for Formation Flying Spacecraft”, *Journal of Guidance, Control and Dynamics*, Vol. 25, No. 2, pp. 387-393.

Schaub, H., & Junkins, J. L., (2003) “Analytical Mechanics of Space Systems”, Reston, Virginia: American Institute of Aeronautics and Astronautics.

Schweighart, S. A., & Sedwick, R. J., (2002) “High Fidelity Linearized J2 Model for Satellite Formation Flight”, *Journal of Guidance, Control and Dynamics*, Vol. 25, No. 6, pp. 1073-1080.

Sengupta, P., & Vadali, S.R., (2007) “Relative Motion and the Geometry of Formation in Keplerian Elliptic Orbits”, *Journal of Guidance, Control and Dynamics*, Vol. 30, No. 4, pp. 953-964.

Sinha, S. C., & Joseph, P., (1994) “Control of General Dynamic Systems with Periodically Varying Parameters via Liapunov-Floquet Transformation”, *Transaction of the ASME*, Vol. 116, pp. 650-658.

Tillerson, M., Inalhan, G. & How, J. P., (2002) “Co-ordination and Control of Distributed Spacecraft Using Convex Optimization Techniques”, *International Journal of Robust and Nonlinear Control*, Vol. 12, No. 2-3, pp. 207-242.

Tschauner, J., & Hempel, P., (1965) “Rendezvous zu einem Min Elliptisher Bahn Umlaufenden Ziel (rendez vous with a Target in Elliptic Orbit)”, *Astronautica Acta*, Vol. 11, No. 2, pp. 104-109.

Ulybyshev, Y., (1998) “Long-Term Formation Keeping of Satellite Constellation Using Linear-Quadratic Controller”, *Journal of Guidance, Control and Dynamics*, Vol. 21, No. 1, pp. 109-115.

Vadali, S. R., Vaddi, S. S. & Alfriend, K. T., (2002) “An Intelligent Control Concept for Formation Flying Satellties”, *International Journal of Robust and Nonlinear Control*, Vol. 12, No. 2-3, pp. 97-115.

Vaddi, S. S., & Vadali, S. R., (2003) “Linear and Nonlinear Control Laws for Formation Flying”, AAS Paper 03-109, *Advances in the Astronautical Sciences*, Vol. 114, Part 1: Spaceflight Mechanics, pp. 171-187.

Vallado, D. A., (2007) “Fundamentals of Astrodynamics and Applications, Third Edition”, Hawthorne, CA: Microcosm Press.

Yamanaka, K., & Ankersen, F., (2002) “New State Transition Matrix for Relative Motion on an Arbitrary Elliptical Orbit”, *Journal of Guidance, Control and Dynamics*, Vol. 25, No. 1, pp. 60-66.